

MEMBRANE RAFTS IN
PLANT–PATHOGEN INTERACTIONS

Inaugural-Dissertation
zur
Erlangung des Doktorgrades
der Mathematisch-Naturwissenschaftlichen Fakultät
der Universität zu Köln
vorgelegt von
Nana Friderike Zappel
aus Göttingen

Köln, Dezember 2008

Die vorliegende Arbeit wurde am Max-Planck-Institut für Züchtungsforschung in Köln in der Abteilung für Molekulare Phytopathologie (Direktor: Prof. Dr. P. Schulze-Lefert) angefertigt.



MAX-PLANCK-GESELLSCHAFT



Max-Planck-Institut für
Züchtungsforschung

Berichterstatter: Prof. Dr. Paul Schulze-Lefert
Prof. Dr. Ulf-Ingo Flügge
Prof. Dr. Ton Bisseling

Prüfungsvorsitzender: Prof. Dr. Martin Hülskamp

Tag der Disputation: 10. Februar 2009

Publications

Teile dieser Arbeit wurden bereits veröffentlicht in:

Zappel NF and Panstruga R (2008) Heterogeneity and lateral compartmentalization of plant plasma membranes. *Curr Opin Plant Biol* **11**: 632-640

Table of contents

| | |
|-------------------------------------------------------------------------------------------|-------------|
| Publications | III |
| Table of contents | V |
| Abbreviations | VII |
| Summary | XI |
| Zusammenfassung | XIII |
| | |
| 1. Introduction | 1 |
| 1.1 Model Membranes | 3 |
| 1.2 Detergent-resistant membranes | 4 |
| 1.3 Membrane rafts and mechanisms of subcellular protein localization | 5 |
| 1.4 Membrane rafts in biotic interactions | 7 |
| 1.5 Membrane rafts and tip growth | 9 |
| | |
| 2. Material and Methods | 12 |
| 2.1 Plant material and growth conditions | 12 |
| 2.2 Metabolic labeling of suspension cell cultures | 14 |
| 2.3 Pathogen infections | 14 |
| 2.4 Microsome preparation and detergent-resistant membrane extraction | 15 |
| 2.5 Protein precipitation and immunoblot analysis | 15 |
| 2.6 Quantitative high-throughput imaging | 16 |
| 2.7 Analysis of callose deposition | 16 |
| 2.8 Oxidative burst assay | 17 |
| 2.9 Allocation of functional categories | 17 |
| 2.10 Experimental set up for quantitative mass spectrometry | 17 |
| 2.11 Plasma membrane preparation and detergent-resistant membrane extraction | 18 |
| 2.12 Mass spectrometry and protein identification | 18 |
| 2.13 Quantitative protein analysis | 19 |
| | |
| 3. Results | 23 |
| 3.1 Quantitative proteomics of flagellin-induced plasma membrane compartmentalization | 23 |
| 3.1.1 The cell culture system is responsive to flg22 treatment | 23 |
| 3.1.2 Identification and quantification of flg22-triggered alterations in DRM composition | 23 |
| 3.1.3 Characteristics and functional classification of identified proteins | 25 |
| 3.1.4 Functional analysis of components identified by the proteomic approach | 29 |

| | | |
|------------|---------------------------------------------------------------------------------------------------------------------------------------------------------------|------------|
| 3.2 | Involvement of sterols and membrane rafts in the Arabidopsis-powdery mildew interaction | 39 |
| 3.2.1 | AtPEN1 associates with detergent-resistant membranes in a sterol-dependent manner | 39 |
| 3.2.2 | Sterol biosynthesis mutants <i>smt1</i> and <i>smt2</i> display enhanced resistance towards the adapted powdery mildew pathogen, <i>Golovinomyces orontii</i> | 42 |
| 3.2.3 | Sterol biosynthesis mutants <i>smt2</i> and <i>dwf5</i> display aberrant focal accumulation of GFP-AtPEN1 underneath fungal attack sites | 45 |
| 3.2.4 | A role for digalactosyldiacylglycerol in the <i>Golovinomyces orontii</i> -host interaction | 47 |
| 3.2.5 | REGGIE-LIKE PROTEINS do not play a major role in the powdery mildew host cell entry | 48 |
| 3.2.6 | Degree of fatty acid desaturation does not affect <i>Golovinomyces orontii</i> host cell entry | 48 |
| 4. | Discussion | 55 |
| 4.1 | Quantitative proteomics of flagellin-induced plasma membrane compartmentalization | 55 |
| 4.1.1 | PM H ⁺ -ATPases and ion transport in PAMP signaling | 56 |
| 4.1.2 | flg22-induced redistribution of FLS2 | 58 |
| 4.1.3 | V-ATPases in PAMP signaling | 58 |
| 4.1.4 | Other components enriched in detergent-resistant membranes upon flg22 treatment with potential roles in pathogen defense | 60 |
| 4.2 | Involvement of sterols and membrane rafts in the Arabidopsis-powdery mildew interaction | 63 |
| 4.2.1 | Sterol-dependent AtPEN1 partitioning into detergent-resistant membranes | 64 |
| 4.2.2 | <i>Golovinomyces orontii</i> host cell entry is compromised in a subset of sterol biosynthesis mutants | 65 |
| 4.2.3 | Sterol biosynthesis mutants display aberrant focal accumulation of GFP-AtPEN1 underneath fungal attack sites | 68 |
| 5. | General conclusion and perspectives | 71 |
| 6. | References | 73 |
| 7. | Supplementary Material | 84 |
| 8. | Author's contributions | 102 |
| | Acknowledgements | 105 |
| | Erklärung | 107 |
| | Lebenslauf | 109 |

Abbreviations

| | |
|-------------------|-------------------------------------------------------------|
| - | fused to (in the context of gene/protein fusion constructs) |
| % (v/v) | volume percent |
| % (w/v) | weight/volume percent |
| % | percent |
| °C | degrees Celsius |
| μ | micro |
| μm | micromolar |
| 5' ASA | 5' aminosalicylic |
| ACA | autoinhibited Ca ²⁺ -ATPase |
| AHA | Arabidopsis H ⁺ -ATPase |
| Arabidopsis | <i>Arabidopsis thaliana</i> |
| ATP | adenosine triphosphate |
| av fold | average fold-change |
| <i>Bgh</i> | <i>Blumeria graminis</i> forma specialis <i>hordei</i> |
| C | carboxy-terminal |
| C18 | C18 bonded silica |
| Ca ²⁺ | calcium ions |
| cDNA | complementary DNA |
| Col-0 | <i>Arabidopsis thaliana</i> ecotype Columbia-0 |
| ConcA | concanamycin A |
| CPR | Constitutive expressor of PR genes |
| CVP | Cotyledon vascular pattern |
| D | distance |
| Da | dalton |
| DET3 | De-etiolated3 |
| dpi | days post infection |
| DRM | detergent-resistant membrane |
| DWF | Dwarf |
| EDTA | ethylenediaminetetraacetic acid |
| enr. | enriched |
| FA | focal accumulation |
| FC | functional category |
| FER | Feronia |
| flg22 | 22 amino acid peptide of flagellin |
| FLS2 | Flagellin Sensing2 |
| FRL1 | Frill1 |
| FTMS | fourier transform mass spectrometer |
| FWHM | full width at half maximum |
| g | gram |
| g | gravity constant (9.81 ms ⁻¹) |
| <i>G. orontii</i> | <i>Golovinomyces orontii</i> |
| GFP | Green fluorescent protein |
| GPI | Glycosylphosphatidylinositol |
| GSL | Glucan synthase-like |
| h | hour |
| HEPES | 4-(2-hydroxyethyl)-1-piperazineethanesulfonic acid |
| HIN1 | Hairpin-induced1 |

ABBREVIATIONS

| | |
|------------------|------------------------------------------------------------|
| hpi | hours post infection |
| HPLC | high-performance liquid chromatography |
| hrs | hours |
| i.e. | <i>id est</i> |
| kDa | kilo Dalton |
| LC | liquid chromatography |
| LCN | Lipocalin |
| l _d | liquid-disordered |
| <i>Ler</i> | <i>Landsberg erecta</i> |
| l _o | liquid-ordered |
| log ₂ | logarithm to the base 2 |
| LTQ | linear ion trap quadrupole |
| m | milli |
| M | molar (mol/l) |
| MAP | Mitogen-activated Protein |
| max fold | maximal fold change |
| MLO | Mildew resistance locus O |
| MS | Murashige and Skoog |
| MS/MS | tandem mass spectrometry |
| MBCD | methyl-β-cyclodextrin |
| n | nano |
| NADPH | Nicotinamide adenine dinucleotide phosphate (reduced form) |
| NHL3 | NDR1/HIN1-like3 |
| NDR1 | Non race-specific disease resistance1 |
| <i>Nt</i> | <i>Nicotiana tabacum</i> |
| OST2 | Open Stomata2 |
| p | probability |
| PAGE | polyacrylamide gel electrophoresis |
| PAMP | pathogen-associated molecular patterns |
| PCR | polymerase chain reaction |
| PEG | poly ethylene glycol |
| PEN1 | Penetration 1 |
| PEST | proline-, glutamic acid-, serine-, and threonine-rich |
| PGP | Plasma glycoprotein |
| pH | negative logarithm of proton concentration |
| PM | plasma membrane |
| PMR4 | Powdery mildew resistant4 |
| PP2C | Protein phosphatase2C |
| ppm | parts per million |
| PR | pathogenesis related |
| Rac5 | Roh of Plant5 |
| rboh | Respiratory burst oxidase homolog |
| RLK | Receptor-like kinase |
| RLP | Reggie-like protein |
| ROR2 | Required for <i>mlo</i> -specific resistance2 |
| ROS | reactive oxygen species |
| rpm | revolutions per minute |
| SA | salicylic acid |
| SDS | sodium dodecylsulfate |
| Ser | serine |
| SID2 | Salicylic acid induction deficient2 |

| | |
|----------|----------------------------------------------------------------------------|
| SMT | Sterol methyltransferase |
| SNAP | Synaptosomal-associated protein |
| SNARE | Soluble <i>N</i> -ethylmaleimide-sensitive factor adaptor protein receptor |
| sqrt | Square root |
| STAGE | stop and go extraction |
| TCR | T-cell receptor |
| T-DNA | transferred DNA |
| Thr | threonine |
| TM | transmembrane |
| Tris | tris-(hydroxymethyl)-aminomethane |
| t-SNARE | target membrane SNARE |
| VAMP | Vesicle-associated membrane protein |
| V-ATPase | Vacuolar H ⁺ -ATPase |
| VHA-C | Vacuolar ATP Synthase Subunit C |
| v-SNARE | vesicle-associated SNARE |

Summary

In the last years, lateral compartmentalization has become a well-recognized topic in plant membrane research. Especially the membrane raft hypothesis receives particular attention, since it gives a conceivable explanation for the spatial and temporal organization of biological membranes. The aim of the work presented here was the investigation of the possible involvement of membrane rafts in biotic stress responses. In this study we elucidated in a quantitative proteomics approach immediate-early protein dynamics in plasma membrane-derived detergent-resistant membranes (DRMs) in response to bacterial flagellin. Proton ATPases and receptor-like kinases were the most prominently enriched protein classes. Strikingly, the flagellin receptor FLS2 was consistently relocalized to DRMs, indicative of its possible recruitment to membrane rafts prior to ligand-induced endocytosis. We performed reverse genetics and pharmacological interference to address the potential contribution of the identified proteins in flg22-triggered responses and thereby identified two novel players of elicitor-dependent oxidative burst control. In a second approach we aimed to elucidate the potential role of membrane rafts and/or sterols during the cellular compartmentalization process in the context of the Arabidopsis–powdery mildew interaction. We showed that the SNARE AtPEN1, which focally accumulates at fungal entry sites, partially associated with DRMs in a sterol-dependent manner. A complementary approach aiming at the genetic interference with membrane raft function revealed that a subset of sterol biosynthesis mutants displayed enhanced resistance towards the adapted powdery mildew pathogen, *Golovinomyces orontii*. This could be partially correlated with an aberrant focal accumulation of GFP-AtPEN1 underneath fungal attack sites, suggesting that the proper sterol composition, which might affect membrane raft integrity, could be important for the focal accumulation of GFP-AtPEN1 at attempted fungal entry sites. In sum our data indicate that membrane rafts might play a role in the compartmentalization of biological processes at the plasma membrane in response to biotic stimuli.

Zusammenfassung

Seit einigen Jahren wird auch in Pflanzen verstärkt die Kompartimentierung von Membranen in verschiedene Domänen betrachtet. Insbesondere die „membrane raft“ Hypothese wird viel diskutiert, da sie eine gute Erklärung für die räumliche und zeitliche Organisation von biologische Membranen liefert. Im Rahmen dieser Arbeit sollte die mögliche Rolle von „membrane rafts“ in biotischen Stressantworten aufgeklärt werden.

Mittels quantitativer Proteomik haben wir die Proteindynamik in Detergenzien-resistenten-Membran (DRM)-Präparationen der Plasmamembran als Folge von Behandlung mit bakteriellem Flagellin untersucht. Protonen-ATPasen und Rezeptor-ähnliche Kinasen waren die am stärksten in DRMs angereicherten Proteinklassen. Auffallend war die konsistente Relokalisierung des Flagellin Rezeptors FLS2. Dies deutet die mögliche Rekrutierung von FLS2 in „membrane rafts“ vor darauf folgender Endozytose an. Anhand reverser Genetik und chemischer Interferenz konnten wir zwei neue Komponenten in dem flg22 induzierten respiratorischen Burst identifizieren.

In einem zweiten Ansatz haben wir zelluläre Kompartimentierungsprozesse in der Arabidopsis–Mehltau Interaktion untersucht. Wir konnten zeigen, dass das SNARE AtPEN1, das unter Angriffsstellen von Mehltausporen akkumuliert, partiell und sterolabhängig mit DRMs assoziiert ist. In einem komplementären genetischen Ansatz konnten wir Sterolbiosynthesemutanten identifizieren, die erhöhte Resistenz gegenüber einem adaptierten Mehltaupilz (*Golovinomyces orontii*) ausweisen. Der Resistenzphänotyp konnte teilweise mit einer veränderten fokalen Akkumulation von GFP-AtPEN1 unter den pilzlichen Angriffsstellen korreliert werden. Dies deutet an, dass eine korrekte Sterolzusammensetzung die Voraussetzung für die Funktionalität potentieller „membrane rafts“ sein könnte und somit möglicherweise in der fokalen Akkumulation von GFP-AtPEN1 eine Rolle spielt. Zusammenfassend deuten unsere Daten auf eine Rolle für „membrane rafts“ in der pathogeninduzierten Membrankompartimentierung hin.

1. Introduction

Since Singer and Nicolson proposed their fluid mosaic model on biological membranes (Singer and Nicolson, 1972) our picture of such membranes has considerably evolved. Today, it is accepted that membranes are highly organized structures providing the necessary heterogeneity to compartmentalize cellular processes (Jacobson et al., 2007). It is plausible that compartmentalization and thereby specialization of cellular processes at the level of biological membranes is essential for the development of organisms and their response to environmental signals. To achieve this membrane specialization, a lateral organization of biological membranes is required. However, so far there is no consensus on the underlying molecular principles and mechanisms driving lateral heterogeneity (Ikonen, 2008). The membrane raft hypothesis is a conceivable explanation for the spatial and temporal organization of membranes (Simons and Ikonen, 1997). Membrane rafts are thought to form distinct domains within the lipid bilayer through the tight interaction of sphingolipids and sterols. Proteins are assumed to be specifically included or excluded from membrane rafts, thereby providing a mechanism for confined protein-clustering (Ikonen, 2008). The membrane raft hypothesis is based on the phase behavior of model membranes, in which liquid-ordered (l_o) and liquid-disordered (l_d) phases can coexist. Sterols have the ability to drive the formation of l_o -phases; however, the precise mechanism of phase separation is unclear (Hancock, 2006). The controversy about the membrane raft hypothesis arises from observations of macroscopically visible coexisting phases in model membranes but not in resting (non-stimulated) living cells. Yet strong evidence has accumulated regarding the existence of very small and highly dynamic l_o -domains in biological membranes (Jacobson et al., 2007). This led to the revised definition of membrane rafts as “small (10–200 nm), heterogeneous, highly dynamic, sterol-enriched and sphingolipid-enriched domains that compartmentalize cellular processes. Small rafts can sometimes be stabilized to form larger platforms through protein–protein and protein–lipid interactions” (Pike, 2006). To finally help resolve the open questions concerning size, composition, stability, mechanism of formation and physical properties of membrane rafts, new technologies and concepts will probably be needed (Jacobson et al., 2007; Ikonen, 2008; van Meer et al., 2008). At the same time, researchers mainly agree that whether small membrane rafts preexist or not, large-scale phase separation can occur through either clustering of preexisting rafts or the stabilization and coalescence of transient rafts

((Kenworthy et al., 2004; van Meer et al., 2008); Figure 1). Examples for such induced large-scale clustering in eukaryotic cells are the vertebrate immunological synapse (Gaus et al., 2005; Seminario and Bunnell, 2008), projection sites of mating yeast cells (Bagnat and Simons, 2002; Proszynski et al., 2006), cell adhesion sites (Gaus et al., 2006) and the tips of growing hyphae in *Candida albicans* (Martin and Konopka, 2004). In addition to the membrane raft hypothesis the meshwork hypothesis also explains the compartmentalization of plasma membranes (PMs). In this model it is assumed that the cortical actin cytoskeleton (so called fences) and transmembrane proteins anchored to it (so called pickets) restrict the lateral diffusion of transmembrane proteins (Marguet et al., 2006). Although the latter model does not account for the compartmentalization of lipids, it is conceivable that the lateral mobility of (trans-) membrane proteins is modulated based on both lipid-dependent and actin-dependent organization forces (Lenne et al., 2006).

In plant research, membrane domains and dynamics, cell polarity and the role of lipids and sterols therein have gained increasing attention in the last few years. Cell polarization and membrane domain formation are indispensable for plants since they rely on cellular and subcellular asymmetry during development. Polar growth of the pollen tube and root hairs depend on cell polarization as well as transporters that are focally localized in membrane domains and that seem to be regulated thereby (Grossmann et al., 2006; Sutter et al., 2006; Boutte et al., 2007; Homann et al., 2007; Kost, 2008). Furthermore, plasticity and the ability to polarize the whole cell including membrane proteins is needed for the plant cells' response to environmental stimuli, such as pathogen attack (Assaad et al., 2004; Bhat et al., 2005; Opalski et al., 2005; Kwon et al., 2008a). Since the mechanisms underlying these membrane polarizations are still largely unknown it will be interesting to investigate the possible involvement of membrane rafts in plant membrane heterogeneity. Membrane raft research in plants may help to substantiate key findings obtained using animal systems but could also open up new possibilities of critically testing the membrane raft hypothesis by employing forward and reverse genetic approaches in a multicellular organism. Here, we review the recent findings on membrane domains and cell polarity in plants with a special focus on the possible role for membrane rafts in various biological processes.

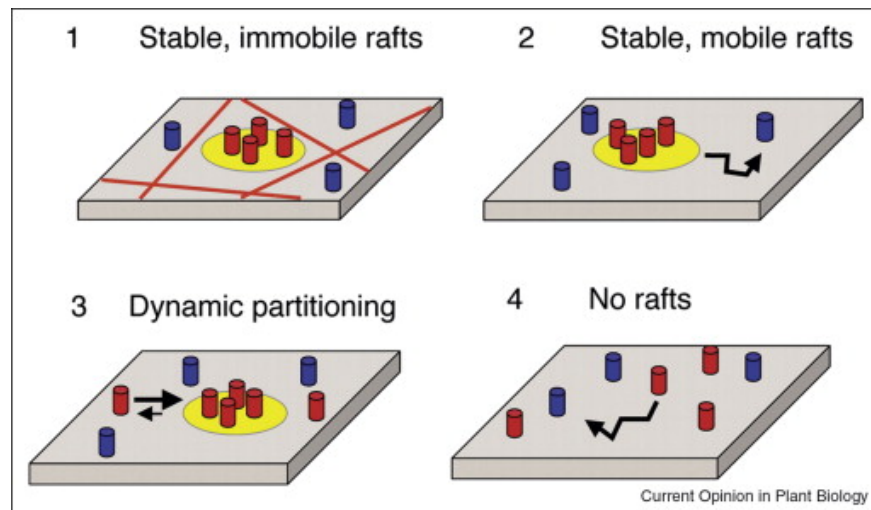


Figure 1. Models for membrane raft dynamics. Models for diffusional mobility of membrane rafts (yellow), raft-associated proteins (red), and nonraft proteins (blue). (1) Stable, immobile rafts. Hypothetical barriers to membrane raft diffusion are depicted by red lines. (2) Stable, mobile rafts. (3) Dynamic partitioning of raft proteins. (4) No rafts. For simplicity, putative barriers to individual protein diffusion are not depicted. Copyright 2004 (Kenworthy et al., 2004), published by The Rockefeller University Press.

1.1 Model Membranes

In contrast to animal membranes where cholesterol is the predominant sterol, plant membranes comprise a more complex sterol mixture. The main sterols in *Arabidopsis* cells are sitosterol, stigmasterol and campesterol, while cholesterol contributes only a minor proportion. One of the basic prerequisites for the existence of membrane rafts in plant cells is the induction of phase separation by phytosterols. The ability of sterols to pack tightly with saturated lipids is the key for their domain-forming activity (Xu and London, 2000). To date, several groups described the domain-promoting activity of phytosterols in two-component and three-component lipid mixtures. They have shown that the order of enriched domains and their stability depends on the structure of the partitioning sterol (Xu et al., 2001; Halling and Slotte, 2004; Wu et al., 2006; Beck et al., 2007; Hac-Wydro et al., 2007). However, probably owing to differences in experimental systems and their methods, no clear ranking of the sterols concerning their domain-forming ability, domain-stabilizing activity or the order of the induced domains has been established. Beck and coworkers demonstrated that the dynamics of three-component mixtures resembling plant membranes are less sensitive to temperature changes than mixtures mimicking animal or fungal membranes (Beck et al., 2007). The domain stability over a wider temperature range suggests that plants evolved a superior mechanism to cope with changing temperatures,

ensuring proper functioning of membrane-associated processes. This feature is possibly one of the many adaptations of plants to their sessile lifestyle.

1.2 Detergent-resistant membranes

Brown and Rose introduced the concept of membrane rafts being resistant to detergent treatment based on the tight interaction of lipids, proteins and cholesterol (Brown and Rose, 1992). During treatment the detergent molecules insert preferentially into the l_d -phase. Above a certain detergent concentration the l_d -phase solubilizes leaving the l_o -phase intact. Due to these characteristics and its practicability, detergent-resistant membrane (DRM) isolation is probably the method most widely used to study membrane rafts, but also most critically discussed (Lichtenberg et al., 2005). Despite all concerns, the differential solubilization of membrane proteins likely depends on their different lipid environment in the membrane. Thus, the enrichment of a protein in DRMs indicates its affinity for presumptive membrane rafts. The most meaningful application of DRM extraction is achieved if there is differential DRM association of a protein before and after a stimulus, thereby linking it to a biological phenomenon (Lingwood and Simons, 2007).

As suggested by the ability of phytosterols to induce phase separation, DRMs could also be isolated from plant material (reviewed in (Bhat and Panstruga, 2005)). In the past two years several groups have enlarged the inventory of DRM-associated plant proteins. Morel and coworkers identified 145 proteins in DRMs of tobacco Bright Yellow-2 (BY-2) cells and analyzed their physicochemical characteristics (Morel et al., 2006). They showed that proteins involved in signaling, response to biotic and abiotic stress, cellular trafficking and cell wall metabolism are over-represented in the DRM fraction. This resembles the protein composition of DRMs in animal cells (Morel et al., 2006). Similarly, DRMs have been isolated from roots of *Medicago truncatula* and their proteomic and lipid compositions extensively analyzed (Lefebvre et al., 2007). Interestingly, several proteins belonging to the PM redox system have been found to associate with DRMs (see also below). Recently, Laloi and coworkers showed how DRM extraction can be combined with genetic approaches (Laloi et al., 2007). The group isolated DRMs from Arabidopsis cell lines *fad2* and *Fad3+* hyperaccumulating 18:1 and 18:3 fatty acids, respectively. The amount of DRMs recovered from the mutant material was 20% of wild-type levels. This underlines

the expected importance of the unsaturation degree of lipid acyl chains in the formation of membrane rafts.

1.3 Membrane rafts and mechanisms of subcellular protein localization

Innate immunity relies on the recognition of pathogen-associated molecular patterns by pattern recognition receptors. Arabidopsis FLAGELLIN SENSITIVE2 (FLS2) is a receptor-like kinase (RLK) and functions as a pattern recognition receptor that senses bacterial flagellin and activates defense signaling. FLS2 exhibits ligand-induced endocytosis that is abolished in a mutant form of FLS2 that cannot be phosphorylated at a C-terminal threonine residue (Robatzek et al., 2006). Plants expressing this mutant form also have disturbed defense signaling, indicating that receptor endocytosis and defense signaling are interconnected. The presumed membrane compartmentalization leading to receptor endocytosis seems to be required for FLS2 function. Recently, a ligand-induced reduction in the membrane mobility of FLS2 was reported (Ali et al., 2007). This finding indicates a change of the environment of the FLS2 receptor upon ligand binding. The cause for the mobility shift could be due to interaction with other proteins, the confinement to less mobile membrane domains, or a combination of both. Indeed, ligand-induced interaction of FLS2 with BRASSINOSTEROID-ASSOCIATED KINASE1 (BAK1), another RLK, was recently reported (Chinchilla et al., 2007; Heese et al., 2007). It is tempting to speculate that the spatial regulation of FLS2, allowing ligand-induced interactions with BAK1 and endocytosis of the receptor, is partly due to its differential association with membrane rafts. In fact, RLKs are over-represented in DRMs of plants, indicating their potential *in vivo* association with membrane rafts (Shahollari et al., 2004; Morel et al., 2006).

The *Chlorella kessleri* hexose-proton symporter HEXOSE UPTAKE1 (HUP1) shows a spotty distribution in the PM of *Chlorella* as well as upon heterologous expression in *Saccharomyces cerevisiae*. However, in yeast strains lacking ergosterol (*erg6*) or sphingolipids (*lcb1-100*), HUP1 is evenly distributed (Grossmann et al., 2006). The catalytic activity of HUP1 is decreased in *erg6* cells, indicating that localization of HUP1 to membrane clusters is important for its function. It has been reported that in yeast ergosterol or sphingolipid biosynthesis mutants, proteins that normally localized to

membrane rafts fail to associate with them (Bagnat and Simons, 2002). Furthermore, these mutants are disrupted in membrane polarization at the mating projection (Bagnat and Simons, 2002). Likewise, the *Arabidopsis* mutant ortholog of *erg6*, *smt1^{orc}* shows defects in cell polarity (Willemsen et al., 2003). In this mutant, the auxin efflux carrier-proteins PIN-FORMED1 (PIN1) and PIN3 that are normally polarly localized within cells are mislocalized, leading to reduced polar auxin transport (Willemsen et al., 2003).

The inwardly rectified K⁺ channel KAT1 is distributed in positionally stable membrane domains in the PM of *Nicotiana benthamiana* and in a distinct radial pattern in turgid guard cells in *Vicia faba* (Sutter et al., 2006; Homann et al., 2007). The radial pattern of KAT1 in guard cells could be attributed to KAT1–cell-wall interactions; however, the refinement of KAT1 to membrane domains seems to depend on other factors. Sutter and coworkers (Sutter et al., 2006) demonstrated that the membrane pattern and the lateral mobility of KAT1 are severely altered upon overexpression of a dominant-negative fragment (Sp2) of the soluble *N*-ethylmaleimide-sensitive factor attachment receptor (SNARE) protein, SYP121. While KAT1 is usually present in non-mobile domains in the PM, it is evenly distributed and becomes mobile when coexpressed with Sp2. These data implicate a role for SNAREs in the distribution and behavior of KAT1 at the PM. Furthermore, Sutter and coworkers showed that the phytohormone abscisic acid selectively triggers KAT1 endocytosis. The exclusion of other proteins from endocytosis requires membrane specialization and the focused recruitment of KAT1 (Sutter et al., 2007). Whether the regulation of KAT1 is in part achieved through its association with presumptive membrane rafts remains unclear, yet the partial localization of KAT1 in DRMs provides a hint to it (Sutter et al., 2006). In yeast, the establishment of polar distribution of slowly diffusing PM proteins has been proposed to be achieved through endocytosis (Valdez-Taubas and Pelham, 2003). Interestingly, the slow diffusion of proteins is affected in the yeast *erg6* mutant, in which also the clustering of membrane rafts seems abolished (Valdez-Taubas and Pelham, 2003; Proszynski et al., 2006).

The first publication clearly showing the importance of sterols in the establishment of plant cell polarity revealed a mislocalization of auxin efflux carriers PIN1 and PIN3 in a sterol-deficient mutant accompanied by a reduction in polar auxin transport (Willemsen et al., 2003). Another auxin efflux carrier, PIN2, was already known to colocalize with sterols at the PM and endocytic compartments (Grebe et al., 2003). Recently, Men and coworkers reported that the polar localization of PIN2 also depends on correct sterol composition (Men et al., 2008). The sterol biosynthesis mutant *cpil-1* displays aberrant PIN2

localization and a defect in root gravitropism. The authors elegantly demonstrated that compromised endocytosis, rather than altered lateral mobility or inappropriate PM targeting, is responsible for defects in PIN2 polarity. Still, the generally slow lateral mobility of PIN2 might be important for its polar localization in a scenario where endocytosis regulates the polar distribution of slowly diffusing proteins (Valdez-Taubas and Pelham, 2003).

It is striking that PIN2 and HUP1, both present in membrane domains, are mislocalized in sterol-deficient mutants that also display compromised endocytosis. Furthermore, KAT1 localization depends on SNARE-mediated trafficking of endomembrane compartments. The correct sterol composition, as well as endocytosis and membrane recycling, thus seem to be reoccurring themes in the establishment of plant cell polarity. It would certainly be interesting to investigate whether the elicitor-triggered internalization of FLS2 and the proper localization of KAT1 also depend on a correct sterol composition.

1.4 Membrane rafts in biotic interactions

As mentioned above, it is essential for an organism to react in a spatially and temporally regulated manner to both beneficial and hostile microbes in close proximity. A prominent example for lateral protein heterogeneity is the focal accumulation of a subset of plant PM proteins underneath attempted fungal entry sites. Upon powdery mildew attack, otherwise evenly distributed fluorophore-tagged Arabidopsis and barley polypeptides such as the PM-resident SNAREs SYP121 and ROR2, the heptahelical defense modulator MLO and the cell-death regulator BAX Inhibitor-1 concentrate in stable circular PM domains of 3–10 μm diameter (Assaad et al., 2004; Bhat et al., 2005; Eichmann et al., 2006). Formation of this pathogen-triggered multi-polypeptide cluster coincides with a marked staining by the sterol-binding dye filipin, which indicates an accumulation of sterols in these membrane areas (Bhat et al., 2005). Cellular polarization, comprising focal rearrangement of the cytoskeleton and altered PM organization, is required for the targeted secretion of cargo during the immune responses in plant and animal systems (reviewed in (Kwon et al., 2008b)). In this context, membrane rafts have been reported to be involved in receptor-mediated activation of many vertebrate immune cell types, including mast cells, B-cells and T-cells (Puri and Roche, 2006). Reminiscent of plant SNAREs SYP121 and ROR2 that cluster at powdery mildew attack sites, exocytic SNAREs also accumulate in T-cells at

the contact site with their respective target cells (Das et al., 2004). Individual human SNARE proteins were found to be enriched in DRMs (Chamberlain et al., 2001) and in cholesterol-dependent clusters that are distinct from typical DRMs (Lang et al., 2001), suggesting that SNAREs associate with different types of membrane rafts, possibly in an isoform-specific and cell type-specific manner. Ternary SNARE complexes, the oligomeric SNARE protein assemblies that ultimately mediate vesicle fusion with target membranes, are enriched in DRMs after mast cell stimulation, indicating that membrane rafts might be the preferred sites for secretion (Lang et al., 2001; Puri and Roche, 2006). This hypothesis is further supported by the finding that cholesterol may promote membrane curvature during endocytic vesicle formation by association with oligomeric cholesterol binding proteins (Thiele et al., 2000).

Though the molecular principles driving large-scale protein assemblies in the PM remain enigmatic, it has recently been suggested that submicrometer-sized SNARE clusters (50–60 nm in diameter) originate from self-organization of multiple SNARE molecules, based on weak homophilic protein–protein interactions (Sieber et al., 2007). Individual SNARE molecules dynamically exchange between clusters and the freely diffusing state. SNARE clusters, which are likely functionally important, are probably stabilized by cholesterol (Lang, 2007; Sieber et al., 2007). It is also conceivable that large-scale PM domains may self-assemble upon a localized stimulus-dependent nucleation event.

Besides polypeptides that are linked to vesicle trafficking/exocytosis, additional proteins implicated in reactions of plants to biotic stimuli have been reported to reside in DRMs. For example, cytochrome b561, which also focally accumulates at fungal attack sites (Bhat et al., 2005), appears to be an integral part of a PM redox system in the DRMs of *Medicago truncatula* roots (Lefebvre et al., 2007). This complex supposedly establishes the redox balance between cytoplasm and apoplast and might be important for the generation and/or detoxification of reactive oxygen intermediates in plant–microbe interactions (Lefebvre et al., 2007). Consistent with this hypothesis, the PM-localized tobacco NADPH oxidase NtRbohD, which is a major source of hydrogen peroxide production in pathogen-challenged cells, was found to be recruited to DRMs of BY-2 cells upon stimulation with the fungal elicitor cryptogein (Mongrand et al., 2004). An epitope-tagged variant of the small Rho GTPase NtRac5, a negative regulator of the NADPH oxidase, likewise accumulates in the DRMs of tobacco BY-2 cells (Mongrand et al., 2004). There is also first evidence for a contribution of membrane rafts to a symbiosis-like plant–microbe interaction. Shahollari and coworkers reported on two genes (At1g13230 and

At5g16590) encoding leucine-rich repeat proteins, both transcriptionally upregulated during the interaction of *Arabidopsis* with the growth-promoting fungus *Piriformospora indica* (Shahollari et al., 2007). Mutant plants defective in At1g13230 (also designated *PIRIFORMOSPORA INSENSITIVE-2*, *Pii-2*) show no growth response to the fungus and no induced transcript accumulation of At5g16590. Interestingly, PII-2 and the gene product of At5g16590 are both associated with DRMs, whereas the At5g16590-encoded polypeptide is absent from DRMs of *pii-2* plants. Additionally, the authors showed that a mutant in a putative sphingosine kinase also exhibits impaired response to *P. indica*. Taken together, these data nicely demonstrate how the DRM association of a protein can be linked to a biological phenomenon, strengthening the assumption that membrane rafts are important for the function of the protein encoded by At5g16590.

1.5 Membrane rafts and tip growth

Rho GTPases are signaling proteins with an important role in polarization of eukaryotic cells, including directional expansion, asymmetric division and differentiation (Kost, 2008). They shuttle between an inactive GDP-bound and an active GTP-bound state and regulate the above processes through their specific localization and activation. RAC/ROP (Rho of plant) GTPases, members of the plant Rho GTPase subfamily, are polarly localized at the apical PM of growing root hairs and pollen tubes. Their signaling properties are required for proper tip growth and are regulated by the interaction with regulatory proteins, membrane lipids and Ca^{2+} (Kost, 2008). RAC/ROP proteins were shown to be equally distributed between DRMs and Triton X-100 soluble membranes, however upon activation RAC/ROPs partitioned into DRMs (Sorek et al., 2007). The authors of this report further investigated the mechanism driving the activation-dependent localization of RAC/ROPs by studying ROP6, a type-I RAC/ROP. In the GDP-bound state ROP6 is prenylated and localized to soluble membranes, whereas it is reversibly acylated upon activation and then localized to DRMs. A constitutive active mutant form of ROP6 accumulated exclusively in DRMs, while in a double mutant, in which the acylated cysteine is also mutated, the protein is again localized to soluble membranes. Similarly, Bloch and coworkers showed that a constitutive active form of RAC10 accumulated in DRMs and induced malformation of root hairs and leaf epidermal cells, probably through deregulation of endocytosis (Bloch et al., 2005). The partitioning of activated RAC/ROPs

into DRMs strongly suggests a role for membrane rafts in the activation-dependent regulation of RAC/ROPs and establishment of cell polarity. The membrane raft association of proteins of the Ras superfamily of small GTPases has been extensively studied in animal cells and similar mechanisms have been suggested for their regulation (Abankwa et al., 2007).

Phosphatidylinositol 4,5-bisphosphate (PtdIns(4,5) P_2) is a signaling lipid that coaccumulates with RAC/ROPs at the apex of growing pollen tubes and root hairs (Cole and Fowler, 2006). PtdIns(4,5) P_2 has been proposed to function as a RAC/ROP effector, thereby influencing membrane fusion events. Indeed, PtdIns(4,5) P_2 has been appointed a role in the regulation of synaptic vesicle endocytosis and exocytosis in animal cells (Cremona and De Camilli, 2001). Furthermore, PtdIns(4,5) P_2 seems to promote the activation of RAC/ROPs (Kost, 2008). In animal cells, PtdIns(4,5) P_2 accumulates at sites of cell surface motility together with a Rho-type GTPase, where it is thought to localize to membrane rafts. PtdIns(4,5) P_2 may thereby coordinate membrane dynamics and actin organization as well as integrate signaling (Golub and Caroni, 2005). It is therefore tempting to speculate that also in plants the localization of PtdIns(4,5) P_2 and RAC/ROPs to membrane rafts provides a mechanism for temporal and spatial organization of signaling and cell polarization. With the help of newly available imaging tools to monitor the PtdIns(4,5) P_2 localization at the subcellular level *in vivo* it will be possible to assess the PtdIns(4,5) P_2 dynamics in response to various stimuli (van Leeuwen et al., 2007).

Similar to the role of RAC/ROPs in cell polarization through the regulation of actin dynamics and membrane trafficking, barley RACB has been implicated in the modulation of actin reorganization and cell polarity in the interaction of barley with the powdery mildew pathogen (Opalski et al., 2005). Additionally, in resemblance of PM-resident SNAREs, MLO and BAX Inhibitor-1 (see above), barley ROP-interactive CRIB (Cdc42/Rac-interactive binding) motif-containing protein (RIC) 171 has been found to accumulate underneath attempted fungal entry sites (Schultheiss et al., 2008). RICs are plant-specific proteins regulating RAC/ROPs by GTP-dependent interactions. Accordingly, GTP-bound RACB supposedly attracts RIC171 to the PM, suggesting that RACB is present in the GTP-bound state at attempted fungal entry sites.

The focal accumulation of RAC/ROP proteins during polarized growth and cell polarization towards fungal attack sites suggests similar mechanisms involving RAC/ROPs for both processes. Possibly the regulation of NADPH oxidase activity, resulting in the localized generation of reactive oxygen species and the subsequent establishment of a local

Ca^{2+} gradient (Foreman et al., 2003), provides a mechanistic link between both phenomena. Indeed, in both cases also the secretory pathway is polarized towards a distinct cellular region (Kost, 2008; Kwon et al., 2008a). It would be interesting to determine whether the signaling lipid $\text{PtdIns}(4,5)\text{P}_2$ also accumulates underneath fungal attack sites.

The aim of this study was to further unravel the importance of lateral membrane compartmentalization in response to biotic stresses. On the one hand we applied ratiometric proteomics based on $^{14}\text{N}/^{15}\text{N}$ -metabolic labeling of Arabidopsis cells to elucidate and quantify immediate-early changes at the PM following PAMP perception. We focused on induced changes in protein DRM localization, which led to the identification of new PAMP signaling components. On the other hand we aimed at the elucidation of the involvement of membrane rafts in plant responses towards a fungal pathogen (powdery mildew). Precisely, we studied the role of sterols in protein DRM localization and in the focal accumulation (FA) of GFP-AtPEN1 underneath fungal attack sites. A biochemical and genetic approach in combination indicate that indeed sterols might have a role in the establishment of cell polarity, which is supposedly required for the correct FA of GFP-AtPEN1 in the Arabidopsis–powdery mildew interaction.

2. Material and Methods

2.1 Plant material and growth conditions

Arabidopsis thaliana (Col-0) cell cultures derived from leaves were grown under continuous light (80 to 100 m⁻²s⁻¹) at 24°C in JPL medium with 10 mM potassium nitrate as sole nitrogen source (Engelsberger et al., 2006). *det3* (*de-etiolated3*) (Schumacher et al., 1999), *ost2-1D* (*open stomata2*) (Merlot et al., 2007), *ammonium transport1* (SALK_106389 and SALK_026874), *nhl3* (*ndr1/hin1-like3*, SALK_035428 and SALK_150318), *aca.1* (autoinhibited Ca²⁺-ATPases, SALK_107029), *gsl06* (*glucan synthase-like06*, (GABI-Kat 401F09 and 867B07), *pmr4-1* (*powdery mildew resistant4*) (Nishimura et al., 2003) and *pmr4-1/sid2-1* (*salicylic acid induction deficient2*, C. Consonni, personal communication) as well as the respective wild type plants were grown on soil for approximately four weeks at a day/night cycle of 10:14 hrs, with 22°C:20°C day/night temperature and a relative humidity of 60%. *Arabidopsis thaliana* T-DNA insertion lines of the SALK (Alonso et al., 2003) and SAIL (Sessions et al., 2002) collections were obtained from the Nottingham Arabidopsis stock centre (NASC; <http://arabidopsis.info/>) and GABI Kat (Rosso et al., 2003). Homozygous T-DNA insertion mutants were selected by PCR using suitable primer combinations. Arabidopsis sterol biosynthesis mutants used in this study are listed in Table 4. Sterol biosynthesis mutants, p35S::GFP-PEN1 in *pen1-1* (Collins et al., 2003), p35S::GFP-PEN1 in *pen1-1/smt2* 443F03, p35S::GFP-PEN1 in *pen1-1/dwf5* 232E05, p35S::GFP-RLP1b (G. Van den Ackerveken, personal communication) and the respective wild type plants were grown on soil at a day/night cycle of 10:14 hrs, with 22°C:20°C day/night temperature and a relative humidity of 60%. Homozygous double mutants *pen1-1/smt2* and *pen1-1/dwf5* expressing p35S::GFP-PEN1 were PCR-selected from F₂ progeny of inter-mutant crosses using the respective lines described above as parents. Seedlings of the *fer* mutant (Escobar-Restrepo et al., 2007), SAK116-6 and SAK97-18 (Table 1) were preselected on Murashige and Skoog (MS) medium (including the appropriate antibiotic) and transferred to soil or liquid medium at approximately 7 days after germination. *Arabidopsis thaliana* mutant lines and overexpressing lines involved in fatty acid desaturation, galactolipid synthesis and unknown processes were obtained from the indicated sources (Table 2) and grown on soil for at a day/night cycle of 10:14 hrs, with 22°C:20°C day/night temperature and a relative humidity of 60%.

Table 2. Mutant and transgenic lines used in this study and functional properties of the proteins encoded by their wild type alleles.

| Biological process | Gene | Mutant allele | Function | AGI code | Line designation | Status | Comment | accession | Source |
|-------------------------|--------------|-----------------------|-------------------------------------------------|------------|------------------|------------|-----------------|---------------|-------------------------|
| Fatty acid desaturation | | | | | | | | | |
| | <i>FAD2</i> | <i>fad2-1</i> | omega-6 fatty acid desaturase activity | At3g12120 | | homozygous | EMS mutant | Col-0 | NASC |
| | <i>FAD3</i> | <i>fad3-2</i> | omega-3 fatty acid desaturase activity | At2g29980 | | homozygous | EMS mutant | Col-0 | NASC |
| | | <i>fad3#</i> | | At2g29980 | | homozygous | T-DNA insertion | Col-0 | NASC |
| | <i>FAD4</i> | <i>fad4-1</i> | | not cloned | | homozygous | EMS mutant | Col-0 | NASC |
| | <i>FAD5</i> | <i>fad5-1</i> | oxidoreductase activity | At3g15850 | | homozygous | EMS mutant | Col-0 | NASC |
| | <i>FAD6</i> | <i>fad6-1</i> | omega-6 fatty acid desaturase activity | At4g30950 | | homozygous | EMS mutant | Col-0 | NASC |
| | <i>FAD7</i> | <i>fad7-1</i> | omega-3 fatty acid desaturase activity | At3g11170 | | homozygous | EMS mutant | <i>gll</i> | NASC |
| | | <i>fad7-2</i> | | | | homozygous | EMS mutant | Col-0 | NASC |
| | <i>FAD8</i> | | omega-3 fatty acid desaturase activity | At5gt05580 | | | | | |
| | | <i>fad7-1, fad8-1</i> | | | | homozygous | EMS mutant | Col-0 | NASC |
| | | <i>fad378</i> | | | | homozygous | EMS mutant | Col-0 | NASC |
| Galactolipid synthesis | | | | | | | | | |
| | <i>DGD1</i> | <i>dgd1-1</i> | galactolipid galactosyltransferase activity | At3g11670 | | homozygous | EMS mutant | Col-2 | (Dörmann et al., 1999) |
| | | <i>dgd1-2</i> | | | SALK_113941 | homozygous | | Col-0 | Salk Institute |
| | | <i>DGD1</i> | | | | homozygous | transgene | <i>dgd1-1</i> | (Härtel et al., 2001) |
| | <i>DGD2</i> | <i>dgd2-1</i> | digalactosyldiacylglycerol synthase | At4g00550 | | homozygous | T-DNA insertion | WS-0 | (Kelly et al., 2003) |
| | | <i>dgd2-2</i> | | | | homozygous | T-DNA insertion | Col-0 | (Kelly et al., 2003) |
| | | <i>dgd2-3</i> | | | GABI_248D03 | homozygous | | Col-0 | Salk Institute |
| | <i>MGDI</i> | | 1,2-diacylglycerol 3-beta-galactosyltransferase | At4g31780 | | homozygous | T-DNA insertion | Col-0 | (Jarvis et al., 2000) |
| Unkown process | | | | | | | | | |
| | <i>RLP1b</i> | <i>rlp1b</i> | unknown | At5g25260 | FLAG_381H02 | homozygous | | Ws-4 | INRA |
| | | <i>RLP1b-GFP</i> | | | | homozygous | transgene | Col-0 | pers. comm., I. Adamska |
| | | <i>RLP1a-GFP</i> | unknown | At5g25250 | | homozygous | transgene | Col-0 | pers. comm., I. Adamska |
| | <i>RLP2</i> | <i>rlp2</i> | unknown | At5g64870 | SALK_143325C | homozygous | | Col-0 | Salk Institute |

Table 1. Mutant and transgenic Arabidopsis lines.

| Name | Genotype | Resistance | Ecotype | Source |
|------------|-------------------------------------------------------|------------|------------|----------------------------------------|
| <i>fer</i> | <i>fer/fer;pp2cDs/pp2cDs</i> | - | <i>Ler</i> | (Escobar-Restrepo et al., 2007) |
| SAK116-6 | <i>fer/fer;pp2cDs/pp2cDs;pFER::FER-GFPkinase dead</i> | Hygromycin | <i>Ler</i> | Sharon Kessler, personal communication |
| SAK97-18 | <i>fer/fer;pp2cDs/pp2cDs;pFER::FER-GFP</i> | Hygromycin | <i>Ler</i> | (Escobar-Restrepo et al., 2007) |

2.2 Metabolic labeling of suspension cell cultures

Full metabolic $^{14}\text{N}/^{15}\text{N}$ -labeling of *Arabidopsis thaliana* (Col-0) suspension cell cultures was carried out as described (Engelsberger et al., 2006). Briefly, for the ^{15}N -labeled cell cultures the conventional ^{14}N -containing nitrogen source in the medium (K^{14}NO_3) was replaced with K^{15}NO_3 (Sigma-Aldrich) as the only nitrogen source, yielding a fully ^{15}N -labeled proteome within two weeks of growth in the labeling medium.

2.3 Pathogen infections

Pathogen infections were carried out as described (Consonni et al., 2006). Briefly, four week-old Arabidopsis plants were inoculated with *G. orontii* spores and quantitative analysis of host cell entry was performed at 48 hpi. The macroscopic sporulation phenotype was evaluated at 7-15 dpi; photographs of infected plants were taken at 10 dpi. For quantitative analysis of the GFP-AtPEN1 FA underneath fungal attack sites two week-old Arabidopsis seedlings were challenged with *Bgh* isolate K1 spores.

Pathogen infections with *E. pisi* were carried out as already described (Consonni et al., 2006). Shortly, four week-old Arabidopsis plants were inoculated with *E. pisi* spores and quantitative analysis of host cell entry was performed at 7 dpi

For visualization of epiphytic fungal structures, specimens were stained with Coomassie Brilliant Blue. For quantification of host cell entry, the proportion of germinated fungal sporelings that developed secondary hyphae was assessed on at least eight leaves (two leaves per plant) per experiment and genotype (minimum of 50 germinated sporelings/leaf evaluated). Fungal penetration success on each genotype was quantified in at least three independent experiments.

2.4 Microsome preparation and detergent-resistant membrane extraction

All steps were carried out on ice or at 4°C. Total membranes were isolated from ground mature *Arabidopsis* rosette leaves using extraction buffer (20 mM Hepes pH 7.5, 13% (w/v) sucrose, 1 mM EDTA) containing protease inhibitor cocktail (Roche) and 1 mM DTT. Total extracts were filtered through two layers of Miracloth (Calbiochem) and centrifuged for 20 minutes at 20,000 x *g*. Microsomes were collected by centrifugation at 100,000 x *g* for 45 minutes and resuspended in 2 ml buffer (20 mM Hepes pH 7.5, 13% (w/v) sucrose, 1 mM EDTA) and centrifuged onto a 1.8M sucrose cushion for 35 minutes at 140,000 x *g*. The interface was collected and diluted at least five-fold for collection of the microsomes by centrifugation at 100,000 x *g* for 1h. The microsomal pellet was resuspended using a dounce glass homogenizer and protein concentration was determined (Bradford, 1976). 50 µg total protein was treated with Triton X-100 at a protein-to-detergent ratio as indicated (final concentration 1%) for 30 minutes at 4°C while continuously shaking at approximately 60 rpm. Solubilized microsomal extracts were adjusted to a final concentration of 1.8 M sucrose, overlaid with a sucrose step gradient (1.4 M, 1.2 M and 0.15 M sucrose, 2 ml, 1ml, and 0.2 ml respectively) and centrifuged at 240,000 x *g* for 18 hrs. Sucrose gradient fractions were collected and proteins precipitated (see below).

2.5 Protein precipitation and immunoblot analysis

Protein precipitation was adapted from a previously described protocol (Wessel and Flügge, 1984). Two volumes of methanol, 0.5 volumes of chloroform and 1.5 volumes of water were added consecutively to the sample and the mixture vortexed thoroughly. Samples were centrifuged for 20 minutes at 4000 rpm (no brake). The upper phase was removed, without disturbing the interphase and at least 3 volumes of methanol were added. Samples were again thoroughly vortexed and centrifuged again for 20 minutes at 4000 rpm. Pellets were air dried and directly resuspended in sample buffer (125 mM Tris pH 6.8, 25% (v/v) glycerol, 5% (v/v) SDS, 0.1% (w/v) Bromophenol Blue, 200mM DTT). After boiling, samples were separated on polyacrylamide gels and immunoblot analysis was carried out using either anti-AtPEN1 (Zhang et al., 2007), anti-GFP (Roche) or anti-AtLCN antiserum. To detect SDS-resistant AtPEN1-containing ternary SNARE complexes boiling was omitted before polyacrylamide gel separation.

2.6 Quantitative high-throughput imaging

Confocal high-throughput imaging was performed with the Perkin Elmer (Hamburg, Germany) Opera™ microscope as previously described (Meyer, 2008). Shortly, excitation of the samples was performed at a 488 nm laser line for GFP. The emission spectrum was taken from 502 to 577 nm.

For high-throughput imaging leaves were prepared in 96-well microplates with an optical glass bottom. Detached cotyledons of two week-old *Arabidopsis* plants inoculated with *Bgh* were placed upside up onto a stamp at 24 hpi. Both cotyledons of each plant were imaged. In total 60 leaves from 30 plants were imaged per genotype and experiment. Due to the natural leaf curvature, not all epidermal cells, the subject of investigation, were in the same optical plane. Thus, images of a consecutive series of 31 planes in the z-direction (z-stack) with a distance of 1 µm were taken per area, with eight areas per leaf. The acquired images were automatically analyzed with a custom-made script of the Acapella™ Software concerning the following parameters: (1) Number of FAs, (2) Number of GFP-PEN1 encased haustoria, (3) Number of FAs per analysable area, (4) Number of FAs per cell, (5) Total integrated FA signal per analysable area, (6) Total integrated FA signal per analysable area, background subtracted, (7) Average intensity of FA, (8) Average area of FA, (9) Total integrated FA signal, over all FAs, (10) Total integrated FA signal, background subtracted, over all FAs, (11) Average length of FA, (12) Average half width of FA, (13) Average width to length ratio of FA, (14) Average roundness of FA, (15) Average contrast of FA compared to the background signal, (16) Average peak intensity of FA, (17) Integrated FA signal per analysable area background subtracted per FA, (18) Number of epidermal leaf cells, (19) Number Of Stomata.

2.7 Analysis of callose deposition

To assess flg22-induced callose deposition in rosette leaves, plants were treated and stained as described previously (Gomez-Gomez et al., 1999). Briefly, 2 µM flg22 was infiltrated in *Arabidopsis* rosette leaves and leaves were harvested 24 hrs later. Leaf samples were cleared with ethanol:acetic acid (1:3 (v/v)), subsequently stained for 24 hrs with 0.01% aniline blue in 150 mM KH₂PO₄ (pH 9.5) and visualized by epifluorescence microscopy.

2.8 Oxidative burst assay

Oxidative burst assays were performed as previously described (Felix et al., 1999). Briefly, cell culture suspensions were distributed in 1 ml aliquots into culture plates and supplied with the peroxidase substrate 5' aminosalicylic acid (5'ASA, 400 μ M). Then flg22 was added to the indicated final concentrations. Alternatively, plants were grown in liquid culture and the reaction mixture, containing horseradish peroxidase (Fluka), luminol (Fluka) and flg22 (100 nM final concentration), was added. Seedlings treated with Concanamycin A (ConcA, Sigma-Aldrich) were preincubated with ConcA (1 mM stock in dimethylsulfoxide, 5 μ M final concentration) for 2 hrs. Control samples were treated with the respective amount of dimethylsulfoxide. The leaf-disc-based oxidative burst assay was performed as described previously (Felix et al., 1999). Briefly, leaf discs were incubated over night in water. Then the reaction mixture, containing horseradish peroxidase (Fluka), luminol (Fluka) and flg22 (1 μ M final concentration), were added.

2.9 Allocation of functional categories

Protein functional categories were assigned according to MapMan (Thimm et al., 2004). Categorization was adjusted manually for obviously wrongly annotated proteins/genes (At1g32050, At1g05570, At2g45820, At3g61260, At4g04720, At2g36910, At4g29900, At3g13380, At3g51740, At1g53100, At3g13560, At5g42100, At3g58100, At4g35230, At2g47060 and At3g17410).

2.10 Experimental set up for quantitative mass spectrometry

The experimental design was as outlined in Figure 2. 15 N and 14 N-labeled parent cell culture suspensions were split up for reciprocal sample pairs and either treated with active flg22 or inactive flg22 Δ 2 (EZBiolab, USA) at 100 nM final concentration. Samples were taken before as well as 5 and 15 minutes after induction. Additionally, cell culture suspensions were treated with flg22 or flg22 Δ 2 and compared to untreated cells, also in reciprocal pairs. Samples were taken 5 minutes after peptide addition. After harvesting, equal amounts (gram fresh weight) of labeled and unlabeled cells were pooled for combined protein extraction, DRM preparation and mass spectrometric analysis.

2.11 Plasma membrane preparation and detergent-resistant membrane extraction

PM preparation and DRM extraction were performed as described (Kierszniowska et al., 2008). Total protein extracts were filtered through Miracloth (Calbiochem) and centrifuged at 10,000 x g. Subsequently, microsomes were collected from the supernatant by centrifugation at 100,000 x g. PM fractions were obtained after two times partitioning in an aqueous two-phase system with PEG/Dextran (each 6.4% (w/w)) and 5 mM KCl (Marmagne et al., 2004). Finally, PMs were collected from the upper phase by centrifugation (120,000 x g) and the protein amount was determined (Bradford, 1976). PMs were resuspended in buffer (50 mM Tris-HCl pH 7.5, 3 mM EDTA) and treated with Triton X-100 at a protein to detergent ratio of 1:13 (final concentration 1%) for 30 minutes on ice while continuously shaking. Solubilized PM extracts were adjusted to a final concentration of 1.8 M sucrose, overlaid with a sucrose step gradient (1.6 M, 1.4 M and 0.15 M sucrose) and centrifuged at 250,000 x g for 18 hrs. An opaque ring (DRM fraction) was collected from below the 1.4 M/0.15 M interface, diluted in buffer (25 mM Tris-HCl pH 7.5, 150 mM NaCl, 5 mM EDTA) and collected by centrifugation at 200,000 x g. All steps were carried out at 4°C.

DRM pellets were resuspended in 30 µl 8 M urea, 2 M thiourea for in-solution tryptic digest. After reduction in 0.5 mM dithiothreitol and alkylation of cysteine groups in 2.5 mM iodoacetamide, proteins were digested with endoproteinase LysC (Wako Chemical, USA) for 3 hrs. Subsequently, the solution was diluted fourfold with 10 mM Tris-HCl (pH 8) before over night digestion with Trypsin (Promega). Digested peptides were desalted over C18 STAGE-tips before mass spectrometric analysis (Rappsilber et al., 2003).

2.12 Mass spectrometry and protein identification

Tryptic peptide mixtures were analyzed by LC/MS/MS using nanoflow HPLC (Proxeon Biosystems, Denmark) and an Orbitrap hybrid mass spectrometer (LTQ-Orbitrap, Thermo Electron, USA) as mass analyzer. Peptides were eluted from a 75 µm analytical column (Reprosil C18, Dr. Maisch GmbH, Germany) on a linear gradient running from 4 % to 64 % acetonitrile in 90 minutes and sprayed directly into the LTQ-Orbitrap mass spectrometer. Proteins were identified by tandem mass spectrometry (MS/MS) by information-dependent acquisition of fragmentation spectra of multiple-charged peptides. Up to five data-dependent MS/MS spectra were acquired in the linear ion trap for each fourier transform mass spectrometer (FTMS) full scan spectrum acquired at 30.000 full

width at half maximum (FWHM) resolution settings. The overall cycle time was approximately one second. Fragment MS/MS spectra from raw files were extracted as DTA-files and then merged to peak lists using default settings of DTASuperCharge version 1.17 (www.msquant.sourceforge.net) with a tolerance for precursor ion detection of 50 ppm. Fragmentation spectra were searched against a non-redundant Arabidopsis protein database (TAIR8, version 2008-04; 31921 entries; www.arabidopsis.org) using the Mascot algorithm (version 2.2.0; Matrix Science, UK, www.matrixscience.com). The database contained the full Arabidopsis proteome and commonly observed contaminants (human keratin, trypsin, lysyl endopeptidase); thus no taxonomic restrictions were used during automated database search. The following search parameters were applied: Trypsin as cleaving enzyme, peptide mass tolerance 10 ppm, MS/MS tolerance 0.8 Da, one missed cleavage allowed. Carbamidomethylation of cysteine was set as a fixed modification, and methionine oxidation was chosen as variable modification. "¹⁵N metabolic labeling" was chosen as a quantitative method for Mascot database searching, allowing identification of labeled and unlabeled peptides within the same database search. Only peptides with a length of more than five amino acids were considered.

In general, peptides were accepted without manual interpretation if they displayed a Mascot score greater than 32 (as defined by Mascot probability (p) < 0.01 significance threshold). Peptides with a score greater than 24 were manually inspected requiring a series of three y or b ions to be accepted. Using the above mentioned criteria for protein identification, the rate of false identifications as determined by the "decoy database" function implemented in Mascot v. 2.2.0 was 0.74% on a 99% (threshold score 32) confidence level and 3.45% at the 95% (threshold score 24) confidence level, indicating increased ambiguity in protein identification as has recently been reported (Nelson et al., 2006). In result tables, peptide assignment to proteins was done according to the Mascot default settings, i.e. each redundant peptide was primarily assigned to the highest scoring protein.

2.13 Quantitative protein analysis

Ratios between labeled and unlabeled forms of tryptic peptides were calculated in MSQuant version 1.4.3 (released 2008-05-03; www.msquant.sourceforge.net). Quantitative information was taken from extracted ion chromatograms of labeled and unlabeled forms of each identified peptide. Thereby, co-elution of both peptide forms was made a requirement and it was manually inspected in MSQuant that the pairs of labeled

and unlabeled forms fit with the expected isotope envelope distributions. Peptides that did not meet these criteria were omitted from the analysis (Engelsberger et al., 2006).

Intensity ratios of labeled ^{15}N -form to unlabeled ^{14}N -form of each identified peptide were averaged across all peptides belonging to the same protein within one experimental set. For each individual peptide, abundance ratios were calculated from the ratio of peak volumes for labeled and unlabeled peptide forms. Peptides conserved in multiple members of a protein family were identified using the "show sub-sets" option in Mascot, and the respective peptides present in multiple proteins were excluded from quantitative analysis if the redundant peptides displayed ratios significantly different ($p < 0.05$; χ^2 -test) from unique peptides of the same protein. Peptides meeting the criteria for sequence identification, but for which only ^{14}N -forms or only ^{15}N -forms were identified, were manually assigned the ratios 0.01 (^{14}N -form only) or 10 (^{15}N -form only). Since quantitative information was extracted from full scan spectra with very low level of noise as obtained in the Orbitrap mass analyzer, no minimum threshold was set for quantitation (Venable et al., 2007). Protein abundance ratios were converted into log₂ values and were normalized to the median log₂ ratio of all proteins identified in the non-treated sample (time point 0). Only those proteins were considered for further analysis, for which intensity ratios were obtained in both of the paired reciprocal experimental sets. Ratios of ^{15}N to ^{14}N forms and the respective standard deviation as calculated in MSQuant for each identified peptide and the number of peptides used for quantitation for each protein are presented in Supplementary Table 2.

Control samples consisting of 1:1 mixtures of labeled and unlabeled cell culture before treatment (time point 0) were analyzed to define the technical and inherent biological variation underlying the experiment. From this control experiment the ratio-dependent standard deviations for specific ratio-bins were calculated as described (Kierszniowska et al., 2008). Log₂ values of ratios for each protein identified in both reciprocal experiment subsets were plotted against each other and the distance to the diagonal (as calculated by $d = |x - y| / \text{sqrt}(2)$) was used as a measure for responsiveness (Figure 4, details see (Kierszniowska et al., 2008)). In the calculation, x and y are the log₂ values of ^{15}N to ^{14}N ratios from each of the reciprocal experiments. Statistical significance of differential protein abundance was assessed by calculating p-values associated with the observed distances to the diagonal compared to the local standard deviation and assuming normal distribution. Specifically, for each data point the ratio between the 'distance' and the local standard deviation was calculated and the p-value was calculated by a 2-tailed t-

distribution. Subsequently, a multiple testing correction was applied to the whole data set using the false discovery rate method introduced by Benjamini and Hochberg (Benjamini and Hochberg, 1995). Reported proteins correspond to a cut-off false discovery rate of 5%.

3. Results

3.1 Quantitative proteomics of flagellin-induced plasma membrane compartmentalization

3.1.1 The cell culture system is responsive to flg22 treatment

To validate the responsiveness of the employed *Arabidopsis* cell culture to flg22 exposure, an oxidative burst assay based on optical color indication was performed. Cell cultures were treated with various amounts of flg22 in the absence or presence of 5'ASA and photographs were taken after 1.5 hrs (Supplementary Figure 1; (Felix et al., 1999)). 5'ASA is a non-specific peroxidase substrate, which is enzymatically converted to a soluble end product that is brown in color. The occurrence of an flg22 concentration-dependent color change, which only took place in samples containing 5'ASA, indicated an flg22-dependent production of ROS and therefore responsiveness of the cell culture to flg22 treatment.

3.1.2 Identification and quantification of flg22-triggered alterations in DRM composition

To elucidate dynamic changes in PM compartmentalization and specialization after flg22 elicitation that are possibly linked to membrane rafts, we performed quantitative mass spectrometric analyses on cell culture DRMs in a time-course experiment. We employed full $^{14}\text{N}/^{15}\text{N}$ metabolic labeling by growing *in vitro* cultured cells on medium with either K^{14}NO_3 or K^{15}NO_3 as the sole nitrogen source. Since ligand-induced endocytosis of FLS2 takes place already within 15 to 20 minutes after flg22 elicitation (Robatzek et al., 2006), PAMP-induced membrane compartmentalization is also expected to occur within or even prior this time frame, whereas changes in protein abundance due to *de novo* protein biosynthesis can be largely excluded at these early time points (Navarro et al., 2004; Benschop et al., 2007). Therefore we induced cell cultures with flg22 (100 nM) or control treatment and collected samples after 0, 5 and 15 minutes (Figure 2). In the first experiment cultures were induced with flg22, and we used the elicitor-inactive flg22 derivative, flg22 Δ 2, as control treatment (Figure 2A). An additional sample set with the identical treatment but reciprocal $^{14}\text{N}/^{15}\text{N}$ labeling was included. In experiment 1 more prominent changes in relative protein abundance were observed after 5 minutes (Figure 3

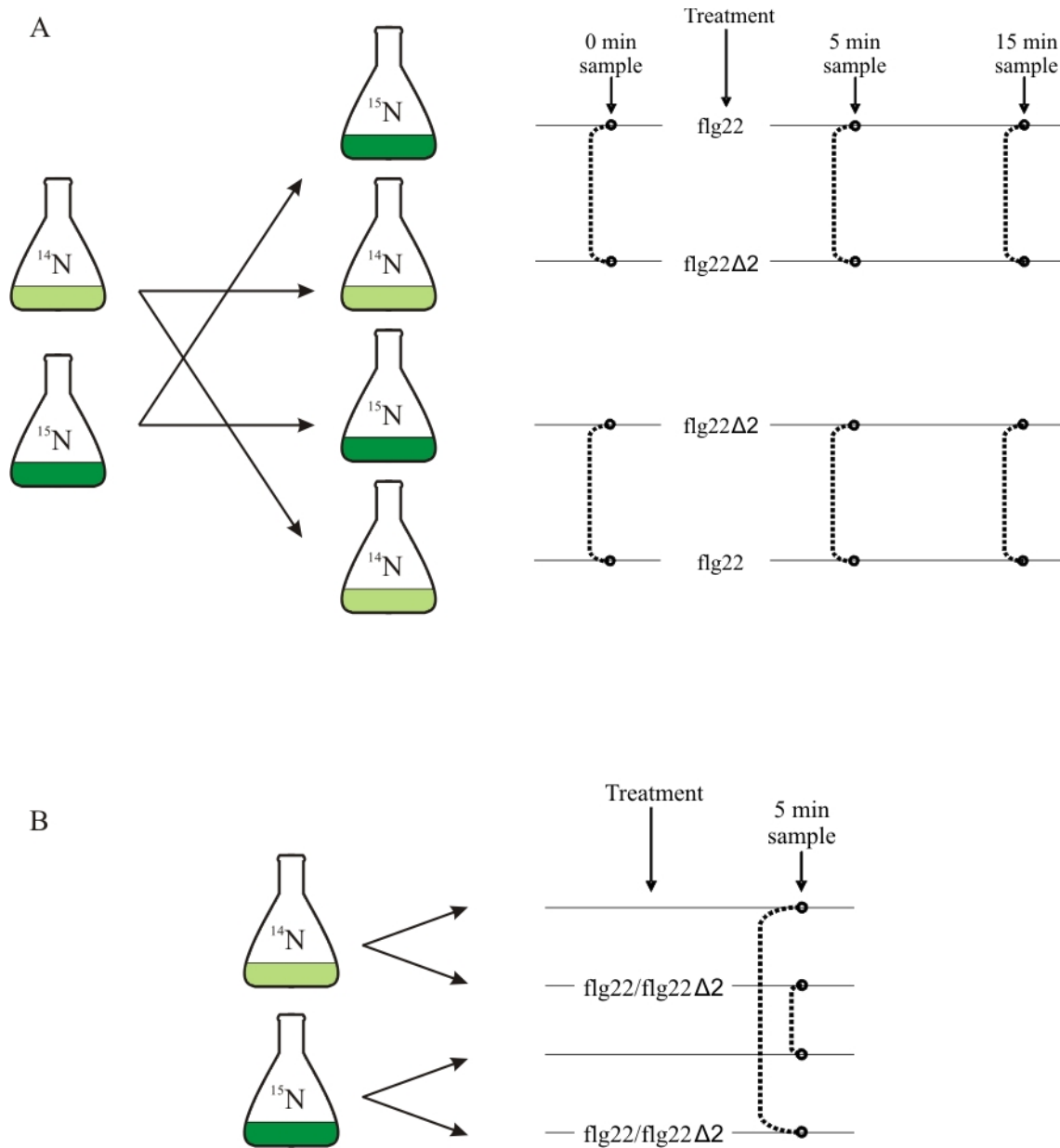


Figure 2. Schematic representation of the experimental set up.

Arabidopsis cell cultures were grown in the presence of either a ^{14}N or ^{15}N -containing nitrogen source. (A) Parent ^{14}N and ^{15}N cultures were split to allow reciprocal treatment. In one case the ^{15}N -labeled cell culture was treated with flg22 and the ^{14}N -labeled with flg22 Δ 2; in the reciprocal experiment the ^{14}N -labeled cell culture was treated with flg22 and the ^{15}N -labeled with flg22 Δ 2. Samples for detergent-resistant membrane extraction and subsequent ratiometric protein quantification were taken before treatment (0 minute sample) as well as 5 and 15 minutes after peptide addition. (B) Differentially labeled parent cultures were split for reciprocal sample treatment. Either ^{15}N -labeled cells were treated with flg22 and compared to untreated ^{14}N -labeled cells or ^{14}N -labeled cells were treated with flg22 and compared to ^{15}N -labeled untreated cells. The same experimental work flow was conducted comparing flg22 Δ 2 versus no treatment. Dotted lines indicate reciprocal sample pairs that were extracted and analyzed together.

and Table 3); accordingly we chose the 5 minute time point for a second experiment (Figure 2B). In the second experiment, flg22 and flg22 Δ 2 treatment was each compared to untreated cells, again using two sets of cell cultures with reciprocal $^{14}\text{N}/^{15}\text{N}$ labeling. PM fractions were extracted from all cell culture samples by two-phase partitioning and subsequently DRMs were isolated by Triton X-100 treatment and sucrose gradient centrifugation (see Materials and Methods for experimental details).

For the analysis of the reciprocal data sets from the first experiment (Figure 2A), the log₂ values of protein ratios from one sample were plotted against log₂ values of the same protein from the reciprocal sample (Figure 3). Each data point represents a given protein that had been quantified in both reciprocal datasets. Statistical significance of differential protein abundance was assessed by calculating p-values associated with the observed distances from the 45° diagonal compared to the local standard deviation and assuming normal distribution (Kierszniowska et al., 2008). The aim of this workflow, adapted from Kierszniowska and coworkers, was to efficiently filter out the between sample variation and at the same time being able to detect subtle stimulus-induced differences (Kierszniowska et al., 2008). The general enrichment of PM proteins in DRMs after flg22 treatment is depicted by the clear shift of the scatterplot of the 5 minute data set and to lesser but also clear extent of the 15 minutes sample set (Figure 3).

3.1.3 Characteristics and functional classification of identified proteins

Based on the procedure outlined above, 316 unique proteins were identified in total, of which 188 were present in reciprocal samples and thus met our criteria for quantitative analysis (Supplementary Table 1). Of these, 34% (64 proteins) were significantly enriched in DRMs after flg22 treatment in a least one of the experiments ($p < 0.05$; Table 3). The number of proteins identified in reciprocal sample sets varied from 55 to 144. Accordingly, the percentage of proteins significantly relocated to DRMs varied between 16 and 45% (Table 3). The averaged “maximal fold change” of the proteins that were found to be significantly enriched was ~ 2 , indicating higher abundance of these proteins in DRMs following PAMP elicitation. In the control samples sets the averaged “maximal fold change” of all proteins was ~ 1.2 , indicative of unaltered DRM localization. No significantly enriched proteins were detected in the sample set induced with the inactive derivative flg22 Δ 2, and only 3 out of 129 proteins (2%) were identified as significantly

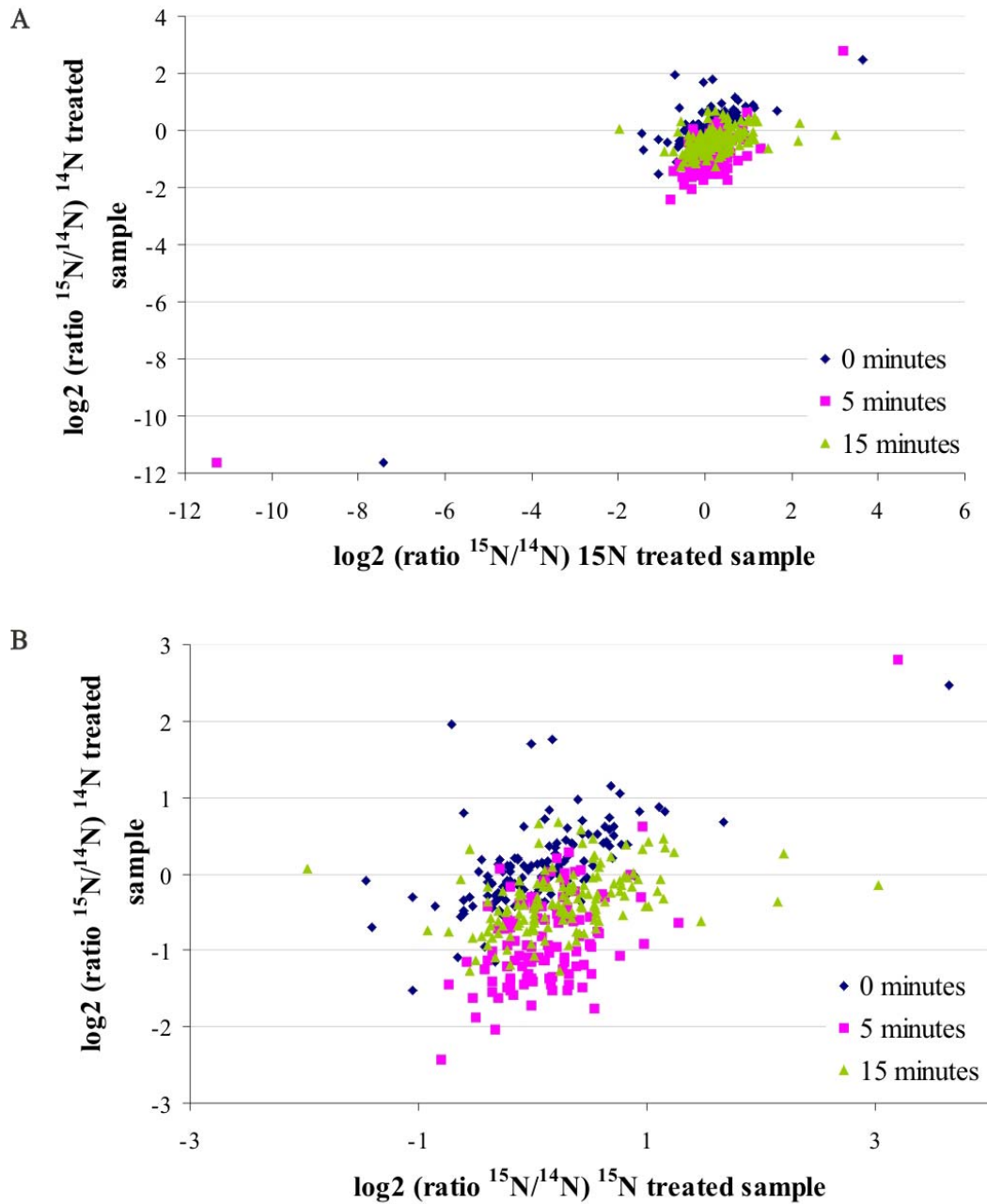


Figure 3. X/Y scatterplots showing \log_2 values of each reciprocal sample set before, 5 and 15 minutes after *flg22* treatment.

\log_2 values of normalized protein abundance ratios from one sample are plotted against \log_2 values of the same protein from the reciprocal sample. (A) All data \log_2 values acquired in the first experiment (see Figure 2A) are plotted. (B) A partial magnification of the core region shown in (A).

responding at the 0 min time point (Table 3). The very low number of proteins being significantly more abundant in the control samples indicates the efficient and successful filtering of false positive polypeptides. Interestingly, all except one protein that showed significantly altered levels after flg22 treatment were more abundant in DRMs. The single protein found to decrease after PAMP exposure is a 60S ribosomal protein (At3g05560), which is probably a contaminant of the PM preparation procedure.

The largest group of signaling proteins which we observed to respond significantly to flg22 treatment comprises 10 RLKs (Table 3). Strikingly, the flagellin receptor FLS2 is one of the two proteins most consistently enriched in DRMs after flg22 elicitation (significantly more abundant in all reciprocal data sets). This finding corroborates the assumption that FLS2 is recruited to specialized membrane domains upon flg22 binding, thereby possibly initiating downstream signaling and/or receptor endocytosis. Next to FLS2, REMORIN 1.3 most consistently shifted into DRMs after PAMP treatment (significant enrichment in all three reciprocal data sets). FERONIA (FER), a RLK identified as a key signaling component in female control of pollen tube perception but ubiquitously expressed throughout the plant (Escobar-Restrepo et al., 2007) also responded significantly to flg22 treatment (for *fer* mutant analysis see additional material).

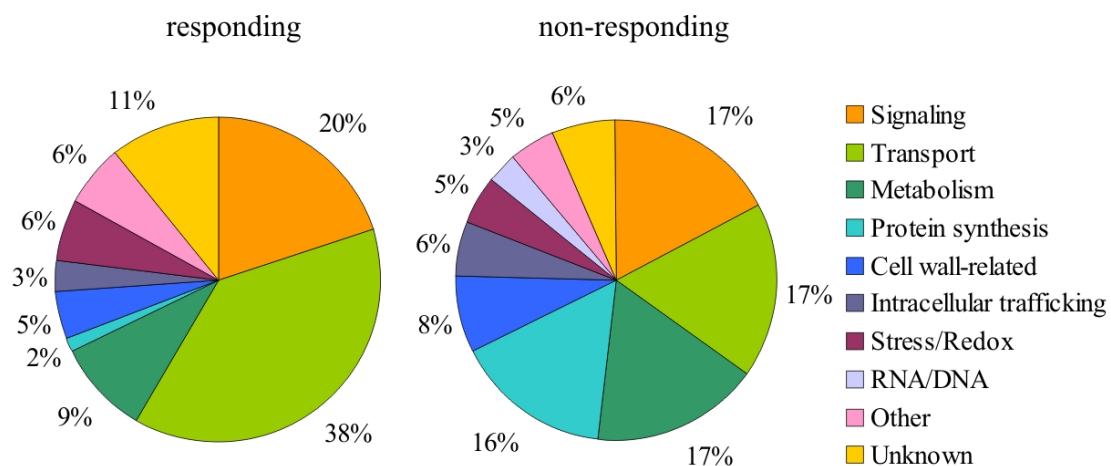


Figure 4. Classification of proteins exhibiting significant redistribution into detergent-resistant membranes after flg22 elicitation and proteins not responding to flg22 treatment.

The functional categories were assigned according to MapMan (Thimm et al., 2004) and manually advanced for some proteins as described in Materials and Methods.

The category of proteins that is enriched most prominently in DRMs upon elicitor treatment is the category of transporters. We identified four PM H⁺-ATPases as

significantly enriched in DRMs upon flg22 elicitation (*Arabidopsis* H⁺-ATPase1 (AHA1), AHA2, AHA3 and AHA4). Interestingly, we also found two isoforms of autoinhibited Ca²⁺-ATPases (ACAs) significantly more abundant in DRMs (ACA8 and ACA10). The significant shift of PM H⁺-ATPases and Ca²⁺-ATPases into DRMs indicates their potential role in PAMP-induced defense responses, which is consistent with their proposed involvement in medium alkalinization and concomitant ROS production (Blumwald et al., 1998; Schaller and Oecking, 1999).

In total we identified 14 Vacuolar H⁺-ATPase (V-ATPase) subunits in our proteomic analysis of which 10 were significantly enriched in DRMs after flg22 treatment. Besides their role in acidification of endomembrane compartments, V-ATPases have been shown to function in secretory and endocytic trafficking (Schumacher, 2006). Based on the potential functional link between endocytosis and membrane rafts (Geldner and Robatzek, 2008; Men et al., 2008) and the enrichment of V-ATPase subunits in DRMs (Borner et al., 2005) it seems thus plausible that their function in membrane traffic is related to membrane raft localization.

Additionally, we identified other transporters of which a subset has been assigned potential functions in plant defense. These include the ammonium transporter AMMONIUM TRANSPORT1 as well as the auxin influx and efflux transporter PLASMA-GLYCOPROTEIN1 (PGP1) and PGP4 (Ninnemann et al., 1994; Benschop et al., 2007; Nühse et al., 2007; Titapiwatanakun et al., 2008). Notably, the PMR4 callose synthase was also significantly enriched in DRMs after PAMP elicitation. PMR4 is known to catalyze biosynthesis of wound- and pathogen-associated callose, which for example is deposited in leaf cells following flg22 treatment (Gomez-Gomez et al., 1999; Jacobs et al., 2003). NHL3 has an already identified role in the *Arabidopsis*–*Pseudomonas syringae* interaction and is significantly more abundant in DRMs after flg22 stimulus. NHL3-overexpressing plants were shown to be more resistant to *Pseudomonas syringae* (Varet et al., 2003).

Of the 188 proteins that fulfilled the criteria for quantification, the majority (73%) possess at least one transmembrane (TM) domain (56%), a glycosylphosphatidylinositol-anchor (12%) or a lipid modification (5%) predicted by the ARAMEMNON database of *Arabidopsis* membrane proteins (Table 3 and Supplementary Table 1; (Schwacke et al., 2003)). For 40% of the polypeptides experimental evidence for PM association exists (Table 3 and Supplementary Table 1; (Schwacke et al., 2003; Alexandersson et al., 2004; Marmagne et al., 2004; Nelson et al., 2006)). Comparison of all proteins found to reside in DRMs based on our study to previously published lists of DRM-associated proteins of

various plant species revealed a substantial overlap. This applies for example to proteins related to cell wall processes, transport, signaling and intracellular trafficking, which are generally highly abundant in DRM preparations (Bhat and Panstruga, 2005).

Interestingly, genes coding for only 12% of the proteins present in reciprocally labeled samples exhibit elevated transcript levels after flg22 treatment (Navarro et al., 2004; Zipfel et al., 2004). No clear difference between genes of proteins significantly more abundant in DRMs (16%) or not (10%) following flg22 treatment was observed. Similarly, only 6% of the respective genes were found to be co-expressed with *FLS2* according to the ATTED database of co-expressed genes (www.atted.jp; (Obayashi et al., 2007)). These comprise 8% of the significantly responding and 5% of the non-responding proteins.

We functionally categorized the 188 identified proteins according to MapMan categories (Figure 4; (Thimm et al., 2004)). When comparing the functional classification of the significantly enriched to the non-enriched groups of proteins, we found the most striking difference in the “transport” category (38% responding *versus* 17% non-responding proteins). Furthermore, pronounced differences were observed in “metabolism” and “protein modification”, with 8 and 14% decreases in the group of significantly responding proteins, respectively. A slight increase in the category “signaling” was observed for the protein group enriched in DRMs (by 3%), whereas “cell wall-related” and “intracellular trafficking” were somewhat decreased (both by 3%).

3.1.4 Functional analysis of components identified by the proteomic approach

Based on our proteomic analysis, a considerable number of membrane-associated proteins, including the flagellin receptor *FLS2*, become rapidly enriched in DRMs following flg22 elicitation. To test whether any of these proteins play an authentic role in flg22-induced cellular responses, we performed *in planta* pharmacological interference experiments and employed reverse genetics. We used the generation of an oxidative burst and the formation of callose-containing cell wall deposits as well-characterized early and late markers of flg22 responsiveness, respectively. Homozygous mutant lines for seven genes of proteins significantly enriched in DRMs after flg22 stress were selected (Table 3). Occurrence of an oxidative burst was quantitatively assessed in 2-week-old wild type and mutant

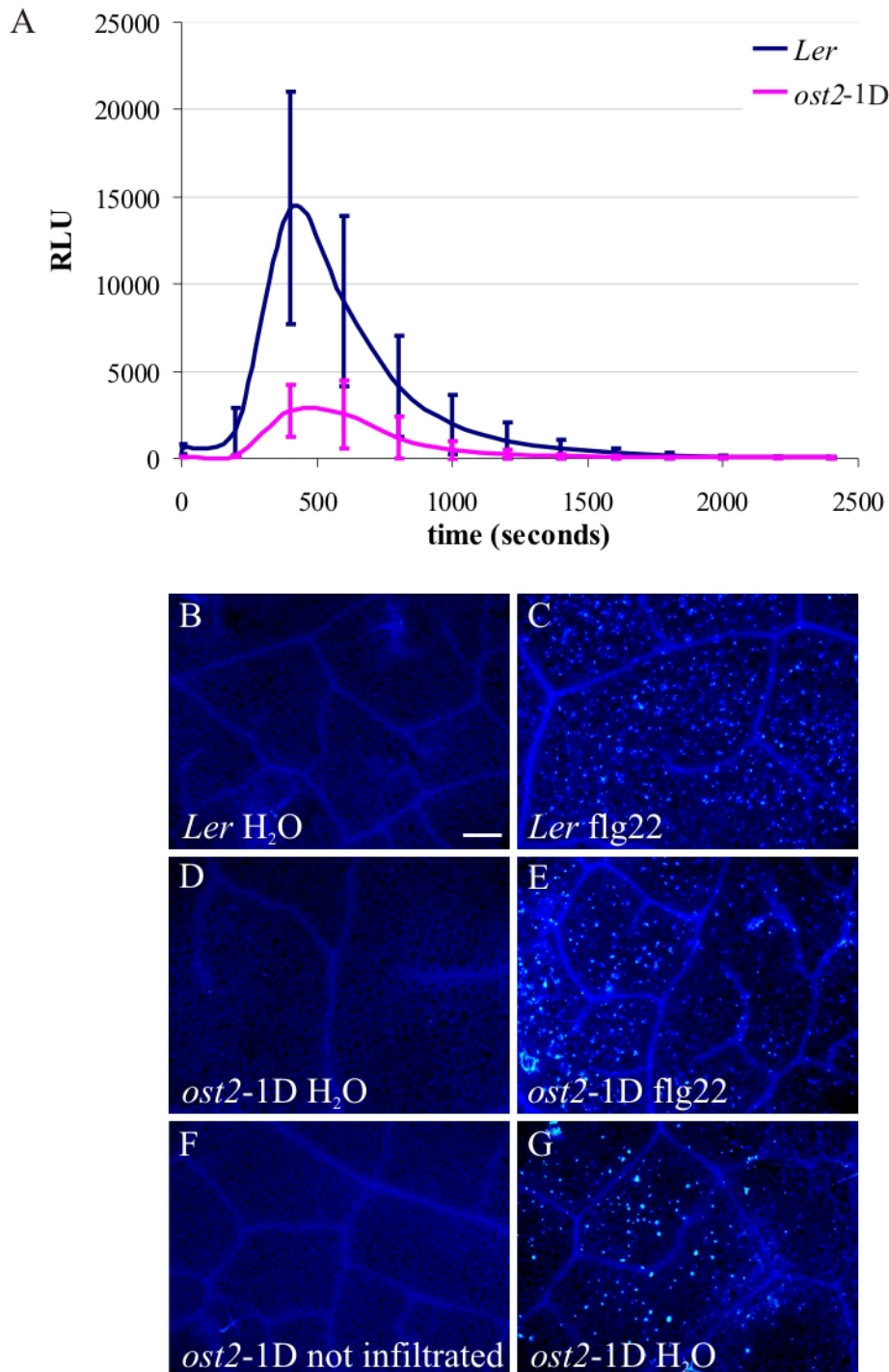


Figure 5. *ost2-1D* mutant plants are impaired in responsiveness to flg22 and show spontaneous as well as flg22-induced callose deposition.

(A) Oxidative burst in response to 100 nM flg22, measured in relative light units (RLU) in wild type (*Ler*) and *ost2-1D* mutant seedlings. The experiment was repeated four times with similar results. Error bars represent standard deviation of ten independent samples measured in a single experiment. (B) – (F) Exemplary micrographs showing callose deposition (as revealed by aniline blue staining) in rosette leaves of wild type (*Ler*, B and C) and *ost2-1D* mutant plants (D to G). B, D and G show micrographs of leaves mock-infiltrated with water. C and E show micrographs of leaves 24 hrs after flg22 infiltration. F shows a micrograph of an untreated leaf. Note the variation in callose deposition in *ost2-1D* plants that is triggered by mock treatment (D and G). Bar = 200 μ m.

seedlings upon application of 100 nM flg22 whereas callose deposition was inspected at 24 hours post infiltration of 2 μ M flg22. While most of the tested mutants retained unaltered responsiveness to flg22 exposure, two mutants showed either a reduced oxidative burst (*det3*) with unaltered callose deposition or abnormalities in both responses (*ost2-1D*) (see also additional material).

ost2-1D is a constitutive active mutant of the PM H⁺-ATPase *AHA1* that is characterized by completely abolished stomatal responses following abscisic acid exposure (Merlot et al., 2007). In our experiments, *ost2-1D* showed a significant reduction in the oxidative burst and occasionally aberrant callose deposition in mock-treated leaves (Figure 5). The latter indicates a generally lowered threshold for stress responses in these plants, which is probably attributed to the reported increase in salicylic acid (SA) levels and the constitutive expression of defense-related genes in the *ost2-1D* mutants (Merlot et al., 2007). However, while mock-treated *ost2-1D* plants only sporadically showed callose deposition, accumulation of this β -D-glucan was always seen upon flg22 treatment (Figure 5E), suggesting that callose deposition was triggered by flg22 in *ost2-1D* plants.

det3 has been isolated based on its deetiolation phenotype. This mutant exhibits reduced transcript levels of the single copy gene *VHA-C* (*VACUOLAR ATP SYNTHASE SUBUNIT C*), which is a core component of all V-ATPase complexes. Consequently, this mutation affects the function of all heterooligomeric V-ATPase complexes (Schumacher et al., 1999). We observed a significantly reduced oxidative burst in *det3* mutant plants (Figure 6A), while flg22-triggered callose deposition was indistinguishable from wild type (data not shown). Notably, also treatment of wild type plants with ConcA, a specific inhibitor of V-ATPases, resulted in a strongly reduced oxidative burst (Figure 6B) and did not interfere with callose deposition (data not shown). This resembles the *det3* phenotype and supports a genuine role for DET3 in early flg22-induced defense responses.

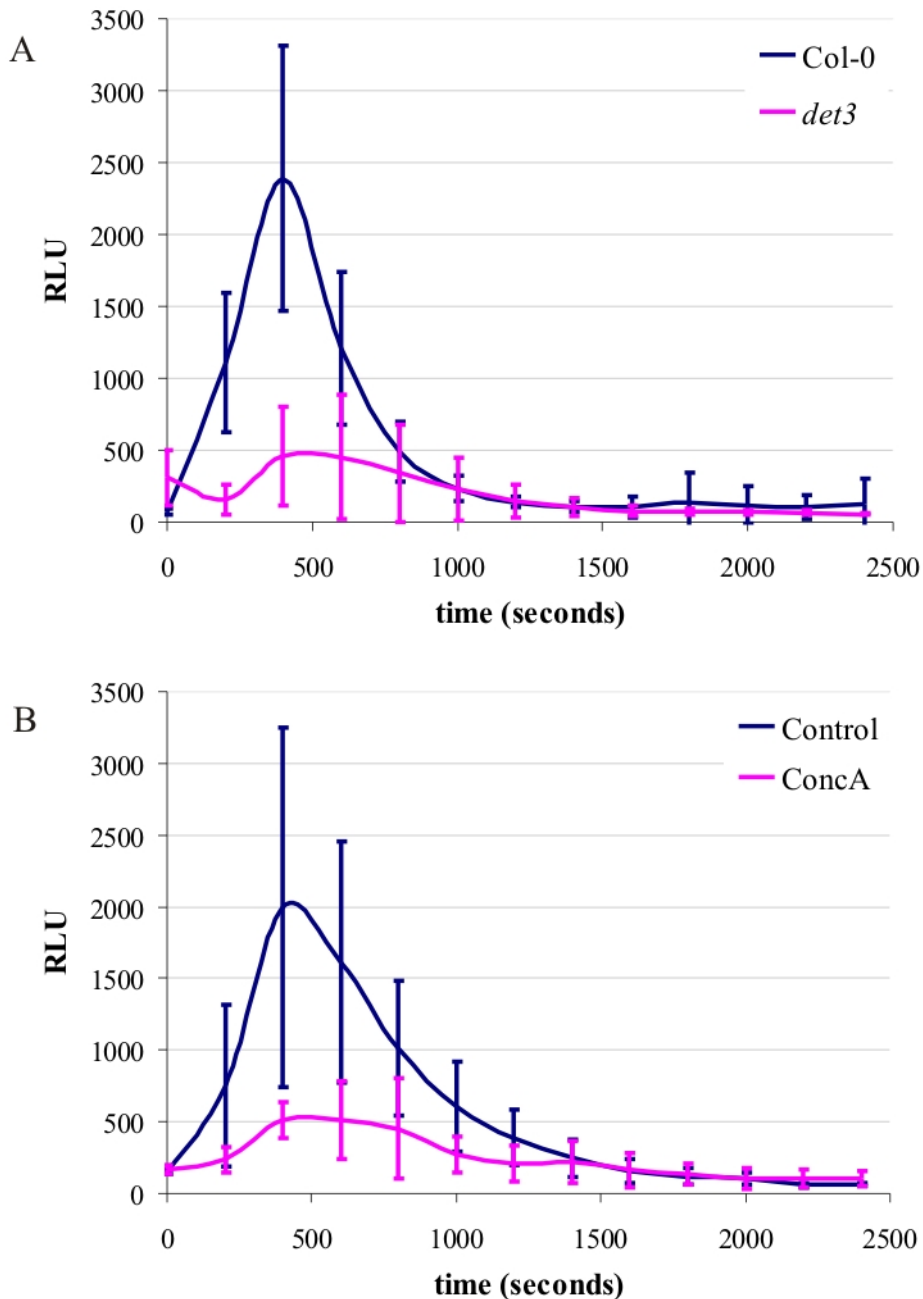


Figure 6. *det3* mutant plants and ConcA-treated wild type plants display reduced responsiveness to flg22 treatment.

(A) Oxidative burst in response to 100 nM flg22, measured in relative light units (RLU) in wild type (Col-0) and *det3* mutant seedlings. The experiment was repeated four times with similar results. Error bars represent standard deviation of 11 independent samples measured in a single experiment. (B) Oxidative burst in response to 100 nM flg22 in Col-0 wild type seedlings treated with either 5 μ M ConcA or with respective amounts of dimethylsulfoxide (drug solvent). The experiment was repeated five times with similar results. Error bars represent standard deviation of six independent samples measured in a single experiment.

FERONIA (*FER*), a RLK, was originally identified as a key signaling component in female control of pollen tube perception (Escobar-Restrepo et al., 2007). According to its identified function in synergids, *FER* is highly expressed there; however, *FER* is also expressed throughout the whole plant, where it might be involved in other processes of cell-autonomous signal transduction or cell-cell communication. In our study we identified *FER* as one of the RLKs that was significantly enriched in DRMs after flg22 treatment (Table 3). Moreover, *FER* is coexpressed with *FLS2* according to the ATTED (www.atted.jp) database of coexpressed genes (Obayashi et al., 2007) and is phosphorylated in response to flg22 treatment (identified in one biological replicate; Benschop et al., 2007). Taken together, these findings suggest in addition to its role in fertilization a PAMP signaling-related function for the *FER* gene product.

To further elucidate the possible involvement of *FER* in plant defense responses, we monitored flg22-triggered callose deposition and employed a set of mutant lines to distinguish between effects that can be directly attributed to the mutation in *FER* and indirect effects through the tightly linked *Ds* element inserted into the neighboring *PROTEIN PHOSPHATASE 2C* (*PP2C*). The analysis of line SAK97-18 allowed us to rule out effects of the *Ds* element in *PP2C*, whereas the line SAK116-6 provided information about the role of the functional kinase domain of *FER* (Table 1). Strikingly, leaves of the *fer* mutant displayed tissue collapse at 24 hrs post infiltration (Figure 7E and I). No callose deposits were observed in flg22-infiltrated leaves, which is likely due to extensive tissue collapse before the onset of callose deposition. All other tested genotypes displayed callose deposition that was indistinguishable from wild type. It would certainly be interesting to further investigate the hypersensitivity of *fer* to flg22 by infiltration of different concentrations of the flg22 peptide or by examining the effect of other less potent peptide variants. Moreover, the collapsed tissue will be examined in more detail by trypan blue staining to assess the occurrence of cell death.

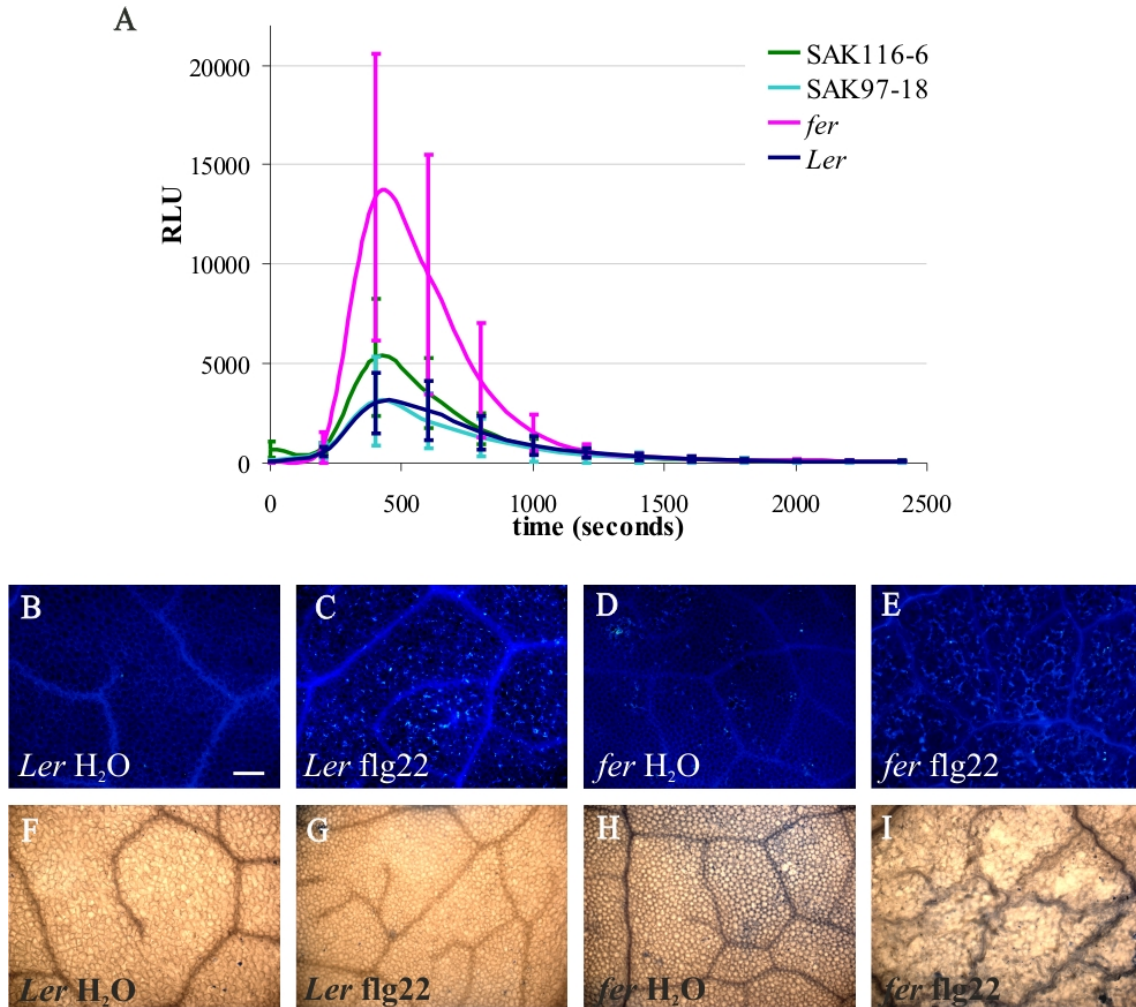


Figure 7. *fer* mutants are hypersensitive to flg22 treatment.

(A) Oxidative burst in response to 100 nM flg22, measured in relative light units (RLU) in wild type seedlings (*Ler*), *fer*, SAK116-6 and SAK97-18 lines. The experiment was repeated twice with similar results. Error bars represent standard deviation of six independent samples measured in a single experiment. (B) – (E) exemplary micrographs showing callose deposition (as revealed by aniline blue staining) in rosette leaves of wild type (*Ler*, B and C) and *fer* mutant plants (D and E). (B and D) show micrographs of leaves mock-infiltrated with water. (C and E) show micrographs of leaves 24 hrs after flg22 infiltration. (F) – (I) Exemplary bright field images of rosette leaves of wild type (*Ler*, F and G) and *fer* mutant plants (H and I). (F and H) show micrographs of leaves mock-infiltrated with water. (G and I) show micrographs of leaves 24 hrs after flg22 infiltration. Bar = 200 μm.

In view of the hypersensitivity of *fer* to flg22 infiltration it seems possible that FER is a negative regulator of PAMP-induced defense responses. Accordingly, an increased oxidative burst in response to flg22 would be expected. However, by an oxidative burst assay using cut leaf discs no conclusive results could be obtained; the data rather suggest a reduced oxidative burst in the *fer* mutant and no difference in the SAK116-6 and SAK97-18 lines (data not shown). However, when seedlings were germinated and preselected on plate before transfer to liquid culture, an enhanced oxidative burst for *fer* but not for the

other genotypes was observed (Figure 7A). It will be necessary to analyze these on the first view contradicting results in more depth. A plausible reason for the seeming discrepancy could be that in the seedling-based oxidative burst assay the plants are not wounded prior to recording the oxidative burst and thus wound responses do not interfere with the measurement.

Interestingly, the SAK116-6 mutant did only partially complement the growth phenotype of the *fer* mutant (data not shown), while ROS production and callose deposition in response to flg22 treatment occurred normally in these plants. Therefore, we assume that the kinase domain of FER is not important for its PAMP signaling-related function, whereas it is crucial for rescuing the growth phenotype.

If our findings can be confirmed and further corroborated, it seems plausible that FER might in fact represent a coreceptor rather than the primary receptor for a ligand. This function could satisfactorily explain the possible involvement of FER in entirely distinct biological processes that take place in different organs/tissues.

Table 3. Proteins significantly enriched in detergent-resistant membranes after flg22 treatment. Proteins significantly enriched in DRMs after flg22 treatment in a least one of the reciprocal sample sets; significant enrichment is indicated in bold ($p < 0.05$). Functional category (FC); average fold-regulation (av fold); probability-value (p); number of TM domains (TM) predicted by ARAMEMNON (Schwacke et al., 2003); experimental evidence for PM association (PM, (Schwacke et al., 2003; Alexandersson et al., 2004; Marmagne et al., 2004; Nelson et al., 2006)); co-expressed with FLS2 (Obayashi et al., 2007), number indicates rank of co-expressed gene according to ATTED; transcriptionally upregulated in response to flg22 treatment (flg22 expr, (Navarro et al., 2004; Zipfel et al., 2004)); phosphorylated after flg22 treatment (Pflg22, (Benschop et al., 2007; Nühse et al., 2007)); mutants of according genes were analyzed for flg22 responsiveness in this study (RG). enriched (enr.), dephosphorylated (de-p), phosphorylation below the significance threshold ((✓)), glycosylphosphatidylinositol (GPI).

| FC | AGI code and annotation | flg22 vs flg22A2 | | | | | | flg22 vs untreated | | flg22A2 vs untreated | | TM | PM | ATTED | flg22 expr | P flg22 | RG |
|-------------------------------------|--------------------------------------------------------------|------------------|--------------|--------------|--------------|--------------|--------------|--------------------|--------------|----------------------|-------|---------|------|-------|------------|---------|----|
| | | 0 minuten | | 5 minuten | | 15 minuten | | 5 minuten | | 5 minuten | | | | | | | |
| | | av fold | p | av fold | P | av fold | p | av fold | p | av fold | p | | | | | | |
| Signalling | | | | | | | | | | | | | | | | | |
| Receptor-like kinase | | | | | | | | | | | | | | | | | |
| | AT5G46330 FLS2 (FLAGELLIN-SENSITIVE 2) | — | — | 1,950 | 0,048 | 1,358 | 0,012 | 1,501 | 0,013 | — | — | 1 | — | 1 | ✓ | — | ✓ |
| | AT3G17840 RLK902 (receptor-like kinase 902) | 0,800 | 0,131 | 1,896 | 0,000 | 1,680 | 0,014 | — | — | — | — | 1 | — | — | — | — | — |
| | AT3G51550 FER (FERONIA) | 0,972 | 0,939 | 1,811 | 0,000 | 1,339 | 0,201 | — | — | — | — | 1 | enr. | 158 | — | — | ✓ |
| | AT3G02880 LRR transmembrane protein kinase, putative | 0,893 | 0,707 | 1,539 | 0,014 | 1,047 | 0,922 | 1,292 | 0,241 | 1,010 | 0,721 | 1 | enr. | — | ✓ | — | — |
| | AT5G16590 LRR transmembrane protein kinase, putative | 0,969 | 0,937 | 1,629 | 0,001 | 1,117 | 0,766 | 1,203 | 0,459 | — | — | 1 | enr. | — | — | — | — |
| | AT2G01820 LRR protein kinase, putative | 1,401 | 0,673 | 1,717 | 0,000 | 2,851 | 0,000 | — | — | 1,154 | 0,617 | 1 | — | — | — | — | — |
| | AT4G36180 LRR family protein | 1,213 | 0,494 | — | — | 2,156 | 0,000 | — | — | — | — | 1 | — | — | — | — | — |
| | AT1G75640 LRR family protein / protein kinase family protein | 0,617 | 0,012 | — | — | 1,421 | 0,024 | — | — | — | — | 1 | — | — | — | — | — |
| | AT3G23750 LRR family protein / protein kinase family protein | 0,892 | 0,673 | 1,590 | 0,030 | 1,266 | 0,563 | — | — | — | — | 1 | ✓ | — | — | — | — |
| | AT3G46290 protein kinase, putative | 0,928 | 0,813 | 1,628 | 0,014 | 1,025 | 0,973 | 1,308 | 0,225 | 1,260 | 0,802 | 1 | — | 224 | — | ✓ | — |
| Other kinases | | | | | | | | | | | | | | | | | |
| | AT4G04720 CPK21 (calcium-dependent protein kinase 21) | 1,033 | 0,937 | 1,918 | 0,001 | 1,163 | 0,593 | — | — | — | — | 0-1/myr | enr. | — | — | — | — |
| | AT5G24010 protein kinase family protein | 0,920 | 0,754 | 1,733 | 0,039 | 1,517 | 0,001 | 1,425 | 0,181 | 0,992 | 0,994 | 1 | — | — | — | — | — |
| Other signalling proteins | | | | | | | | | | | | | | | | | |
| | AT1G05150 calcium-binding EF hand family protein | 0,864 | 0,600 | 1,435 | 0,179 | 1,067 | 0,875 | 1,422 | 0,013 | — | — | 0 | — | — | — | ✓ | — |
| Transport | | | | | | | | | | | | | | | | | |
| Plasma membrane ATPases | | | | | | | | | | | | | | | | | |
| | AT2G18960 AHA1 (H(+)-ATPase 1) | 0,909 | 0,754 | 1,673 | 0,000 | 1,306 | 0,268 | 1,456 | 0,013 | 1,024 | 0,692 | 10 | ✓ | — | — | de-p | ✓ |
| | AT4G30190 AHA2 (H(+)-ATPase 2) | 0,971 | 0,930 | 1,828 | 0,014 | 1,224 | 0,488 | 1,435 | 0,013 | 0,976 | 0,994 | 10 | enr. | — | — | de-p | — |
| | AT5G57350 AHA3 (H(+)-ATPase 3) | — | — | 4,652 | 0,919 | 2,700 | 0,009 | — | — | — | — | 10 | enr. | — | — | — | — |
| | AT3G47950 AHA4 (H(+)-ATPase 4) | — | — | 2,000 | 0,001 | 1,109 | 0,748 | 0,999 | 0,947 | — | — | 10 | ✓ | — | — | — | — |
| Calcium-transporting ATPases | | | | | | | | | | | | | | | | | |
| | AT5G57110 ACA8 (autoinhibited Ca ²⁺ -ATPase 8) | 0,986 | 0,973 | 1,509 | 0,008 | 1,131 | 0,766 | 1,437 | 0,013 | 1,001 | 0,994 | 8-9 | enr. | — | — | — | — |
| | AT4G29900 ACA10 (autoinhibited Ca ²⁺ -ATPase 10) | 1,008 | 0,983 | 1,556 | 0,004 | 1,245 | 0,255 | 1,165 | 0,538 | — | — | 9 | ✓ | — | ✓ | ✓ | — |
| Vacuolar H(+)-ATPases | | | | | | | | | | | | | | | | | |
| | AT3G28715 VHA-d2 | 1,174 | 0,653 | 1,540 | 0,043 | 1,482 | 0,087 | — | — | — | — | 0 | — | — | — | — | — |

Table 3 continued.

| FC | AGI code and annotation | flg22 vs flg22A2 | | | | | | flg22 vs untreated | | flg22A2 vs untreated | | TM | PM | ATTED | flg22 expr | P flg22 | RG |
|----------------------------------|------------------------------------------------------------------------|------------------|-------|--------------|--------------|--------------|--------------|--------------------|--------------|----------------------|-------|-------|------|-------|------------|---------|----|
| | | 0 minuten | | 5 minuten | | 15 minuten | | 5 minuten | | 5 minuten | | | | | | | |
| | | av fold | p | av fold | p | av fold | p | av fold | p | av fold | p | | | | | | |
| | AT3G28710 VHA-d1 | 1,098 | 0,766 | — | — | 1,450 | 0,089 | 1,252 | 0,300 | 0,964 | 0,741 | 0 | ✓ | — | — | — | — |
| | AT4G39080 VHA-a3 | 1,068 | 0,846 | 1,550 | 0,053 | 1,590 | 0,024 | — | — | 1,042 | 0,994 | 6 | — | — | — | — | — |
| | AT1G78900 VHA-A | 1,027 | 0,955 | 1,580 | 0,000 | 1,255 | 0,363 | — | — | — | — | 0-1 | enr. | — | — | — | — |
| | AT2G21410 VHA-a2 | 1,272 | 0,585 | 1,394 | 0,147 | 1,651 | 0,025 | 1,262 | 0,293 | — | — | 6 | — | — | — | — | — |
| | AT4G11150 VHA-E1 | 1,008 | 0,983 | 1,791 | 0,014 | 1,328 | 0,286 | 1,305 | 0,225 | 0,960 | 0,862 | 0 | ✓ | — | — | — | — |
| | AT1G76030 VHA.B1 | 0,648 | 0,225 | 1,410 | 0,128 | 1,659 | 0,016 | — | — | 0,931 | 0,594 | 0 | ✓ | — | — | — | — |
| | AT3G58730 VHA-D | 0,981 | 0,908 | 2,048 | 0,004 | 1,358 | 0,012 | — | — | — | — | 0 | ✓ | — | — | — | — |
| | AT3G42050 VHA-H | — | — | 1,588 | 0,001 | 1,353 | 0,103 | — | — | — | — | 0 | ✓ | — | — | — | — |
| | AT1G12840 VHA-C/DET3 (DE-ETIOLATED 3) | — | — | — | — | 1,552 | 0,011 | — | — | — | — | 0 | — | — | — | — | ✓ |
| ABC Transporter | | | | | | | | | | | | | | | | | |
| | AT2G36910 PGP1 (P-Glycoprotein 1) | — | — | 1,764 | 0,041 | 1,282 | 0,599 | 1,227 | 0,443 | 2,141 | 0,710 | 10 | — | — | — | ✓ | — |
| | AT2G47000 PGP4 (P-Glycoprotein 4) | 1,023 | 0,957 | 1,783 | 0,001 | 1,204 | 0,493 | 1,311 | 0,225 | — | — | 12 | — | — | — | ✓ | — |
| Other Transporter | | | | | | | | | | | | | | | | | |
| | AT5G50200 WR3 (WOUND-RESPONSIVE 3); nitrate transporter | 1,066 | 0,859 | 1,985 | 0,003 | 1,290 | 0,299 | 1,337 | 0,217 | 1,009 | 0,994 | 1 | — | — | — | — | — |
| | AT4G13510 AMT1;1 (AMMONIUM TRANSPORT 1) | 0,889 | 0,698 | 1,849 | 0,006 | 1,460 | 0,227 | 1,313 | 0,225 | 0,918 | 0,947 | 12 | ✓ | — | ✓ | ✓ | ✓ |
| | AT1G11260 STP1 (SUGAR TRANSPORTER 1) | 1,026 | 0,912 | 1,586 | 0,025 | 1,153 | 0,754 | 1,427 | 0,140 | 1,015 | 0,459 | 12 | ✓ | 32 | — | — | — |
| | AT3G19930 STP4 (SUGAR TRANSPORTER 4) | 1,144 | 0,919 | 1,607 | 0,020 | 1,203 | 0,585 | 1,312 | 0,225 | 1,154 | 0,738 | 12 | ✓ | — | — | — | — |
| | AT4G21120 AAT1 (CATIONIC AMINO ACID TRANSPORTER 1) | — | — | — | — | 1,134 | 0,686 | 1,436 | 0,013 | — | — | 14 | — | — | — | — | — |
| | AT5G40780 LHT1 (LYSINE HISTIDINE TRANSPORTER 1) | — | — | 2,411 | 0,004 | 1,136 | 0,707 | 1,492 | 0,013 | — | — | 11-12 | ✓ | — | ✓ | — | — |
| | AT3G54140 proton-dependent oligopeptide transport (POT) family protein | 0,938 | 0,813 | 1,867 | 0,048 | 1,181 | 0,632 | 1,549 | 0,049 | 0,810 | 0,817 | 11 | ✓ | — | — | — | — |
| Cell wall-related | | | | | | | | | | | | | | | | | |
| | AT1G03870 FLA9 (FLA9) | 1,097 | 0,997 | 1,133 | 0,684 | 1,610 | 0,048 | — | — | — | — | 0-1 | enr. | — | — | — | — |
| | AT4G12420 SKU5 (skewed 5); copper ion binding | 0,712 | 0,303 | 1,580 | 0,038 | 4,621 | 0,000 | 1,660 | 0,902 | 1,075 | 0,902 | 0/GPI | enr. | — | — | — | — |
| | AT1G05570 CALS1/GSL6 (CALLOSE SYNTHASE 1) | — | — | — | — | 1,498 | 0,047 | — | — | — | — | 16 | — | — | — | — | ✓ |
| Intracellular trafficking | | | | | | | | | | | | | | | | | |
| | AT3G09740 SYP71 (SYNTAXIN OF PLANTS 71) | 1,109 | 0,832 | 2,203 | 0,016 | 1,445 | 0,686 | 1,569 | 0,049 | — | — | 1 | ✓ | — | — | — | — |
| | AT1G32050 SCAMP4 (secretory carrier-associated membrane protein 4) | 0,982 | 0,947 | 1,821 | 0,000 | 1,213 | 0,477 | 1,327 | 0,225 | 1,000 | 0,540 | 4 | ✓ | — | — | — | — |
| Metabolism | | | | | | | | | | | | | | | | | |
| | AT4G03550 GSL05/PMR4 (GLUCAN SYNTHASE-LIKE 5) | 1,046 | 0,919 | 1,832 | 0,004 | 1,546 | 0,041 | 1,359 | 0,181 | — | — | 14 | ✓ | — | — | (✓) | ✓ |
| | AT3G16860 phytochelatin synthetase-related | 0,900 | 0,736 | 1,590 | 0,030 | 1,381 | 0,156 | — | — | — | — | 0/GPI | — | — | ✓ | — | — |
| | AT3G25290 auxin-responsive family protein | 1,179 | 0,573 | 1,919 | 0,007 | 1,111 | 0,741 | — | — | — | — | 5 | ✓ | — | — | — | — |
| | AT4G12980 auxin-responsive protein, putative | 0,967 | 0,780 | 1,726 | 0,014 | 1,467 | 0,585 | 1,195 | 0,456 | — | — | 5 | ✓ | — | — | — | — |
| | AT3G07570 membrane protein, putative | 1,209 | 0,481 | 1,642 | 0,016 | 1,486 | 0,001 | — | — | — | — | 5-6 | — | — | — | — | — |
| | AT1G73650 expressed protein | 1,387 | 0,707 | 2,441 | 0,107 | 1,311 | 0,463 | 1,604 | 0,026 | — | — | 4 | ✓ | — | — | — | — |
| Stress/Redox | | | | | | | | | | | | | | | | | |
| | AT5G06320 NHL3 (NDR1/HIN1-like 3) | 0,879 | 0,661 | 1,623 | 0,001 | 1,388 | 0,198 | 1,379 | 0,175 | 0,955 | 0,994 | 1 | ✓ | — | ✓ | — | ✓ |

Table 3 continued.

| FC | AGI code and annotation | flg22 vs flg22A2 | | | | | | flg22 vs untreated | | flg22A2 vs untreated | | TM | PM | ATTED | flg22 expr | P flg22 | RG |
|----|-------------------------------------------------------------|------------------|-------|--------------|--------------|--------------|--------------|--------------------|--------------|----------------------|-------|---------|------|-------|------------|---------|----|
| | | 0 minuten | | 5 minuten | | 15 minuten | | 5 minuten | | 5 minuten | | | | | | | |
| | | av fold | p | av fold | p | av fold | p | av fold | p | av fold | p | | | | | | |
| | AT1G30360 ERD4 (EARLY-RESPONSIVE TO DEHYDRATION 4) | 0,986 | 0,919 | 1,778 | 0,017 | 1,290 | 0,131 | 1,420 | 0,013 | 1,033 | 0,539 | 8-9 | enr. | — | — | — | — |
| | AT3G54200 expressed protein; similar to Harpin-induced 1 | 0,982 | 0,939 | 1,835 | 0,024 | 1,119 | 0,787 | — | — | — | — | 1 | ✓ | — | ✓ | — | — |
| | AT1G19110 inter-alpha-trypsin inhibitor heavy chain-related | 1,100 | 0,769 | 2,073 | 0,001 | 1,572 | 0,107 | 1,548 | 0,027 | 0,984 | 0,539 | 0-1 | — | — | — | — | — |
| | Protein modification | | | | | | | | | | | | | | | | |
| | AT3G05560 60S ribosomal protein L22-2 (RPL22B) | 1,120 | 0,766 | — | — | 0,604 | 0,000 | 4,550 | 0,817 | — | — | 0 | — | — | — | — | — |
| | Other | | | | | | | | | | | | | | | | |
| | AT2G45820 REM1.3 (REMORIN) | 1,209 | 0,519 | 1,660 | 0,017 | 1,738 | 0,012 | 1,623 | 0,048 | 0,981 | 0,710 | 0 | enr. | — | — | ✓ | — |
| | AT3G61260 REM1.2 (remorin family protein) | 0,834 | 0,325 | 1,683 | 0,012 | 1,190 | 0,541 | 1,427 | 0,162 | 1,087 | 0,817 | 0 | enr. | — | — | — | — |
| | AT1G11330 S-locus lectin protein kinase family protein | — | — | 2,131 | 0,030 | — | — | — | — | — | — | 1 | — | — | — | — | — |
| | AT1G72230 plastocyanin-like domain-containing protein | — | — | 1,384 | 0,303 | 1,267 | 0,093 | 1,105 | 0,721 | 1,128 | 0,568 | 0/GPI | — | — | — | — | — |
| | Unknown | | | | | | | | | | | | | | | | |
| | AT1G32190 expressed protein | 0,904 | 0,748 | 1,863 | 0,001 | 1,526 | 0,048 | 1,415 | 0,148 | 1,001 | 0,568 | 0-1/myr | — | — | — | — | — |
| | AT3G44150 expressed protein | — | — | 1,825 | 0,048 | 1,256 | 0,432 | 1,430 | 0,013 | — | — | 1 | — | — | — | — | — |
| | AT1G17620 expressed protein | 1,053 | 0,919 | 1,606 | 0,006 | 1,219 | 0,470 | 1,331 | 0,225 | 1,016 | 0,538 | 1 | ✓ | — | — | — | — |
| | AT3G01290 band 7 family protein | 1,042 | 0,919 | 1,659 | 0,014 | 1,342 | 0,198 | 1,264 | 0,293 | — | — | 0-1/myr | enr. | — | ✓ | — | — |
| | AT1G69840 band 7 family protein | 0,982 | 0,942 | 1,950 | 0,000 | 1,431 | 0,325 | 1,437 | 0,013 | 0,927 | 0,568 | 0 | ✓ | 154 | ✓ | — | — |
| | AT5G62740 band 7 family protein | 1,511 | 0,455 | 1,996 | 0,009 | 1,554 | 0,364 | 1,448 | 0,013 | — | — | 0 | ✓ | — | — | — | — |

3.2 Involvement of sterols and membrane rafts in the Arabidopsis-powdery mildew interaction

3.2.1 AtPEN1 associates with detergent-resistant membranes in a sterol-dependent manner

DRM extraction is a commonly applied method as a first approach to address the potential localization of a protein of interest to membrane rafts. The extraction is based on the hypothesis that membrane rafts are resistant to treatment with anionic, non-denaturing detergents due to the tight interactions between sterols, sphingolipids and proteins in the l_o -phase (Brown and Rose, 1992). To analyze the potential association of AtPEN1 with DRMs, microsomes were isolated from rosette leaves of GFP-AtPEN1 overexpressing Arabidopsis plants and DRMs extracted at a range of Triton-X 100-to-protein ratios. Subsequently, samples were fractionated by sucrose gradient centrifugation and analyzed by immunoblot analysis using a polyclonal antiserum directed against AtPEN1 (Figure 8A). At a Triton-X 100-to-protein ratio of 15, which represents stringent conditions for the isolation of DRMs from plant membranes (Mongrand et al., 2004; Borner et al., 2005), still a substantial amount of GFP-AtPEN1 was recovered in the low density DRM fractions (indicated by black bar). Similar results were obtained upon DRM extraction from Col-0 wild type plants and immunological detection of native AtPEN1 using the anti-AtPEN1 polyclonal antiserum (Figure 8B). Reggie-like proteins (RLPs) are presumptive homologues of flotillin-1, which commonly serves as a lipid raft marker protein in mammalian cells (Babuke and Tikkanen, 2007). When isolating DRMs from AtRLP1b-GFP overexpressing Arabidopsis plants we observed the association of AtRLP1b-GFP with DRMs (Figure 8B). Similarly, we found partitioning into DRMs for AtRLP1a-GFP and even more pronounced for AtRLP2 (data not shown). Based on a proteomic approach Borner and coworkers previously reported the enrichment of AtRLP1a in DRMs (Borner et al., 2005). Taken together, these findings suggest that AtRLPs associate with DRMs across kingdoms, indicative of a conserved function in membrane raft-related processes. Arabidopsis LIPOCALIN (AtLCN) is a cold-responsive PM protein (Kawamura and Uemura, 2003), which did not associate with DRMs under our conditions (Figure 8B). This indicates that it is surrounded by a different lipid environment in the membrane than AtPEN1 and AtRLPs, suggesting its localization solely in the l_d -phase, outside of

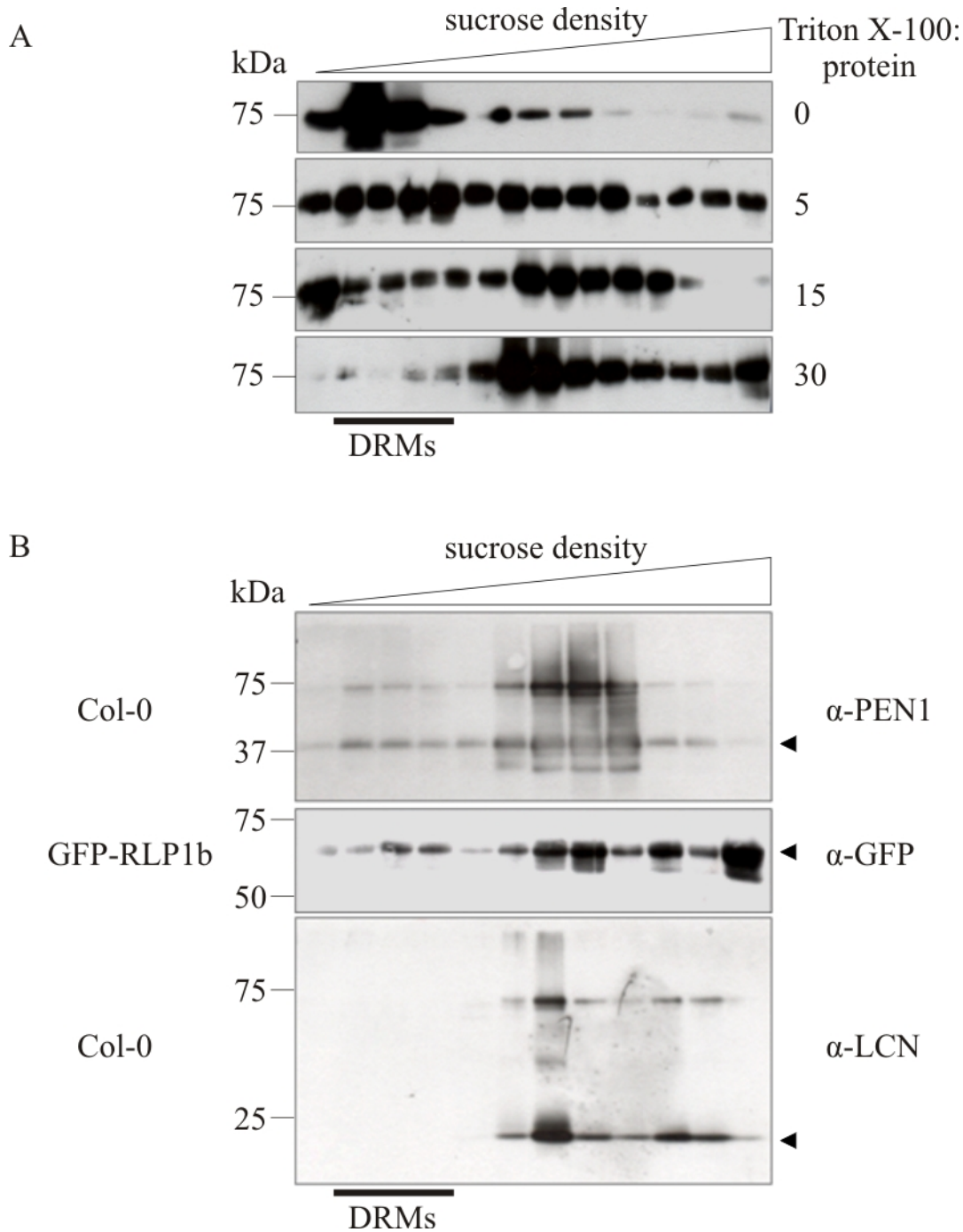


Figure 8. AtPEN1 partially associates with detergent-resistant membranes.

DRMs were isolated from rosette leaves of GFP-AtPEN1 overexpressing Arabidopsis plants (A) as well as Col-0 and RLP1b-GFP overexpressing plants (B) and subsequently fractionated by sucrose gradient centrifugation. Proteins of the recovered fractions were precipitated, separated by SDS-PAGE and transferred to nitrocellulose for immunoblot analysis. (A) DRMs were isolated using a range of Triton-X 100-to-protein ratios (as indicated) and immunoblot analysis was performed using an antiserum directed against GFP. (B) DRMs were extracted using a Triton-X 100-to-protein ratio of 15 and immunoblot analysis was performed using antisera against the respective protein or peptide-tag as indicated. Arrowheads indicate the expected molecular weight of the respective full-size proteins.

membrane rafts. To test whether the DRM association of AtPEN1 is dependent on sterols, microsomes were preincubated prior to detergent treatment and DRM isolation with 5 or 10 mM methyl- β -cyclodextrin (M β CD), a compound which selectively extracts sterols from membranes (Roche et al., 2008). We observed a clear and M β CD concentration-dependent reduction in AtPEN1 DRM association (Figure 9), suggesting that the residence of AtPEN1 in DRMs requires the presence of sterols.

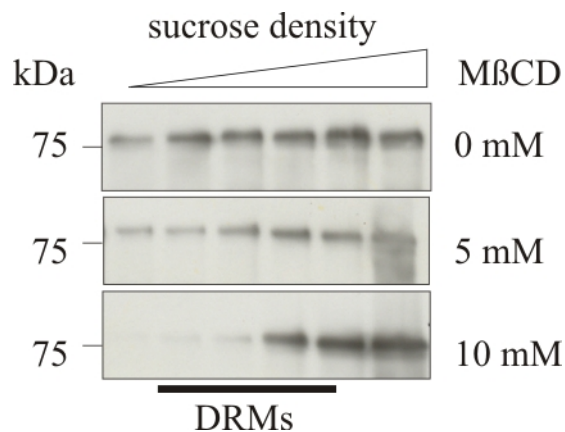


Figure 9. AtPEN1 association with detergent-resistant membranes is sterol-dependent.

DRMs were isolated from GFP-AtPEN1 overexpressing Arabidopsis rosette leaves at a Triton-X 100-to-protein ratio of 15. To analyze the sterol dependence of the GFP-AtPEN1 DRM association, microsomal fractions were preincubated with either 5 mM or 10 mM M β CD before Triton-X 100 treatment and subsequently fractionated by sucrose gradient centrifugation. Proteins of the recovered fractions were precipitated, separated by SDS-PAGE and transferred to nitrocellulose membrane for immunoblot analysis using an antiserum directed against AtPEN1. The upper (low density) half of each gradient was analyzed.

Heterooligomeric ternary SNARE complexes but not monomeric SNARE proteins are the functionally active protein complexes that ultimately drive vesicle fusion at target membranes (Lipka et al., 2007). These ternary SNARE complexes are SDS-resistant but heat sensitive (Hayashi et al., 1994; Kwon et al., 2008a) and thus can be visualized as high molecular weight complexes by SDS-PAGE and subsequent immunoblot analysis. To analyze the presence of AtPEN1-containing ternary SNARE complexes in DRMs, we isolated DRMs from Col-0 Arabidopsis rosette leaves and the fractions recovered after sucrose gradient centrifugation were either directly separated by SDS-PAGE (Figure 10, right panel) or boiled before loading on the gel (Figure 10, left panel). AtPEN1-containing ternary SNARE complexes were clearly detected in the low density fractions of the sucrose gradient but were absent or below the detection limit in the low buoyant density fractions (Figure 10, right panel). When DRMs were isolated from powdery mildew-challenged

plant material (non-adapted powdery mildew pathogen, *Blumeria graminis* forma specialis *hordei* (*Bgh*)) we did not observe any difference in DRM association of the monomeric AtPEN1 protein or the AtPEN1-containing ternary SNARE complexes (data not shown).

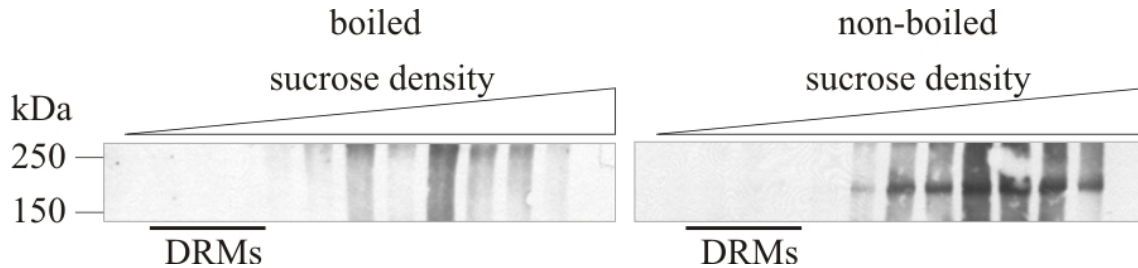


Figure 10. Detergent-resistant membranes are devoid of AtPEN1-containing ternary SNARE complexes.

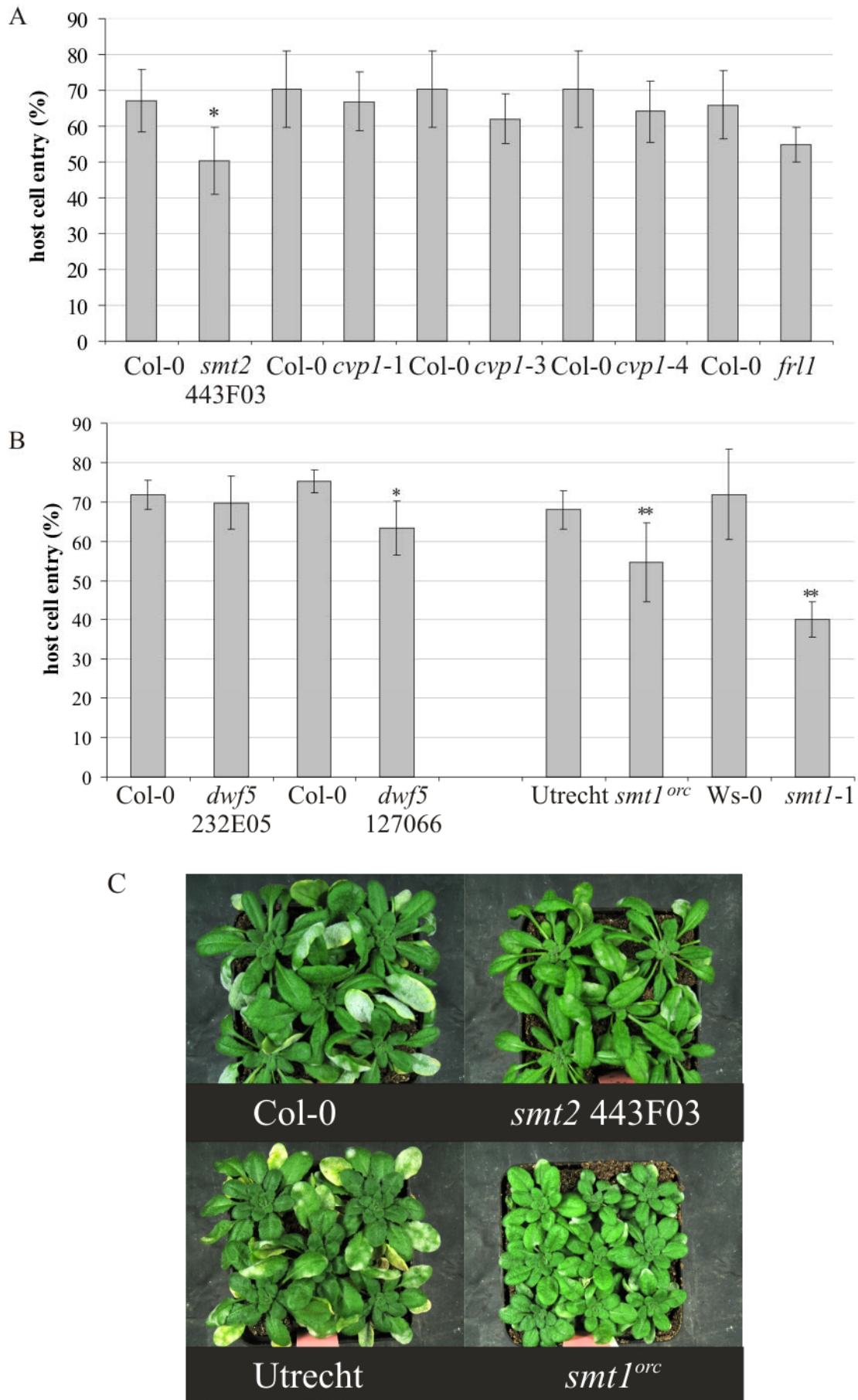
DRMs were isolated from Col-0 Arabidopsis rosette leaves applying a Triton-X 100-to-protein ratio of 15 and fractionation *via* sucrose gradient centrifugation. For the analysis of SDS-resistant AtPEN1-containing ternary SNARE complexes proteins of the recovered fractions were precipitated, directly separated by SDS-PAGE without boiling and transferred to nitrocellulose membrane (right panel). SDS resistant AtPEN1-containing ternary SNARE complexes dissociate after boiling (left panel). Immunoblot analysis was performed using an antiserum directed against AtPEN1.

3.2.2 Sterol biosynthesis mutants *smt1* and *smt2* display enhanced resistance towards the adapted powdery mildew pathogen, *Golovinomyces orontii*

With the aim to genetically interfere with membrane raft formation and/or function *in planta* we took advantage of the available mutants in genes encoding enzymes of the sterol biosynthesis pathway. In plants, mutants in genes encoding enzymes acting in most of the biosynthetic steps have been described (Clouse, 2002). Notably, some of the respective mutants are gametophytic or embryonic lethal, while others are viable, but often associated with developmental defects. All available mutant lines (Table 4, see also additional material for further mutant plants investigated) were assessed for their macroscopic and microscopic powdery mildew infection phenotype. For the latter, we challenged 4 week-old plants with the adapted powdery mildew pathogen, *G. oronti*, and performed quantitative analysis of host cell entry at 48 hpi (Figure 11A and B as well as Supplementary Figure 2). We identified mutants in two genes (*SMT1*, *SMT2*) that each showed an altered pathogen phenotype in multiple independent alleles. *SMT1* and *SMT2* both encode methyltransferases in the sterol biosynthetic pathway, mutants of which have perturbed sterol compositions (Carland et al., 2002; Willemsen et al., 2003; Hase et al., 2005), probably causing the described cell polarity defects (Fischer et al., 2004). In the

context of powdery mildew infection we observed enhanced disease resistance in both mutants (reduced host cell entry as compared to Col-0 wild type plants). This phenotype was found in two independent *smt1* alleles (Figure 11B) and a third allele showed that same tendency, while a fourth allele, which carries a T-DNA insertion in the 5'UTR, did not display compromised host cell entry (Supplementary Figure 2). The analysis of five independent *smt2* alleles revealed that four out of five mutants showed a moderately reduced fungal entry rate (Figure 11A). *smt2* 443F03 carries a T-DNA insertion, whereas *cotyledon vascular pattern (cvp)1-3* as well as *cvp1-4* harbor single nucleotide exchanges that probably all result in complete null alleles (Carland et al., 2002). Similarly, the single nucleotide deletion in *frill 1 (frl1)* results in aberrant translation and an early stop codon, suggesting that also this allele results in a complete null mutant (Hase et al., 2005), while *cvp1-1* has a single amino acid exchange that probably only causes a partial loss of function (Carland et al., 2002). This provides a plausible explanation for the absence of a pathogen phenotype in the *cvp1-1* mutant (Figure 11A). *DWARF (DWF)5* encodes a sterol reductase in the sterol biosynthesis pathway close to where it feeds into the brassinosteroid synthesis route (Choe et al., 2000). Accordingly, *dwf5* mutant plants display a typical brassinosteroid-deficient growth phenotype (Choe et al., 2000). The *dwf5* 127066 mutant showed a less pronounced but nevertheless statistically significant reduction of host cell penetration (Figure 11B). A second allele (*dwf5* 232E05) did not display this phenotype, which could be due to residual DWF5 enzymatic activity in this line in which the T-DNA insertion resides more downstream in the open reading frame. However, the *dwf5* 232E05 allele showed the described brassinosteroid-deficient growth phenotype to a similar degree as *dwf5* 127066, indicative of similarly disrupted DWF5 activity in both mutants (Choe et al., 2000). This suggests that the observed effect on pathogen entry in *dwf5* 127066 is not related to the *dwf5* mutation but possibly caused by a second T-DNA insertion/mutational event. Macroscopic infection phenotypes for all mutant lines were evaluated at 7-15 dpi and were indistinguishable from wild type plants for most sterol biosynthesis mutants

RESULTS



(data not shown), except for reduced sporulation on *smt1* and *smt2* mutant plants (Figure 11C).

To assess how strongly membrane composition is disturbed in the sterol biosynthesis mutants we examined if DRMs can still be extracted from their membranes and whether AtPEN1 yet associated with them. For all tested mutants (*smt1^{orc}*, *smt2* as well as *dwf5* 127066) neither a difference in DRM recovery nor in AtPEN1 association with DRMs was observed (data not shown). This indicates that, despite of perturbed sterol compositions, membrane rafts are largely intact in these mutant membranes. The findings do, however, not exclude an impairment of their functionality.

3.2.3 Sterol biosynthesis mutants *smt2* and *dwf5* display aberrant focal accumulation of GFP-AtPEN1 underneath fungal attack sites

To quantitatively analyze the FA of GFP-AtPEN1 underneath fungal attack sites, the Opera™, an automated confocal micro plate imaging reader, and the image analysis software Acapella™ were applied. This instrumentation allows the quantitative analysis of a large amount of parameters concerning the pathogen-triggered FA of GFP-AtPEN1, thereby revealing also subtle alterations that cannot be observed by eye (Meyer, 2008).

Two week-old wild type as well as *dwf5* 232E05 and *smt2* 443F03 mutant plants overexpressing GFP-AtPEN1 under the control of the 35S promoter in the *pen1-1* genetic background were inoculated with *Bgh* conidiospores and analyzed at 24 hpi. Quantitative image analysis concerning 19 parameters revealed a significant increase in the average intensity and average area of the GFP-AtPEN1 FA sites in the *smt2* 443F03 mutant background (Figure 12A and B). While the average area remained unaltered in the *dwf5* 232E05 mutant, the average area of the GFP-AtPEN1 FAs was significantly reduced (Figure 12C and D). For all other parameters *smt2* 443F03 and *dwf5* 232E05 mutants plants did not differ from wild type (data not shown). Taken together these data suggest that a proper membrane sterol composition is decisive for wild type-like accumulation of GFP-AtPEN1 at attempted fungal entry sites.

Figure 11. *Golovinomyces orontii* host cell entry and sporulation is compromised in sterol biosynthesis mutant plants.

(A) and (B) Quantitative analysis of host cell entry was performed at 48 hpi. Results represent mean \pm s.d. of three to seven independent experiments (for details see supplementary Figure 2). Asterisks indicate a significant difference from wild type accessions Col-0 or Ws-0 (** = $p < 0.01$; * = $p < 0.05$, Student's t-test). (C) Infection phenotypes of representative wild type (Col-0 and Utrecht) and *smt1^{orc}* and *smt2* 443F03 mutant plants at 10 dpi.

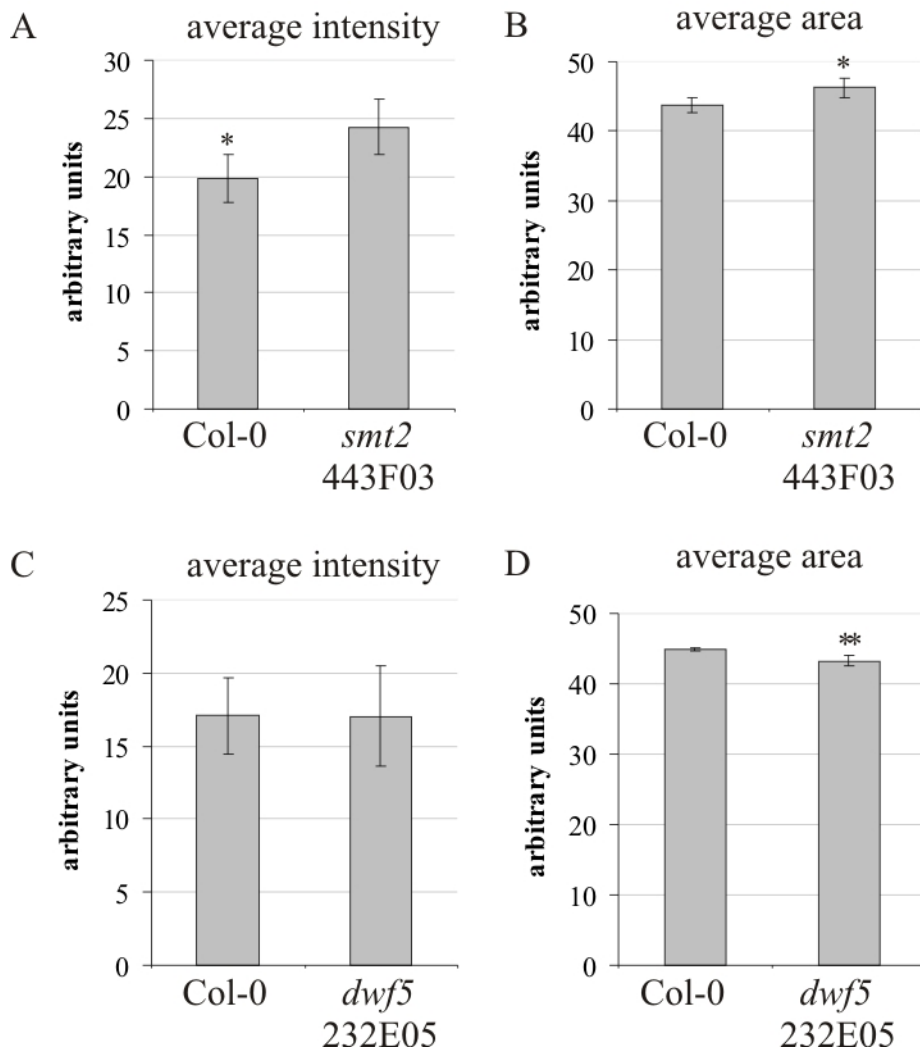


Figure 12. Sterol biosynthesis mutants display aberrant focal accumulation of GFP-AtPEN1 underneath fungal attack sites.

Two-week old wild type *Arabidopsis* plants (Col-0) as well as *smt2* 443F03 and *dwf5* 232E05 mutant plants expressing GFP-AtPEN1 under the control of the 35S promoter in *pen1-1* background were inoculated with *Bgh* and analyzed at 24 hpi. For data acquisition the Opera™ confocal microscope and for image analysis the Acapella™ software were used. (A) – (D) Quantitative analyses of the GFP-At PEN1 focal accumulation in *smt2* 443F03 (A and B) and *dwf5* 232E05 (C and D). Average intensity of spots (A and C) and average area of spots (B and D). Results represent mean \pm s.d. of four and five independent experiments for *dwf5* 232E05 and *smt2* 443F03, respectively. Asterisks indicate a significant difference from control plants (** = $p < 0.01$, * = $p < 0.05$, Student's t-test). The mutant plants did not differ from wild type for 17 other parameters analyzed with the Acapella™ image analysis software.

3.2.4 A role for digalactosyldiacylglycerol in the *Golovinomyces orontii*-host interaction

Glycoglycerolipids are the predominant lipids in plant chloroplasts, with monogalactosyldiacylglycerol (MGDG) and digalactosyldiacylglycerol (DGDG) being the most abundant molecules. It has previously been shown that galactolipid mutants display a reduced chlorophyll content and photosynthetic activity as well as an impairment of growth (Dörmann et al., 1999; Hölzl and Dörmann, 2007). Under phosphate-limiting conditions the accumulation of DGDG in extraplastidial membranes including the PM was observed (Hölzl and Dörmann, 2007). It is thought that DGDG might replace phospholipids under these conditions. Notably, DGDG also accumulates in the peribacteroid membrane of nitrogen-fixing nodules in soybean and *Lotus japonicus* (Gaude et al., 2004). The authors speculate that during nodulation the phosphate requirement is enhanced and that therefore DGDG, a non-phosphorus lipid, replaces phospholipids, making phosphate available for other essential cellular processes. In our study we observed strongly reduced host cell entry of *G. orontii* on *dgd1* mutant plants, which was reversed in a respective transgenic complementation line (Figure 13B). *dgd2* mutants were also significantly affected in two out of three analyzed alleles, however to a smaller degree (Figure 13B). While *dgd2-1* and *dgd2-3* both displayed reduced host cell entry, *dgd2-2* did not show this phenotype. This can probably be attributed to only partial loss of DGD2 function in this allele due to the position of the T-DNA insertion in the last exon. The less severe phenotype of *dgd2* mutant plants likely reflects the subordinate role of DGD2 in DGDG biosynthesis (Hölzl and Dörmann, 2007). Consistently, macroscopic evaluation of fungal sporulation revealed reduced conidiation of *G. orontii* on *dgd1-1*, but not on *dgd2-1* mutants (Figure 14). Quantitative analysis of the YFP-AtPEN1 FA underneath fungal attack sites in the *dgd2-1* background based on the Opera imaging system was indistinguishable from wild type YFP-AtPEN1 FA (data not shown). Interestingly, *mgd1* mutant plants did not show enhanced resistance towards *G. orontii* and conversely to DGDG, MGDG was also not found outside of plastidial membranes (Jouhet et al., 2004; Hölzl and Dörmann, 2007). It is tempting to speculate that DGDG might, in parallel to its accumulation in peribacteroid membranes, play a role in the establishment of the extrahaustorial membrane around fungal feeding structures. However, Fiehn and colleagues showed that the *dgd1-1* mutant displays a dramatically altered metabolite profile compared to wild type plants (Fiehn et al., 2000). 153 out of 326 quantified metabolites were significantly changed in the mutant, among them indole-3-acetonitrile

and other unidentified indole derivatives, indicating a possible hormonal defect and the potential constitutive accumulation of defence-related indolic compounds. These profound changes in the *dgd1-1* mutant could at least in part account for the observed increased resistance through (a) not yet determined secondary effect(s).

3.2.5 REGGIE-LIKE PROTEINs do not play a major role in the powdery mildew host cell entry

RLPs are presumptive homologues of mammalian flotilin-1, which commonly serves as a membrane raft marker protein in animal cells (Babuke and Tikkanen, 2007). Even though their precise biochemical activity is still unknown they have been proposed to function as scaffolding proteins for a subset of membrane rafts (Langhorst et al., 2007). Moreover, they have been implicated in raft-mediated endocytosis, phagocytosis as well as in the regulation of the cytoskeleton and neurite outgrowth (Babuke and Tikkanen, 2007). In plants the function of RLPs remains completely enigmatic; however, RLP1a was found to be enriched in DRMs, indicating the conserved association of RLPs with DRMs across kingdoms (Borner et al., 2005). In extension of these findings, we could also demonstrate the association of RLP1b and RLP2 with DRMs (Figure 8). In the context of RLPs acting as scaffolding proteins and therefore assuming a general function in membrane raft integrity, we assessed mutants in genes of RLPs and RLP overexpressing plants for their powdery mildew infection phenotype. *rlp1b* displayed a slight but significant reduction in host cell entry and a line overexpressing RLP1b-GFP showed increased susceptibility (Figure 13C). *rlp2* mutant plants and RLP1a-GFP overexpressing lines did not show an infection phenotype distinguishable from wild type (Figure 13D). Based on preliminary data, no clear trend could be observed upon challenge of *rlp1b*, *rlp2* and RLP1a and RLP1b-GFP overexpressing lines with the non-adapted powdery mildew pathogen, *Erysiphe pisi* (Figure 13D).

3.2.6 Degree of fatty acid desaturation does not affect *Golovinomyces orontii* host cell entry

According to the current model, the tight interaction of sphingolipids and sterols in membrane rafts is partly based on straight hydrocarbon chains due to their high saturation degree (Simons and Ikonen, 1997). Indeed, Laloi and colleagues showed that the amount of DRMs recovered from Arabidopsis cell lines *fatty acid desaturation (fad)2* and *Fad3+*, hyperaccumulating 18:1 and 18:3 fatty acids, respectively, was reduced to 20% of wild

type levels (Laloi et al., 2007). In the present study we tested a comprehensive set of *fad* mutants for their powdery mildew infection (*G. orontii*) phenotype and did not observe any significant difference to wild type plants with respect to fungal host cell entry (Figure 13A) and conidiation (data not shown). This finding suggests that membrane fluidity, which is altered in *fad2* and *Fad3*⁺ mutants (Vaultier et al., 2006), does not affect *G. orontii* pathogenesis.

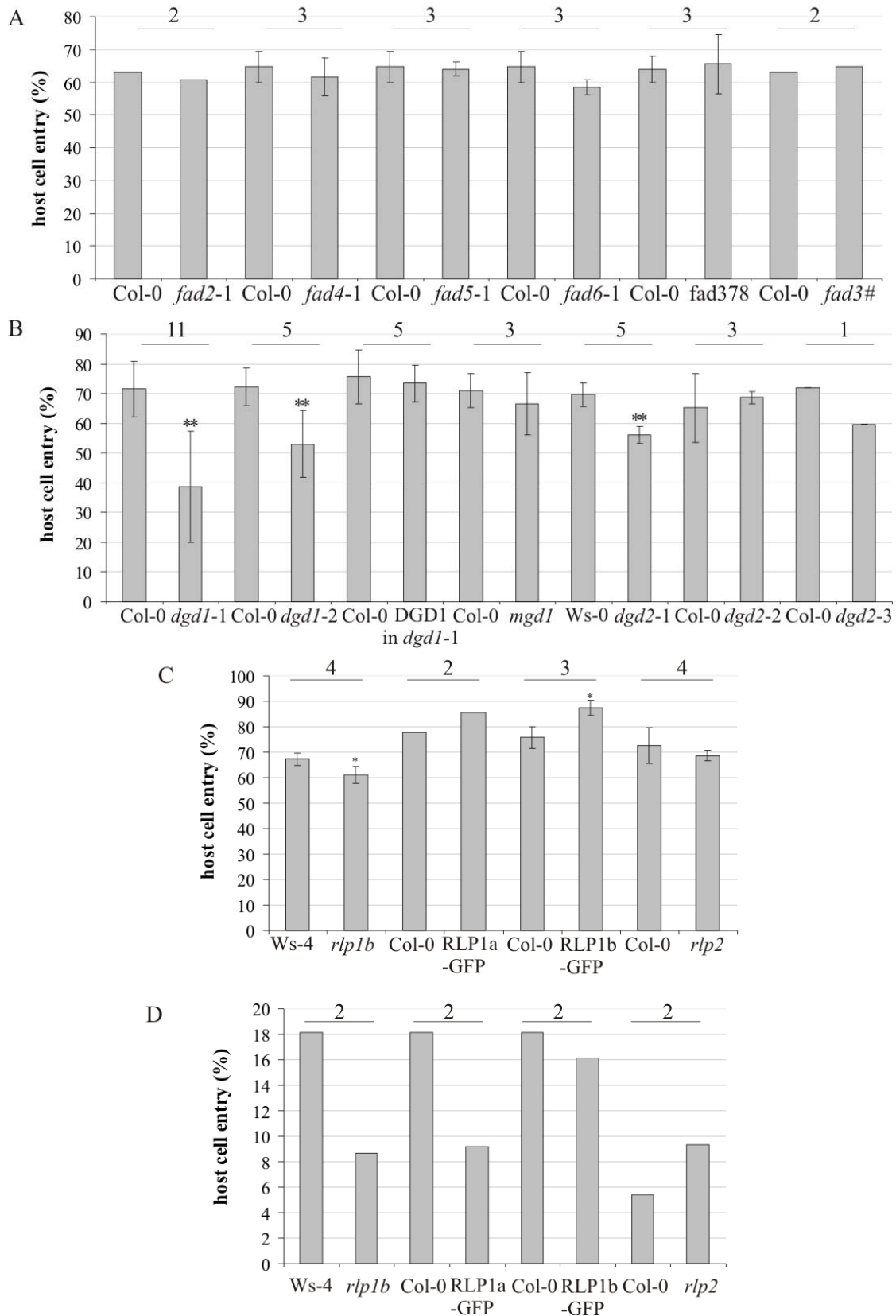


Figure 13. Host cell entry rates of additional mutants and transgenic lines used in this study. (A) to (C) Quantitative analysis of *G. orontii* host cell entry was performed at 48 hpi. (D) Quantitative analysis of *Erysiphe pisi* host cell entry was performed 7 dpi. Results represent mean \pm s.d. Number of biological replicates is indicated above the bars. Asterisks indicate a significant difference from wild-type accessions (** = $p < 0.01$; * = $p < 0.05$, Student's t-test).

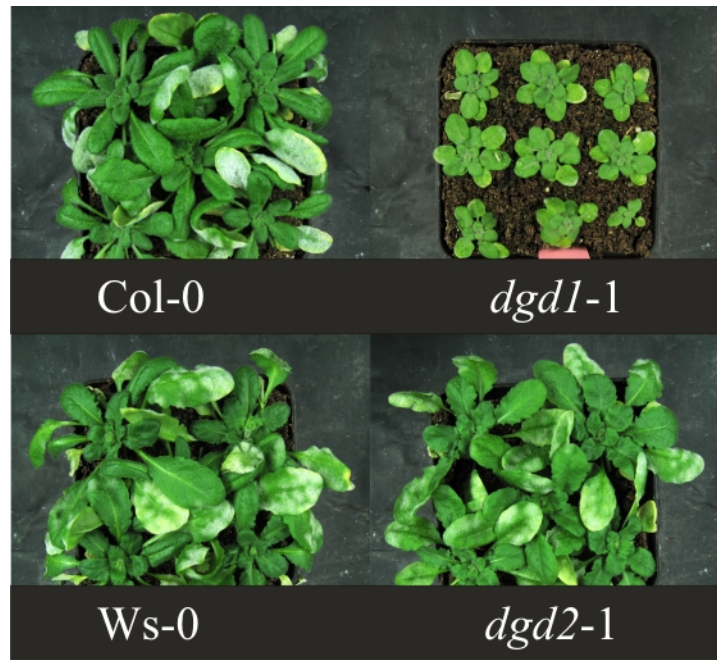


Figure 14. Sporulation of *Golovinomyces orontii* is reduced on *dgd1-1* mutant plants. Infection phenotypes of representative wild type (Col-0 and Ws-0) and *dgd1-1* and *dgd2-1* mutant plants at 10 dpi.

Table 4. Mutant alleles of sterol biosynthesis genes used in this study.

| Biological process | Gene | Mutant allele | Function | AGI code | Line designation | Status | Comment | Accession | Source | |
|---------------------|-----------------|---------------|-------------------------|-------------|------------------|-------------------|--------------------------|-----------|------------------------|----------------|
| Sterol biosynthesis | <i>DWF1/DIM</i> | | C-24 reductase | At3g19820 | SALK_006925 | no insert | | Col-0 | Salk Institute | |
| | | | | | SALK_006932 | homozygous | | Col-0 | Salk Institute | |
| | | | | | GABI_614D03 | waiting for seeds | | Col-0 | GABI-Kat | |
| | <i>DWF5</i> | | A7 sterol reductase | At1g50430 | SALK_127041 | no insert | | Col-0 | Salk Institute | |
| | | | | | SALK_127058 | no insert | | Col-0 | Salk Institute | |
| | | | | | SALK_127066 | homozygous | | Col-0 | Salk Institute | |
| | | | | | SALK_127074 | no insert | | Col-0 | Salk Institute | |
| | | | | | SAIL_232_E05 | homozygous | | Col-0 | NASC | |
| | | | | | SALK_002937 | no insert | | Col-0 | Salk Institute | |
| | | | | | <i>DWF7/STE1</i> | | A7 sterol C-5 desaturase | At3g02580 | SALK_136258 | no insert |
| | GABI_446H09 | homozygous | | Col-0 | | | | | GABI-Kat | |
| | SALK_136266 | no insert | | Col-0 | | | | | Salk Institute | |
| | <i>SMT2</i> | <i>smt2</i> | C-28 methyl transferase | At1g20330 | GABI_443F03 | homozygous | | Col-0 | GABI-Kat | |
| | | <i>frl1</i> | | | | homozygous | EMS mutant | Col-0 | (Hase et al., 2000) | |
| | | <i>cvp1-1</i> | | | | homozygous | EMS mutant | Col-0 | (Carland et al., 2002) | |
| | | <i>cvp1-3</i> | | | | homozygous | EMS mutant | Col-0 | (Carland et al., 2002) | |
| | | <i>cvp1-4</i> | | | | homozygous | EMS mutant | Col-0 | (Carland et al., 2002) | |
| | <i>HYDRA1</i> | | A8-A7 sterol isomerase | At1g20050 | GABI_366D06 | lethal | | Col-0 | GABI-Kat | |
| | <i>FAKCEL</i> | | C-14 sterolreductase | At3g52940 | | no line available | | | | |
| | <i>CYP51</i> | | C-14 demethylase | At1g11680 | SALK_067630 | lethal | | | Col-0 | Salk Institute |
| | | | | | SAIL_12_A11 | lethal | in 5'UTR ~280bp | Col-0 | NASC | |
| GABI_575H03 | | | | | homozygous | in 5'UTR ~350 bp | Col-0 | GABI-Kat | | |
| GABI_696D07 | | | | | homozygous | in 5'UTR ~350 bp | Col-0 | GABI-Kat | | |
| | | | | SAIL_12_F10 | lethal | in 5'UTR | Col-0 | NASC | | |

Table 4 continued.

| | | | | | | | |
|---------------------------|---------------------------------------|------------|---------------|--------------------------|--------------|-------|-----------------------|
| <i>CPII</i> | cycloeucaleenol cycloisomerase | At5g50375 | SALK_053963 | in progress | in 5'UTR | Col-0 | Salk Institute |
| | | | SALK_135330 | in progress | in 5'UTR | Col-0 | Salk Institute |
| <i>CASI</i> | cycloartenol synthase | At2g07050 | SALK_119879 | in progress | | Col-0 | Salk Institute |
| | | | SALK_056272 | waiting for seeds | | Col-0 | Salk Institute |
| | | | SALK_152551 | waiting for seeds | | Col-0 | Salk Institute |
| <i>SMT1 (CPH)</i> | C-24 methyl transferase | At5g13710 | GABI_059A04 | lethal | | Col-0 | GABI-Kat |
| | | | SALK_098551 | no insert | | Col-0 | Salk Institute |
| | | | SALK_098552 | no insert | | Col-0 | Salk Institute |
| | | | SAIL_772_B06 | homozygous | in 5'UTR | Col-0 | NASC |
| | | | GABI_214H04 | lethal | | Col-0 | GABI-Kat |
| | | | <i>smt1-1</i> | homozygous | EMS mutant | Ws-0 | (Diener et al., 2000) |
| | | | <i>smt1-3</i> | homozygous | EMS mutant | Ws-0 | (Diener et al., 2000) |
| <i>smt1^{orc}</i> | homozygous | EMS mutant | Utrecht | (Willemsen et al., 2003) | | | |
| <i>FPS1</i> | farnesyl diphosphate synthase | At5g47770 | SALK_122668 | homozygous | | Col-0 | Salk Institute |
| | | | SALK_004298 | lethal | | Col-0 | Salk Institute |
| | | | SALK_073576 | homozygous | | Col-0 | Salk Institute |
| <i>SQS1</i> | squalene synthase | At4g34640 | SAIL_1284_H07 | lethal | | Col-0 | NASC |
| | | | SALK_087515 | lethal | | Col-0 | Salk Institute |
| | | | SALK_077057 | homozygous | 180 bp 5'UTR | Col-0 | Salk Institute |
| <i>SQS2</i> | squalene synthase | At4g34650 | GABI_768A06 | homozygous | | Col-0 | GABI-Kat |
| | | | GABI_651C05 | homozygous | | Col-0 | GABI-Kat |
| <i>FPS2</i> | farnesyl diphosphate synthase | At4g17190 | SAIL_328_G06 | homozygous | | Col-0 | NASC |
| <i>HMG1</i> | 3-hydroxy-3-methylglutaryl coenzyme A | At1g76490 | SALK_061790 | homozygous | | Col-0 | Salk Institute |
| | | | SALK_125435 | homozygous | | Col-0 | Salk Institute |
| | | | GABI_338D08 | waiting for seeds | | Col-0 | GABI-Kat |
| <i>HMG2</i> | 3-hydroxy-3-methylglutaryl coenzyme A | At2g17370 | SALK_073557 | homozygous | | Col-0 | Salk Institute |
| | | | SALK_094623 | homozygous | | Col-0 | Salk Institute |
| | | | GABI_248D08 | in progress | | Col-0 | GABI-Kat |

4. Discussion

4.1 Quantitative proteomics of flagellin-induced plasma membrane compartmentalization

To reveal PAMP-induced protein dynamics at the PM of Arabidopsis cells we performed a quantitative proteomics approach, especially aiming at the elucidation of protein relocalization to DRMs after flg22 treatment. By ratiometric quantification we identified proteins that were significantly enriched in DRMs in response to flg22. By a subsequent reverse genetic approach to investigate an authentic role of these proteins in PAMP-induced defense responses we identified two novel components in this pathway (see also preliminary data for a third component in additional material).

In total we identified 316 proteins associated with DRMs. When we compared these to the inventory of DRM-associated plant proteins previously reported (Bhat and Panstruga, 2005; Morel et al., 2006) an extensive overlap was observed. This applied in particular to the categories of transporters, signaling, intracellular trafficking and cell-wall related proteins. 188 proteins were present in reciprocally labeled samples and thus quantification based on protein abundance ratios could be pursued for them. 34% of the quantified proteins were enriched significantly in at least one of the reciprocal sample sets. Importantly, only up to 2% of the proteins responded in a statistically significant manner in the control samples, which were either treated with the inactive peptide or untreated. We thus conclude that our workflow successfully identified proteins that specifically respond to flg22 treatment, unambiguously distinguishing between inherent biological and experimental variation and responses to the biological treatment (Kierszniowska et al., 2008).

The proteins for which quantification was pursued were classified into MapMan categories (Figure 4). While the class of transporters comprised 17% among the non-responding proteins, they accounted for 38% of the group of significantly responding proteins. This drastic difference supposedly highlights the importance of transport processes across the PM in response to PAMPs (Blumwald et al., 1998; Beffagna et al., 2005). The apparently large change in the category of protein synthesis reflects the successful exclusion of putative contaminants (proteins not associated with membranes) from the significantly responding proteins. The assumed contaminants were mainly ribosomal proteins and

therefore fell into the class of protein synthesis. Accordingly, for most of the proteins in this group neither PM localization nor a TM domain was predicted. One of the main characteristics attributed to membrane rafts is their enrichment in signaling components and their putative function as signaling platforms (Simons and Toomre, 2000). Accordingly, RLKs are also enriched in plant DRMs (e.g., Shahollari et al., 2004; Morel et al., 2006) and constitute the largest group of proteins identified in the present study.

4.1.1 PM H⁺-ATPases and ion transport in PAMP signaling

The rapid generation of ROS is a characteristic reaction of host cells in response to elicitor treatment and pathogen attack (Lamb and Dixon, 1997; Felix et al., 1999). ROS are implicated in the induction of the hypersensitive response, the regulation of defense gene induction as well as crosslinking of structural proteins and lignin polymers, thereby rendering the cell wall less digestible (Felix et al., 1999; Hüchelhoven and Kogel, 2003). Moreover ROS, such as ¹O₂, O₂⁻, H₂O₂ and •OH, have a direct cytotoxic capacity (Miller et al., 2008). The current model proposes that upon elicitor treatment H⁺-ATPase activity is downregulated through phosphorylation, inducing membrane depolarization and alkalinization of the extracellular medium (Schaller and Oecking, 1999; Nühse et al., 2007). Concomitantly, calcium influx is triggered, which in turn stimulates a calcium-dependent and PM-associated NADPH oxidase (AtRBOHD; (Ogasawara et al., 2008)). Most likely the same is true for a second NADPH oxidase (AtRBOHF) that also contributes to ROS production in response to pathogen attack (Torres et al., 2006). In parallel, the increased cytosolic pH leads to a higher production of NADPH, which is used as an electron source by NADPH oxidases (Beffagna et al., 2005). Since high calcium concentrations are cytotoxic, and also to reset the cellular machinery for the next encountered stimulus, cytoplasmic Ca²⁺ extrusion driven by Ca²⁺-ATPases is essential. Rapid elimination of elevated cytoplasmic Ca²⁺ levels thus supposedly conditions the transient nature of the ROS burst (Beffagna et al., 2005; Lecourieux et al., 2006). Both, H⁺-ATPases and Ca²⁺-ATPases have long been proposed to play an essential role in triggering and terminating the oxidative burst (Blumwald et al., 1998; Felix et al., 1999; Schaller and Oecking, 1999; Lecourieux et al., 2006). A large body of evidence, however mainly based on biochemical studies including pharmacological interference, indeed supports these hypotheses (Beffagna et al., 2005). In the present study we identified four PM H⁺-ATPases to be significantly enriched in DRMs upon flg22 elicitation (AHA1, AHA2, AHA3 and AHA4), including the two major H⁺-ATPases AHA1 and AHA2.

Furthermore, two Ca^{2+} -ATPases were found to be significantly enriched in DRMs after PAMP stimulus (ACA8 and ACA10). Interestingly, AHA1, AHA2 and ACA10 were also shown to be rapidly dephosphorylated and phosphorylated, respectively, in response to flg22 treatment (Benschop et al., 2007; Nühse et al., 2007). Additionally, *ACA10* transcript levels increase in response to flg22 treatment (Zipfel et al., 2004), further supporting its genuine involvement in elicitor-induced defense responses.

By taking a reverse genetic approach we demonstrated the contribution of the PM H^+ ATPase AHA1 in the production of ROS in response to flg22 (Figure 5A). Mutant plants expressing a constitutive active variant of AHA1 (Merlot et al., 2007) showed a significantly reduced oxidative burst compared to wild type seedlings. In these mutant plants a constant hyperpolarization of the PM leading to acidification of the extracellular medium (Merlot et al., 2007) seems to cause a reduced production of ROS, probably through a less efficient membrane depolarization and accordingly perturbed ion fluxes in response to elicitor treatment. Additionally, this mutant was described to have elevated levels of the stress signaling molecule SA and constitutive defense gene induction, leading to spontaneous cell death and leaf necrosis (Merlot et al., 2007). Consistently, we observed aberrant (spontaneous) callose deposition in *ost2-1D*, which could be a consequence of the elevated SA levels (Consonni et al., 2006). It is unlikely that the high SA levels have a direct effect on the flg22-induced oxidative burst, especially since an elevated defense status of these plants would rather suggest an elevated oxidative burst response.

For H^+ -ATPases it has already been proposed that the activity of these proton pumps is regulated at the posttranslational level, likely through events of phosphorylation and dephosphorylation (Gaxiola et al., 2007). Our data suggest that the regulation of H^+ -ATPases might also involve their recruitment to specialized membrane domains (membrane rafts). This is further corroborated by the fact that immunodetection studies consistently showed that PM H^+ -ATPases are present in patches at the PM (Gaxiola et al., 2007). Interestingly, Lefebvre and coworkers identified a DRM-associated PM redox system in *Medicago truncatula* root cells which could participate in the production or degradation of ROS *via* the regulation of the redox balance between the cytoplasm and apoplast (Lefebvre et al., 2007). Moreover, the tobacco NADPH oxidase NtRBOHD and its negative regulator, a small Rho GTPase (NtRac5), were shown to associate with DRMs after treatment with a fungal elicitor (Mongrand et al., 2004). Thus, it seems that not only H^+ -ATPases but also other players implicated in the oxidative burst in response to biotic stimuli might be associated with membrane rafts and may be regulated thereby.

4.1.2 flg22-induced redistribution of FLS2

Strikingly, the flg22 receptor FLS2 was consistently enriched in DRMs after flg22 induction in all sample sets, displaying an up to 3-fold enrichment. Benschop and coworkers did not observe any change in FLS2 protein abundance in total PMs at 10 minutes after addition of flg22 (Benschop et al., 2007). Therefore the significant enrichment of FLS2 in DRMs observed in this study reflects its PAMP-induced redistribution within the PM.

FLS2 represents the first documented example of ligand-induced receptor endocytosis in plants (Robatzek et al., 2006). BAK1, a coreceptor rapidly forming a complex with FLS2 after flg22 elicitation, is necessary for the internalization of FLS2 (Chinchilla et al., 2007; Heese et al., 2007). Consistent with an altered membrane environment, ligand-induced reduction in lateral mobility of FLS2 was reported (Ali et al., 2007). These observations are in accordance with the current model that receptor endocytosis is preceded by formation of oligomeric complexes and coalescence of membrane rafts at the receptor site (Geldner and Robatzek, 2008). Indeed, in mammals, the epidermal growth factor receptor is thought to localize to membrane rafts that also recruit the machinery for receptor endocytosis (Puri et al., 2005). The presence of TUBULIN ALPHA-4 CHAIN and SECRETORY CARRIER MEMBRANE PROTEIN (SCAMP) 4 in DRMs (both constitutively present in all samples in the present study) strengthens the notion that endocytosis might be initiated at membrane rafts also in plant cells. SCAMP4 is a presumptive homolog of rice SCAMP1, which was recently shown to localize to the PM and early endosomes (Lam et al., 2007). Further experimental support for a role of membrane rafts in endocytosis stems from Grebe and coworkers who showed by filipin labeling that sterols accumulate in ARA6 (early endosome Rab5 GTPase homolog)-GFP-positive endosomes (Grebe et al., 2003). Moreover, a sterol-deficient mutant (*cyclopropylsterol isomerase1*) was recently found to display aberrant localization of the otherwise strictly polarized auxin efflux carrier PIN-FORMED2, which most likely is a consequence of disturbed endocytosis (Men et al., 2008).

4.1.3 V-ATPases in PAMP signaling

Vacuolar H⁺-ATPases (V-ATPases) are multi-subunit enzymes comprised of the peripheral V1 complex (composed of eight subunits) and the membrane integral V0 subunit complex (comprised of five different subunits in Arabidopsis) (Gaxiola et al., 2007). In total we identified 14 of these subunits in our proteomic analysis of which 10 underwent

relocalization into DRMs after flg22 treatment. The most prominent role for V-ATPases is the acidification of endomembrane compartments, but they also act in secretory and endocytic trafficking (Dettmer et al., 2006; Marshansky and Futai, 2008). It is well accepted that V-ATPases are not only present in vacuolar membranes, but in all types of endomembranes (Schumacher, 2006) and PMs (Alexandersson et al., 2004; Marmagne et al., 2004; Borner et al., 2005; Jefferies et al., 2008). Dettmer and coworkers showed that VHA-A1 localizes to the trans-Golgi network, where endocytic and secretory vesicles are found, and that V-ATPases are important for their trafficking (Dettmer et al., 2006). Notably, *det3*, affected in *VHA-C*, which consequently affects all V-ATPases, exhibits a reduced sensitivity to brassinosteroids (Schumacher et al., 1999).

Here we showed that V-ATPases also play a role in PAMP-triggered defense responses. Both, *det3* mutants and ConcA-treated wild type seedlings displayed a reduced oxidative burst upon flg22 elicitation, while callose deposition was undistinguishable from wild type plants. This indicates that FLS2 trafficking may involve the trans-Golgi network-endocytic pathway, which might lead to disturbed downstream signaling responses in *det3* mutants and ConcA-treated plants. Preliminary data showing an unaltered FLS2-GFP signal at the PM of ConcA-treated plants (data not shown) likely rules out that reduced levels of FLS2 at the PM (e.g. due to improper secretion of newly synthesized receptor) caused the described oxidative burst phenotype. In contrast, BRASSINOSTEROID INSENSITIVE1 (BR11)-GFP was found to accumulate in intracellular compartments after ConcA treatment (Dettmer et al., 2006), reflecting its constant cycling between the PM and internal cell compartments. In mammals, V-ATPases have an established role in the acidification of early endosomes, as well as directly at the PM in the acidification of the extracellular space (Marshansky and Futai, 2008). Indeed the recurrent identification of V-ATPases in plant PM-derived DRMs might also indicate additional not yet identified functions.

It is interesting to note that in both mutants, *ost2-1D* and *det3*, only the production of ROS in response to flg22 treatment was affected, while callose deposition still occurred normally. This demonstrates that the oxidative burst, a marker for early defense responses, and callose deposition, occurring at later time points after flg22 challenge, can be genetically and pharmacologically uncoupled. The identification of *ost2-1D* and *det3* as new components in plant immunity also reflects the different subcellular localization of FLS2. As outlined above, AHA1 likely functions directly in the establishment of altered ion fluxes across the PM, which eventually leads to the activation of NADPH oxidases and the occurrence of an oxidative burst. In the case of V-ATPase we propose a function in the

flg22-induced membrane trafficking events, either directly related to FLS2 endocytosis or downstream of it.

4.1.4 Other components enriched in detergent-resistant membranes upon flg22 treatment with potential roles in pathogen defense

PGPs are members of the ATP-Binding Cassette protein superfamily. PGP1, PGP4 and PGP19 are the best-characterized proteins of this class and play a role in the maintenance of cellular auxin levels. While PGP1 and PGP19 export auxin from cells, PGP4 functions in auxin import (Blakeslee et al., 2007; Titapiwatanakun et al., 2008). In this study we observed an flg22-elicited increase of PGP1 and PGP4 in DRM fractions, indicative of a role for these auxin transporters in plant immune responses. A link between the repression of auxin signaling and basal defense signaling has already been described, suggesting that auxin promotes susceptibility to the bacterial speck disease (Navarro et al., 2006; Wang et al., 2007). At the posttranslational level PGP4 and PGP1 were shown to be phosphorylated in response to PAMP treatment (Benschop et al., 2007; Nühse et al., 2007).

The PMR4 callose synthase, which is required for wound and papillary callose formation (Jacobs et al., 2003; Nishimura et al., 2003), is significantly enriched in DRMs after flg22 elicitation. PMR4 is also phosphorylated upon flg22 treatment (just below the significance threshold, (Nühse et al., 2007)). We also identified another callose synthase, CALLOSE SYNTHASE1/GSL6, to be enriched in DRMs. Yet, neither GSL6 nor any other callose synthase seems to have a redundant function in flg22-induced callose deposition, since *pmr4-1* plants are completely devoid of callose deposition after elicitor treatment (Kim et al., 2005). We could further rule out a function of PMR4 in the flg22-induced production of ROS because *pmr4-1* mutant plants exhibited an unaltered ROS burst (data not shown). Since *pmr4-1* mutants display elevated SA levels (Nishimura et al., 2003), we also tested *pmr4-1 sid2-1* double mutants for altered ROS production and did not observe any differences as compared to wild type or the according single mutants (data not shown). This not only rules out a role for PMR4 in the PAMP-induced oxidative burst but also excludes a role for SA in the PAMP-triggered ROS production. This is especially interesting, in the light of the important role of SA in PAMP-triggered resistance to *Pseudomonas syringae* and the finding that *sid2-2* mutant plants are strongly affected in PAMP-triggered responses (as revealed by expression profiling; (Tsuda et al., 2008)).

NHL3 is a pathogen-responsive member of the *NDR1/HIN1*-like (*NON-RACE-SPECIFIC DISEASE RESISTANCE1/HAIRPIN-INDUCED-LIKE*) gene family. Accumulation of

NHL3 transcripts was observed during the interaction with avirulent *Pseudomonas syringae* strains, while no transcript accumulated during interactions with virulent strains (Varet et al., 2002). The function of *NHL3* in plant defense has further been supported by the finding that *NHL3*-overexpressing plants are more resistant to *Pseudomonas syringae* (Varet et al., 2003). We found that *NHL3* is also enriched in DRMs after *flg22* treatment. However, we did not observe clear differences between *nhl3* and wild type plants concerning PAMP-induced ROS production and callose deposition (data not shown), which could be due to redundancy in this large gene family. Interestingly, *NDR1*, one of the founders of the *NDR1/HIN1*-like gene family, was shown to interact with RPM1 INTERACTING PROTEIN4 (*RIN4*), a negative regulator of plant immunity (Kim et al., 2005). This interaction is required for the activation of resistance signaling and was proposed to control the amount of available free negative regulator in the plant cell (Day et al., 2006).

Next to *FLS2*, *REMORIN 1.3* is the protein most consistently shifted into DRMs after PAMP treatment (significant response in all three reciprocal data sets), and also *REMORIN1.2* was identified in *flg22*-responsive DRMs. They both belong to the 1b group of canonical plant remorins; however their biological roles still remain to be elucidated (Raffaele et al., 2007). Providing first leads towards their function, group 11b remorins have been observed to be differentially expressed during *Arabidopsis-Pseudomonas syringae* interactions (Raffaele et al., 2007). Interestingly, group 1b remorins seem to associate with the PM and moreover have been identified in DRMs before (Mongrand et al., 2004). In addition, a group 2 remorin from *Lotus japonicus* was shown to exhibit elevated transcript levels during the interaction with a mycorrhizal fungus (Raffaele et al., 2007), further supporting a role of remorins in plant-microbe interactions.

In this part of the study we aimed at the elucidation of immediate-early *flg22*-triggered responses at the PM. Therefore we performed a proteomics study revealing the quantitative changes in protein abundance in DRMs upon *flg22* treatment. We showed that elicitor treatment triggered profound changes in the protein composition of DRMs, including a significant enrichment of the *FLS2* receptor, other RLKs, H^+ -ATPases and V-ATPases. By a reverse genetic approach, we confirmed a role for *AHA1* and V-ATPases, two new components of PAMP signaling, in plant immunity. Taken together we demonstrated how the successful combination of a quantitative proteomics approach and subsequent functional analyses can lead to the identification of new players in a biological process.

4.2 Involvement of sterols and membrane rafts in the Arabidopsis-powdery mildew interaction

In this part of the study we investigated the possible involvement of membrane rafts in PM compartmentalization events in the context of Arabidopsis–powdery mildew interactions. By biochemical characterization we showed that the t-SNARE AtPEN1 partially associated with DRMs in a sterol-dependent manner, indicating its possible *in vivo* localization to membrane rafts. Moreover, we revealed increased resistance of a subset of sterol biosynthesis mutants towards the adapted powdery mildew pathogen, *G. orontii*. In case of the sterol biosynthesis mutant *smt2* we were able to correlate this partial reduction in host cell entry with aberrant FA of GFP-AtPEN1 underneath fungal attack sites. This indicates a possible contribution of sterols to the GFP-AtPEN1 FA and suggests an involvement of this process in determining the outcome of the powdery mildew–plant interaction.

Events at the plant PM, especially around the site of attempted fungal penetration, play a central role in the establishment of fungal infections. Together with the cell wall, the PM is amongst the first barriers fungi have to cope with to successfully invade a plant cell and colonize the host. In case of powdery mildews, the host PM is the intimate contact site of the emerging fungal feeding organ, the haustorium, and the plant cell (O'Connell and Panstruga, 2006). Accordingly, the entire plant cell rearranges upon powdery mildew attack, including the movement of cytoplasm and organelles towards the attempted penetration site and the local deposition of cell wall material (Underwood and Somerville, 2008). It is thought that this cell polarization is largely achieved through rearrangement of the cytoskeleton (Miklis et al., 2007). In previous studies it was shown that PM-resident plant proteins playing a crucial role in the interaction with powdery mildews (AtPEN1, AtPEN3, HvROR2, HvBAX Inhibitor-1 and HvMLO) focally accumulate at the site of attempted fungal penetration (Collins et al., 2003; Assaad et al., 2004; Bhat et al., 2005; Consonni et al., 2006; Eichmann et al., 2006; Stein et al., 2006). Furthermore, Kwon and coworkers observed focal vesicle trafficking (highlighted by the GFP-labeled v-SNARE VAMP722) towards the attack sites (Kwon et al., 2008a). In the same study, vesicle fusion, mediated by AtPEN1-containing ternary SNARE complexes, was shown to contribute to plant defense at the cell periphery. A recent study uncovered that the FA of plant proteins at powdery mildew attack sites possibly is the consequence of local exosomal protein delivery into the apoplastic space (Meyer et al., 2008). Consistent with this hypothesis, the delayed formation of papillae associated with defects in restriction of powdery mildew

entry observed in *pen1-1* was also found in VAMP721^{+/-} VAMP722^{-/-} mutant plants (Kwon et al., 2008a). This underlines the suggested importance of focal delivery of possibly toxic cargo and cell wall building blocks towards fungal attack sites and is reminiscent of the secretion of toxic compounds at contact sites (immunological synapses) between, for example, natural killer cells and their target cells in humans (Kwon et al., 2008b). Taken together these data suggest that the focal secretion at fungal attack sites might take place through membrane rafts (Kwon et al., 2008b). Notably, the first and most prominent example of large-scale phase separation in living cells has been described for the immunological synapse by employing Laurdan, a phase-sensitive membrane dye (Gaus et al., 2005). Reminiscent of plant SNAREs clustering at powdery mildew attack sites, also in T-cells exocytic SNAREs accumulate at the immunological synapse (Das et al., 2004).

4.2.1 Sterol-dependent AtPEN1 partitioning into detergent-resistant membranes

To biochemically address the potential association of AtPEN1 with membrane rafts we isolated DRMs from microsomes of Arabidopsis rosette leaves. DRMs from plant membranes are commonly extracted at Triton-X 100-to-protein ratios of 4/6:1 to 15:1 (Mongrand et al., 2004; Borner et al., 2005). For our study we chose highly stringent conditions to probe DRM association, extracting at a Triton-X 100-to-protein ratio of 15:1 (Figure 8). According to Mongrand and colleagues the maximal enrichment of sterols and sphingolipids in DRMs from tobacco PMs was found at this ratio (Mongrand et al., 2004). Notably, we recovered a substantial amount of AtPEN1 in DRM fractions under these conditions (Figure 8A and B).

MBCD has recently been shown to selectively extract sterols from plant membranes, leaving other lipids and the protein content unaltered (Roche et al., 2008). In this study it was reported that the specific extraction of sterols from tobacco PMs induced alterations in the lateral membrane organization. The authors observed a decrease in the liquid-phase heterogeneity that they attributed to the loss of l_o -domains after sterol extraction. Additionally, they showed that almost no DRM-associated proteins were extracted from MBCD-treated membranes, indicating the successful disruption of membrane rafts by MBCD-mediated sterol depletion (Roche et al., 2008). To test whether also the partitioning of AtPEN1 into DRM fractions was dependent on sterols, microsomes were preincubated with either 5 mM or 10 mM MBCD before Triton-X 100 application. We found that the association of AtPEN1 with DRMs was MBCD treatment-dependent (Figure 9). This suggests a sterol-dependence of DRM association, indicating the potential residence of

AtPEN1 in membrane rafts *in vivo*. Indeed, in animal cells microscopic studies revealed that SNAREs concentrate in submicron-sized (50-60 nm in diameter), cholesterol-dependent self-organizing clusters at which vesicles fuse (Lang, 2007; Sieber et al., 2007). Moreover, SNAREs are enriched in DRMs in animal cells (Chamberlain et al., 2001; Puri and Roche, 2006). To drive membrane fusion, SNAREs form heterooligomeric SNARE protein assemblies, so called ternary SNARE complexes (Hayashi et al., 1994). Puri and Roche addressed the question to what extent monomeric SNAREs and ternary SNARE complexes associate with DRMs during mast cell exocytosis (Puri and Roche, 2006). They found that especially syntaxin 4 in its monomeric form associated with DRMs only to a small degree, whereas syntaxin 4 engaged in ternary SNARE complexes completely partitioned into DRMs. This finding prompted us to investigate the association of AtPEN1-containing ternary SNARE complexes with DRMs. Notably, AtPEN1-containing ternary SNARE complexes were clearly present in solubilized membrane fractions but either absent or below the detection limit in DRM fractions (Figure 10). These findings rather argue for AtPEN1-mediated exocytosis taking place outside of membrane rafts.

In animal cells membrane partitioning of individual SNAREs seems highly specific (Lang 2007, Lang 2001), thereby providing a potential mechanism for their isoform-specific regulation. Especially when considering the membrane localization of SNAREs as a regulatory mechanism, it would be interesting to monitor the possible dynamic relocation of monomeric AtPEN1 and AtPEN1-containing ternary SNARE complexes after pathogen infection. Since, however, AtPEN1 is part of a cell-autonomous defense mechanism and moreover, even when densely inoculated with powdery mildew conidia, only few leaf cells are attacked by the fungus, it is unlikely to detect such changes by the present experimental setup. Indeed, no difference in AtPEN1 DRM association before and after powdery mildew challenge could be observed in whole leaf extracts (data not shown).

4.2.2 *Golovinomyces orontii* host cell entry is compromised in a subset of sterol biosynthesis mutants

To further support the biochemical analysis we aimed at genetic interference with membrane raft formation. Since the sterol biosynthesis pathway in Arabidopsis is particularly well characterized (Clouse, 2002) we isolated homozygous mutants of genes encoding enzymes in this pathway (Table 4). A high proportion of the homozygous mutants were lethal whereas others did not show obvious developmental phenotypes. This resembled the already described gametophytic and embryonic defects in certain sterol

biosynthesis mutants (Clouse, 2002). However, it also denotes the potential problem that homozygous mutant lines that can be isolated as viable plants are not affected strongly and thus might only display subtle to intermediate phenotypes.

A large number of sterol biosynthesis mutant lines were tested for their macroscopic and microscopic powdery mildew infection phenotype. While most investigated mutants did not show a significant difference from wild type plants (Supplementary Figure 2), mutants affected in either of the methyltransferases *SMT1* or *SMT2* consistently displayed reduced powdery mildew host cell penetration (Figure 11A and B). For mutants of either gene also reduced sporulation of *G. orontii* was observed macroscopically (Figure 11C).

SMT1 is a C-24 methyltransferase and responsible for the first dedicated catalytic step in sterol biosynthesis, the conversion of cycloartenol to 24-methylene-cycloartenol. The *smt1^{orc}* mutant is characterized by a mutation in a splice acceptor site resulting in truncated *SMT1* protein variants. Mutant plants have reduced sterol levels and display defects in cell polarity and auxin efflux (Willemsen et al., 2003). *smt1-1* carries an *AC* transposon insertion and 222 bp duplication in the second intron probably leading to complete absence of *SMT1* function (Diener et al., 2000). Both mutant lines showed a highly significant reduction in host cell penetration (Figure 11B). Correlating with the less severe cell polarity defects in *smt2* as compared to *smt1*, we also observed a less pronounced, however statistically significant and repeatable resistance to the adapted powdery mildew pathogen in *smt2* (Figure 11A). *SMT2* acts at a branching point in sterol biosynthesis, directing 24-methylenelophenol towards sitosterol and away from campesterol and downstream brassinosteroids. Unlike sterol biosynthesis mutants defective in enzymes that act upstream of *smt2* (including *smt1*), it does not display embryonic defects; however, unlike mutants defective in enzymes acting downstream of it, the *smt2* phenotype cannot be rescued by brassinosteroids (Clouse, 2002). For *smt1* and *smt2* perturbed alignment of cells into vascular cell files has been described, suggesting a similar defect in cell polarity for both mutants. This is probably attributed to their similarly reduced amount of the major plant sterol, sitosterol, while campesterol and cholesterol levels are elevated in these mutants (Fischer et al., 2004). Notably, mutants in the yeast homolog of *smt1* (*erg6*), which are devoid of ergosterol, the main yeast sterol, also have various cell polarity abnormalities, including the abolishment of membrane raft clustering at mating projection (Valdez-Taubas and Pelham, 2003; Proszynski et al., 2006). Moreover, a reverse genetic approach recently identified another Arabidopsis sterol biosynthesis mutant with aberrant cell polarity. The *cyclopropylsterol isomerase1-1* mutant displays mislocalization of an auxin

efflux carrier protein (PIN-FORMED2) that is polarly localized in wild type cells (Men et al., 2008). It is striking, that of the large number of sterol biosynthesis mutants investigated in this study only *smt1* and *smt2*, having similarly perturbed sterol profiles, showed a clear and reproducible pathogen phenotype. This suggests that sterol-dependent cell polarity might be crucial for this plant–microbe interaction.

Notably, for *smt1^{orc}* and *smt2* mutants we found a tendency towards elevated *PR-1* (*PATHOGENESIS RELATED-1*) transcript levels compared to wild type plants in unchallenged conditions (data not shown). This phenomenon was more pronounced in the *smt1^{orc}* mutant and indicates a lowered threshold for *PR-1* induction in these mutants. More importantly, elevated *PR-1* transcript levels could possibly account for the observed pathogen phenotypes. This is reminiscent of *cpr* (*constitutive expressor of PR genes*) mutants that have constitutively activated defense pathways, leading to constitutive systemic resistance (Clarke et al., 2000). The genetic dissection of the *cpr*-dependent defense mechanisms revealed that they are strongly dependent on the defence signaling molecule salicylic acid (SA) (Clarke et al., 2000). This stands in contrast to the early events in the powdery mildew–*Arabidopsis* interaction, where defenses at the cell periphery that limit host cell entry were shown to occur fully independently of SA biosynthesis/signaling (Zimmerli et al., 2004). Concerning *smt1* and *smt2* we therefore conclude that the moderately elevated *PR-1* transcript levels, most likely leading to SA accumulation and enhanced defense activation, did not affect fungal host cell entry. We rather propose that the disturbed sterol profiles are the cause for reduced host cell entry in both mutants. However, this is not necessarily true for the reduced fungal sporulation on *smt1^{orc}* and *smt2*, which can be partially due to elevated *PR-1* expression (Van Damme et al., 2005). To finally resolve the role of elevated *PR-1* transcript levels we crossed *smt1* and *smt2* mutants to a mutant deficient in SA biosynthesis (*sid2-1*). Resulting double mutants will be analyzed for their host cell entry rate and sporulation phenotype in the near future.

DWF7, DWF5 and DWF1 are located downstream of SMT2 in the sterol biosynthesis pathway. Mutants of the respective genes all have a dwarfed growth phenotype and, like brassinosteroid-deficient mutants, can be rescued by exogenous brassinolide treatment (Clouse, 2002). As indicated above, mutants in this part of the sterol biosynthesis pathway do not display embryonic defects. Only a single allele of the *dwf5* mutants among the four tested *dwf* mutants showed a slight but statistically significant reduction of powdery mildew host cell entry (Figure 11B and Supplementary Figure 2). Therefore, the observed

reduced host cell entry cannot be attributed to the developmental phenotypes of the plant, its brassinosteroid deficiency or the mutation in *DWF5*, but must be caused by another effect that is specific for the *dwf5* 127066 allele. A second T-DNA insertion at a distinct locus is the most likely explanation for these findings.

4.2.3 Sterol biosynthesis mutants display aberrant focal accumulation of GFP-AtPEN1 underneath fungal attack sites

The quantitative multiparametric analysis of GFP-AtPEN1 FAs at fungal attack sites based on the OPERA™ imaging system and Acapella™ image analysis software allows the identification of subtle changes that cannot be observed by eye (Meyer, 2008). This setting has been proven crucial to capture slight deviations from wild type FA sites in a forward genetic screen, since it turned out that mutants with strongly aberrant GFP-AtPEN1 FA mostly resulted in juvenile plant lethality (Meyer, 2008). This finding agrees with our assumption that only intermediate to weak sterol biosynthesis mutants can be isolated, since severe interference results in gametophytic or embryonic lethality. In combination with reverse genetics, the quantitative characterization of GFP-AtPEN1 FA provides thus the ideal means to assess possible defects in this process in an unbiased and highly sensitive manner.

To quantitatively analyze the GFP-AtPEN1 FA underneath fungal attack sites, *smt2* and *dwf5* 232E05 plants were crossed to GFP-AtPEN1 overexpressing Arabidopsis plants in the *pen1-1* genetic background (*smt1* mutant crosses are in progress). Two week-old seedlings were challenged with powdery mildew sporelings and analyzed at 24 hpi. The statistical analysis of all 19 parameters revealed a highly significant difference of GFP-AtPEN1 FA in the *smt2* background concerning the average FA intensity and average FA area (Figure 12A and B). In the *dwf5* 232E05 background a significant difference was only observed for the average FA area (Figure 12C and D). These findings indicate that a reduced host cell entry phenotype can be correlated to aberrant FA of GFP-AtPEN1 underneath fungal attack sites. While *smt2* showed a more pronounced pathogen phenotype, GFP-AtPEN1 FA is also affected in more parameters than *dwf5* 232E05 that did not exhibit a significantly altered host cell entry rate. Notably, the average area of the GFP-AtPEN1 FA was decreased in *smt2* while it was increased in *dwf5* 232E05. Thus, alterations in the FA of GFP-AtPEN1 in *dwf5* 232E05 were not correlated with a compromised fungal entry rate, indicating that rather a decrease in average area and intensity, as observed for *smt2*, impacted on the infection phenotype. Taken together the

data suggest a proper sterol composition may play a role in the FA of GFP-AtPEN1 at attempted fungal entry sites. They indicate that the FA might be important for successful establishment of compatibility. Future experiments aiming at the analysis of GFP-AtPEN1 FAs in *smt1^{orc}* mutant plants, which displayed a more drastic infection phenotype, promise further insight. However, it already now seems plausible that the targeted and spatially defined pathogen-triggered secretion of GFP-AtPEN1 and its ternary SNARE complex-forming partner AtSNAP33 into the paramural space (Meyer et al., 2008) might be regulated through selective membrane raft association. Indeed, in animal cell–parasite interactions membrane remodeling and accommodation of the parasite within the host cell involves the recruitment of membrane rafts to the interaction sites (Underwood and Somerville, 2008).

As an indirect parameter for membrane raft integrity in the sterol biosynthesis mutants we extracted DRMs from respective rosette leaves and assessed the association of AtPEN1 with low buoyant density fractions. AtPEN1 association with DRMs in *smt1^{orc}*, *smt2* as well as *dwf5* 127066 was indistinguishable from wild type extracts (data not shown). From these findings we can conclude on the one hand that DRMs can still be extracted from the mutant tissues and that on the other hand AtPEN1 association is not noticeably affected by a (moderately) altered sterol profile. It seems plausible that in spite of an altered sterol composition DRMs can form to the same degree as under wild type conditions, since the induction of phase separation has been described for various phytosterols, while no clear ranking could be established (Zappel and Panstruga, 2008). However, despite of the fact that DRMs can be extracted from the mutant tissues, the *in vivo* membrane raft function, which might be more sensitive to compositional changes, could be perturbed in the sterol biosynthesis mutants. At the same time we cannot exclude that DRMs are not linked to potential membrane rafts that might play a role in the plant–powdery mildew interaction and therefore do not provide an appropriate measure. We must also take into consideration that AtPEN1 might not be localized to membrane rafts *in vivo* and therefore the assessment of GFP-AtPEN1 FAs underneath fungal attack sites might not be a proper means to elucidate the potential aggregation of membrane rafts at the interactions sites. However, the role of sterols in the pathogen-induced and spatially-defined exocytosis can be addressed.

To further unravel the importance of sterols and/or sterol-dependent cell polarization the use of conditionally rescued sterol biosynthesis mutants that would otherwise not be viable and might therefore display stronger phenotypes promises great help (Babiychuk et al.,

DISCUSSION

2008). Combining the analyses of these mutants with new imaging approaches involving Laurdan, which has been successfully used to visualize phase separation in animal cells *in vivo* (Gaus et al., 2005), might provide additional new insights.

5. General conclusion and perspectives

The ongoing controversy about membrane rafts mainly stems from the fact that numerous studies in the animal field use DRM association as the only evidence to attribute membrane raft localization to the protein under investigation (Kenworthy, 2008). This practice resulted in long lists of proteins and processes that are supposedly linked to membrane rafts. Similarly, extensive proteomic studies in plant research have created a large inventory of DRM-associated proteins from various plant species (Bhat and Panstruga, 2005; Morel et al., 2006; Laloi et al., 2007; Lefebvre et al., 2007). Lingwood and Simons however underlined the strength of detergent insolubility when it is not used as a criterion *per se* but the differential DRM association of a protein upon physiologically relevant stimuli is used as an initial lead towards membrane raft involvement (Lingwood and Simons, 2007). In one study presented in this work (chapter 2), we provide to our knowledge the first example how also in plant research the differential DRM association of plasma membrane proteins can serve as a lead for the identification of new components of a biological process (here: flagellin-elicited defense responses). Future studies will aim at the elucidation of the molecular mechanisms underlying the function of these newly identified components. Thereby new insight into cell-autonomous plant innate immunity will be gained. Especially the investigation of the RLK FERONIA promises to broaden our knowledge about the involvement of an RLK with an apparently negative regulatory function in plant immunity.

To date several studies have demonstrated the importance of sterols in plant cell polarity. First, auxin efflux carriers were shown to mislocalize in sterol biosynthesis mutants (*smt1* and *cpil*), accompanied by a reduction in auxin transport and gravitropism defects (Willemsen et al., 2003; Fischer et al., 2004; Men et al., 2008). Second, these mutants display perturbed arrangement of vascular cell files (*smt1* and *smt2*) (Fischer et al., 2004). Men and colleagues revealed that the defective polarity acquisition in *cpil* probably originates from aberrant endocytosis in this mutant (Men et al., 2008). In the second study presented here (chapter 3) we found first evidence for the role of sterols in compatibility/resistance of Arabidopsis towards the powdery mildew pathogen and the FA of GFP-AtPEN1 underneath fungal attack sites. Furthermore, we showed that AtPEN1 associates with DRMs in a sterol-dependent manner. In analogy to the aberrant endocytosis

found in *cpi1* it will be interesting to also test the sterol biosynthesis mutants used in this study for this phenotype. These mutants could be of great value to investigate the so far scarcely appreciated role of endocytosis in plant-microbe interactions. To understand in more detail the contribution of sterols in the FA of GFP-AtPEN1 the use of mutants that display stronger defects, as for example *smt1* and *cpi1*, and conditionally rescued sterol biosynthesis mutants (Babiychuk et al., 2008) might yield more conclusive results. The analysis of (a) mutant(s) more strongly affected in GFP-AtPEN1 FA (Meyer, 2008) might finally allow determining the role of this process in the Arabidopsis-powdery mildew interaction.

6. References

- Abankwa D, Gorfe AA, Hancock JF** (2007) Ras nanoclusters: molecular structure and assembly. *Semin Cell Dev Biol* **18**: 599-607
- Alexandersson E, Saalbach G, Larsson C, Kjellbom P** (2004) Arabidopsis Plasma Membrane Proteomics Identifies Components of Transport, Signal Transduction and Membrane Trafficking. *Plant Cell Physiol* **45**: 1543-1556
- Ali GS, Prasad KV, Day I, Reddy AS** (2007) Ligand-Dependent Reduction in the Membrane Mobility of FLAGELLIN SENSITIVE2, an Arabidopsis Receptor-Like Kinase. *Plant Cell Physiol* **48**: 1601-1611
- Alonso J, Stepanova A, Leisse T, Kim C, Chen H, Shinn P, Stevenson D, Zimmerman J, Barajas P, Cheuk R, Gadrinab C, Heller C, Jeske A, Koesema E, Meyers C, Parker H, Prednis L, Ansari Y, Choy N, Deen H, Geralt M, Hazari N, Hom E, Karnes M, Mulholland C, Ndubaku R, Schmidt I, Guzman P, Aguilar-Henonin L, Schmid M, Weigel D, Carter D, Marchand T, Risseuw E, Brogden D, Zeko A, Crosby W, Berry C, Ecker J** (2003) Genome-wide insertional mutagenesis of *Arabidopsis thaliana*. *Science* **301**: 653-657
- Assaad FF, Qiu JL, Youngs H, Ehrhardt D, Zimmerli L, Kalde M, Wanner G, Peck SC, Edwards H, Ramonell K, Somerville CR, Thordal-Christensen H** (2004) The PEN1 syntaxin defines a novel cellular compartment upon fungal attack and is required for the timely assembly of papillae. *Mol Biol Cell* **15**: 5118-5129
- Babiychuk E, Bouvier-Nave P, Compagnon V, Suzuki M, Muranaka T, Van Montagu M, Kushnir S, Schaller H** (2008) Allelic mutant series reveal distinct functions for *Arabidopsis* cycloartenol synthase 1 in cell viability and plastid biogenesis. *PNAS* **105**: 3163-3168
- Babuke T, Tikkanen R** (2007) Dissecting the molecular function of reggie/flotillin proteins. *Eur J Cell Biol* **86**: 525-532
- Bagnat M, Simons K** (2002) Cell surface polarization during yeast mating. *Proc Natl Acad Sci U S A* **99**: 14183-14188
- Bauer Z, Gomez-Gomez L, Boller T, Felix G** (2001) Sensitivity of Different Ecotypes and Mutants of *Arabidopsis thaliana* toward the Bacterial Elicitor Flagellin Correlates with the Presence of Receptor-binding Sites. *J Biol Chem* **276**: 45669-45676
- Beck JG, Mathieu D, Loudet C, Buchoux S, Dufourc EJ** (2007) Plant sterols in "rafts": a better way to regulate membrane thermal shocks. *Faseb J* **21**: 1714-1723
- Beffagna N, Buffoli B, Busi C** (2005) Modulation of Reactive Oxygen Species Production During Osmotic Stress in *Arabidopsis thaliana* Cultured Cells: Involvement of the Plasma Membrane Ca²⁺-ATPase and H⁺-ATPase. *Plant Cell Physiol* **46**: 1326-1339
- Benjamini Y, Hochberg Y** (1995) Controlling the false discovery rate: a practical and powerful approach to multiple testing. *J R Stat Soc* **57**: 289-300
- Benschop JJ, Mohammed S, O'Flaherty M, Heck AJR, Slijper M, Menke FLH** (2007) Quantitative Phosphoproteomics of Early Elicitor Signaling in Arabidopsis. *Mol Cell Proteomics* **6**: 1198-1214
- Bhat RA, Miklis M, Schmelzer E, Schulze-Lefert P, Panstruga R** (2005) Recruitment and interaction dynamics of plant penetration resistance components in a plasma membrane microdomain. *PNAS* **102**: 3135-3140
- Bhat RA, Panstruga R** (2005) Lipid rafts in plants. *Planta* **223**: 5-19
- Blakeslee JJ, Bandyopadhyay A, Lee OR, Mravec J, Titapiwatanakun B, Sauer M, Makam SN, Cheng Y, Bouchard R, Adamec J, Geisler M, Nagashima A, Sakai**

- T, Martinoia E, Friml J, Peer WA, Murphy AS** (2007) Interactions among PIN-FORMED and P-glycoprotein auxin transporters in Arabidopsis. *Plant Cell* **19**: 131-147
- Bloch D, Lavy M, Efrat Y, Efroni I, Bracha-Drori K, Abu-Abied M, Sadot E, Yalovsky S** (2005) Ectopic expression of an activated RAC in Arabidopsis disrupts membrane cycling. *Mol Biol Cell* **16**: 1913-1927
- Blumwald E, Aharon GS, C-H. Lam B** (1998) Early signal transduction pathways in plant-pathogen interactions. *Trends in Plant Science* **3**: 342-346
- Borner GH, Sherrier DJ, Weimar T, Michaelson LV, Hawkins ND, Macaskill A, Napier JA, Beale MH, Lilley KS, Dupree P** (2005) Analysis of detergent-resistant membranes in Arabidopsis. Evidence for plasma membrane lipid rafts. *Plant Physiol* **137**: 104-116
- Boutte Y, Ikeda Y, Grebe M** (2007) Mechanisms of auxin-dependent cell and tissue polarity. *Curr Opin Plant Biol* **10**: 616-623
- Bradford MM** (1976) A rapid and sensitive method for the quantitation of microgram quantities of protein utilizing the principle of protein-dye binding. *Anal Biochem* **72**: 248-254
- Brown DA, Rose JK** (1992) Sorting of GPI-anchored proteins to glycolipid-enriched membrane subdomains during transport to the apical cell surface. *Cell* **68**: 533-544
- Büschges R, Hollricher K, Panstruga R, Simons G, Wolter M, Frijters A, van Daelen R, van der Lee T, Diergaarde P, Groenendijk J, Topsch S, Vos P, Salamini F, Schulze-Lefert P** (1997) The barley *Mlo* gene: a novel control element of plant pathogen resistance. *Cell* **88**: 695-705
- Carland FM, Fujioka S, Takatsuto S, Yoshida S, Nelson T** (2002) The Identification of *CVPI* Reveals a Role for Sterols in Vascular Patterning. *Plant Cell* **14**: 2045-2058
- Chamberlain LH, Burgoyne RD, Gould GW** (2001) SNARE proteins are highly enriched in lipid rafts in PC12 cells: implications for the spatial control of exocytosis. *PNAS* **98**: 5619-5624
- Chinchilla D, Bauer Z, Regenass M, Boller T, Felix G** (2006) The Arabidopsis receptor kinase FLS2 binds flg22 and determines the specificity of flagellin perception. *Plant Cell* **18**: 465-476
- Chinchilla D, Zipfel C, Robatzek S, Kemmerling B, Nurnberger T, Jones JD, Felix G, Boller T** (2007) A flagellin-induced complex of the receptor FLS2 and BAK1 initiates plant defence. *Nature* **448**: 497-500
- Choe S, Tanaka A, Noguchi T, Fujioka S, Takatsuto S, Ross AS, Tax FE, Yoshida S, Feldmann KA** (2000) Lesions in the sterol delta reductase gene of Arabidopsis cause dwarfism due to a block in brassinosteroid biosynthesis. *Plant J* **21**: 431-443
- Clarke JD, Volko SM, Ledford H, Ausubel FM, Dong X** (2000) Roles of salicylic acid, jasmonic acid, and ethylene in *cpr*-induced resistance in Arabidopsis. *Plant Cell* **12**: 2175-2190
- Clouse SD** (2002) Arabidopsis mutants reveal multiple roles for sterols in plant development. *Plant Cell* **14**: 1995-2000
- Cole RA, Fowler JE** (2006) Polarized growth: maintaining focus on the tip. *Curr Opin Plant Biol* **9**: 579-588
- Collins NC, Thordal-Christensen H, Lipka V, Bau S, Kombrink E, Qiu JL, Huckelhoven R, Stein M, Freialdenhoven A, Somerville SC, Schulze-Lefert P** (2003) SNARE-protein-mediated disease resistance at the plant cell wall. *Nature* **425**: 973-977
- Consonni C, Humphry ME, Hartmann HA, Livaja M, Durner J, Westphal L, Vogel J, Lipka V, Kemmerling B, Schulze-Lefert P, Somerville SC, Panstruga R**

- (2006) Conserved requirement for a plant host cell protein in powdery mildew pathogenesis. *Nat Genet* **38**: 716-720
- Cremona O, De Camilli P** (2001) Phosphoinositides in membrane traffic at the synapse. *J Cell Sci* **114**: 1041-1052
- Das V, Nal B, Dujancourt A, Thoulouze M-I, Galli T, Roux P, Dautry-Varsat A, Alcover A** (2004) Activation-induced polarized recycling targets T cell antigen receptors to the immunological synapse: Involvement of SNARE complexes. *Immunity* **20**: 577-588
- Day B, Dahlbeck D, Staskawicz BJ** (2006) NDR1 interaction with RIN4 mediates the differential activation of multiple disease resistance pathways in Arabidopsis. *Plant Cell* **18**: 2782-2791
- de Torres M, Mansfield JW, Grabov N, Brown IR, Ammoun H, Tsiamis G, Forsyth A, Robatzek S, Grant M, Boch J** (2006) *Pseudomonas syringae* effector AvrPtoB suppresses basal defence in Arabidopsis. *The Plant Journal* **47**: 368-382
- Dettmer J, Hong-Hermesdorf A, Stierhof YD, Schumacher K** (2006) Vacuolar H⁺-ATPase activity is required for endocytic and secretory trafficking in Arabidopsis. *Plant Cell* **18**: 715-730
- de Wet B, Harder T** (2008) Are rafts involved in T-cell receptor signalling? Introduction to the Talking Point on the involvement of lipid rafts in T-cell activation. *EMBO Rep* **9**: 523-524
- Diener AC, Li H, Zhou W-x, Whoriskey WJ, Nes WD, Fink GR** (2000) *STEROL METHYLTRANSFERASE 1* Controls the Level of Cholesterol in Plants. *Plant Cell* **12**: 853-870
- Dörmann P, Balbo I, Benning C** (1999) Arabidopsis Galactolipid Biosynthesis and Lipid Trafficking Mediated by DGD1. *Science* **284**: 2181-2184
- Eichmann R, Dechert C, Kogel K-H, Hüchelhoven R** (2006) Transient over-expression of barley BAX Inhibitor-1 weakens oxidative defence and MLA12-mediated resistance to *Blumeria graminis* f.sp. *hordei*. *Mol Plant Pathol* **7**: 543-552
- Engelsberger W, Erban A, Kopka J, Schulze W** (2006) Metabolic labeling of plant cell cultures with K¹⁵NO₃ as a tool for quantitative analysis of proteins and metabolites. *Plant Methods* **2**: 14
- Escobar-Restrepo JM, Huck N, Kessler S, Gagliardini V, Gheyselinck J, Yang WC, Grossniklaus U** (2007) The FERONIA receptor-like kinase mediates male-female interactions during pollen tube reception. *Science* **317**: 656-660
- Felix G, Boller T** (1995) Systemin induces rapid ion fluxes and ethylene biosynthesis in *Lycopersicon peruvianum* cells. *Plant J* **7**: 381-389
- Felix G, Duran JD, Volko S, Boller T** (1999) Plants have a sensitive perception system for the most conserved domain of bacterial flagellin. *Plant J* **18**: 265-276
- Fiehn O, Kopka J, Dormann P, Altmann T, Trethewey RN, Willmitzer L** (2000) Metabolite profiling for plant functional genomics. *Nature Biotechnology* **18**: 1157-1161
- Fischer U, Men S, Grebe M** (2004) Lipid function in plant cell polarity. *Curr Opin Plant Biol* **7**: 670-676
- Foreman J, Demidchik V, Bothwell JH, Mylona P, Miedema H, Torres MA, Linstead P, Costa S, Brownlee C, Jones JD, Davies JM, Dolan L** (2003) Reactive oxygen species produced by NADPH oxidase regulate plant cell growth. *Nature* **422**: 442-446
- Freialdenhoven A, Peterhansel C, Kurth J, Kreuzaler F, Schulze-Lefert P** (1996) Identification of genes required for the function of non-race-specific *mlo* resistance to powdery mildew in barley. *Plant Cell* **8**: 5-14

- Gaude N, Tippmann H, Fletmetakis E, Katinakis P, Udvardi M, Dormann P** (2004) The galactolipid digalactosyldiacylglycerol accumulates in the peribacteroid membrane of nitrogen-fixing nodules of Soybean and Lotus. *J Biol Chem* **279**: 34624-34630
- Gaus K, Le Lay S, Balasubramanian N, Schwartz MA** (2006) Integrin-mediated adhesion regulates membrane order. *J Cell Biol* **174**: 725-734
- Gaus K, Chklovskaja E, Fazekas de St Groth B, Jessup W, Harder T** (2005) Condensation of the plasma membrane at the site of T lymphocyte activation. *J Cell Biol* **171**: 121-131
- Gaxiola RA, Palmgren MG, Schumacher K** (2007) Plant proton pumps. *FEBS Lett* **581**: 2204-2214
- Geldner N, Robatzek S** (2008) Plant Receptors Go Endosomal: A Moving View on Signal Transduction. *Plant Physiol* **147**: 1565-1574
- Golub T, Caroni P** (2005) PI(4,5)P₂-dependent microdomain assemblies capture microtubules to promote and control leading edge motility. *J Cell Biol* **169**: 151-165
- Gómez-Gómez L, Boller T** (2000) FLS2: An LRR Receptor-like Kinase Involved in the Perception of the Bacterial Elicitor Flagellin in *Arabidopsis*. *Mol Cell* **5**: 1003-1011
- Gomez-Gomez L, Felix G, Boller T** (1999) A single locus determines sensitivity to bacterial flagellin in *Arabidopsis thaliana*. *Plant J* **18**: 277-284
- Grebe M, Xu J, Mobius W, Ueda T, Nakano A, Geuze HJ, Rook MB, Scheres B** (2003) Arabidopsis sterol endocytosis involves actin-mediated trafficking via ARA6-positive early endosomes. *Curr Biol* **13**: 1378-1387
- Grossmann G, Opekarova M, Novakova L, Stolz J, Tanner W** (2006) Lipid raft-based membrane compartmentation of a plant transport protein expressed in *Saccharomyces cerevisiae*. *Eukaryot Cell* **5**: 945-953
- Hac-Wydro K, Wydro P, Jagoda A, Kapusta J** (2007) The study on the interaction between phytosterols and phospholipids in model membranes. *Chem Phys Lipids* **150**: 22-34
- Halling KK, Slotte JP** (2004) Membrane properties of plant sterols in phospholipid bilayers as determined by differential scanning calorimetry, resonance energy transfer and detergent-induced solubilization. *Biochim Biophys Acta* **1664**: 161-171
- Hancock JF** (2006) Lipid rafts: contentious only from simplistic standpoints. *Nat Rev Mol Cell Biol* **7**: 456-462
- Härtel H, Dörmann P, Benning C** (2001) Galactolipids not associated with the photosynthetic apparatus in phosphate-deprived plants. *J Photochem Photobiol B* **61**: 46-51
- Hase Y, Fujioka S, Yoshida S, Sun G, Umeda M, Tanaka A** (2005) Ectopic endoreduplication caused by sterol alteration results in serrated petals in *Arabidopsis*. *J Exp Bot* **56**: 1263-1268
- Hase Y, Tanaka A, Baba T, Watanabe H** (2000) FRL1 is required for petal and sepal development in *Arabidopsis*. *Plant J* **24**: 21-32
- Hayashi T, McMahon H, Yamasaki S, Binz T, Hata Y, Südhof TC, Niemann H** (1994) Synaptic vesicle membrane fusion complex: action of clostridial neurotoxins on assembly. *EMBO J* **13**: 5051-5061
- He HT, Marguet D** (2008) T-cell antigen receptor triggering and lipid rafts: a matter of space and time scales - Talking Point on the involvement of lipid rafts in T-cell activation. *EMBO Rep* **9**: 525-530

- Heese A, Hann DR, Gimenez-Ibanez S, Jones AM, He K, Li J, Schroeder JI, Peck SC, Rathjen JP** (2007) The receptor-like kinase SERK3/BAK1 is a central regulator of innate immunity in plants. *PNAS* **104**: 12217-12222
- Hölzl G, Dörmann P** (2007) Structure and function of glycolycerolipids in plants and bacteria. *Prog Lipid Res* **46**: 225-243
- Homann U, Meckel T, Hewing J, Hutt MT, Hurst AC** (2007) Distinct fluorescent pattern of KAT1::GFP in the plasma membrane of *Vicia faba* guard cells. *Eur J Cell Biol* **86**: 489-500
- Hückelhoven R, Kogel K-H** (2003) Reactive oxygen intermediates in plant-microbe interactions: Who is who in powdery mildew resistance? *Planta* **216**: 891-902
- Ikonen E** (2008) Cellular cholesterol trafficking and compartmentalization. *Nat Rev Mol Cell Biol* **9**: 125-138
- Jacobs AK, Lipka V, Burton RA, Panstruga R, Strizhov N, Schulze-Lefert P, Fincher GB** (2003) An Arabidopsis callose synthase, GSL5, is required for wound and papillary callose formation. *Plant Cell* **15**: 2503-2513
- Jacobson K, Mouritsen OG, Anderson RG** (2007) Lipid rafts: at a crossroad between cell biology and physics. *Nat Cell Biol* **9**: 7-14
- Jarvis P, Dörmann P, Peto CA, Lutes J, Benning C, Chory J** (2000) Galactolipid deficiency and abnormal chloroplast development in the Arabidopsis MGD synthase 1 mutant. *PNAS* **97**: 8175-8179
- Jefferies KC, Cipriano DJ, Forgac M** (2008) Function, structure and regulation of the vacuolar H⁺-ATPases. *Arch Biochem Biophys* **476**: 33-42
- Jones JDG, Dangl JL** (2006) The plant immune system. *Nature* **444**: 323-329
- Jouhet J, Marechal E, Baldan B, Bligny R, Joyard J, Block MA** (2004) Phosphate deprivation induces transfer of DGDG galactolipid from chloroplast to mitochondria. *J Cell Biol* **167**: 863-874
- Kawamura Y, Uemura M** (2003) Mass spectrometric approach for identifying putative plasma membrane proteins of Arabidopsis leaves associated with cold acclimation. *Plant J* **36**: 141-154
- Kelly AA, Froehlich JE, Dörmann P** (2003) Disruption of the two *Digalactosyldiacylglycerol Synthase* genes *DGD1* and *DGD2* in Arabidopsis reveals the existence of an additional enzyme of galactolipid synthesis. *Plant Cell* **15**: 2694-2706
- Kenworthy AK** (2008) Have we become overly reliant on lipid rafts? Talking Point on the involvement of lipid rafts in T-cell activation. *EMBO Reports* **9**: 531-535
- Kenworthy AK, Nichols BJ, Remmert CL, Hendrix GM, Kumar M, Zimmerberg J, Lippincott-Schwartz J** (2004) Dynamics of putative raft-associated proteins at the cell surface. *J Cell Biol* **165**: 735-746
- Kierszniowska S, Walther D, Schulze WX** (2008) Ratio-dependent significance thresholds in reciprocal ¹⁵N-labeling experiments as a robust tool in detection of candidate proteins responding to biological treatment. *Proteomics*: in press
- Kim M, da Cunha L, McFall A, Belkadir Y, DebRoy S, Dangl J, Mackey D** (2005) Two *Pseudomonas syringae* type III effectors inhibit RIN4-regulated basal defense in Arabidopsis. *Cell* **121**: 749-759
- Kost B** (2008) Spatial control of Rho (Rac-Rop) signaling in tip-growing plant cells. *Trends in Cell Biology* **18**: 119-127
- Kwon C, Neu C, Pajonk S, Yun HS, Lipka U, Humphry M, Bau S, Straus M, Kwaaitaal M, Rampelt H, El Kasmi F, Jürgens G, Parker J, Panstruga R, Lipka V, Schulze-Lefert P** (2008a) Co-option of a default secretory pathway for plant immune responses. *Nature* **451**: 835-840

- Kwon C, Panstruga R, Schulze-Lefert P** (2008b) Les liaisons dangereuses: immunological synapse formation in animals and plants. *Trends Immunol* **29**: 159-166
- Laloi M, Perret AM, Chatre L, Melser S, Cantrel C, Vaultier MN, Zachowski A, Bathany K, Schmitter JM, Vallet M, Lessire R, Hartmann MA, Moreau P** (2007) Insights into the role of specific lipids in the formation and delivery of lipid microdomains to the plasma membrane of plant cells. *Plant Physiol* **143**: 461-472
- Lam SK, Siu CL, Hillmer S, Jang S, An G, Robinson DG, Jiang L** (2007) Rice SCAMP1 defines clathrin-coated, *trans*-Golgi-located tubular-vesicular structures as an early endosome in tobacco BY-2 cells. *Plant Cell* **19**: 296-319
- Lamb C, Dixon RA** (1997) The oxidative burst in plant disease resistance. *Annu Rev Plant Physiol Plant Mol Biol* **48**: 251-275
- Lang T** (2007) SNARE proteins and 'membrane rafts'. *J Physiol* **585**: 693-698
- Lang T, Bruns D, Wenzel D, Riedel D, Holroyd P, Thiele C, Jahn R** (2001) SNAREs are concentrated in cholesterol-dependent clusters that define docking and fusion sites for exocytosis. *EMBO J* **20**: 2202-2213
- Langhorst M, Solis G, Hannbeck S, Plattner H, Stuermer C** (2007) Linking membrane microdomains to the cytoskeleton: regulation of the lateral mobility of reggie-1/flotillin-2 by interaction with actin. *FEBS Letters* **581**: 4697-4703
- Lanquar V, Kuhn L, Lelièvre F, Khafif M, Espagne C, Bruley C, Barbier-Brygoo H, Garin J, Thomine S** (2007) ¹⁵N-metabolic labeling for comparative plasma membrane proteomics in Arabidopsis cells. *Proteomics* **7**: 750-754
- Lecourieux D, Ranjeva R, Pugin A** (2006) Calcium in plant defence-signalling pathways. *New Phytol* **171**: 249-269
- Lefebvre B, Furt F, Hartmann MA, Michaelson LV, Carde JP, Sargueil-Boiron F, Rossignol M, Napier JA, Cullimore J, Bessoule JJ, Mongrand S** (2007) Characterization of lipid rafts from *Medicago truncatula* root plasma membranes: a proteomic study reveals the presence of a raft-associated redox system. *Plant Physiol* **144**: 402-418
- Lenne PF, Wawrezynieck L, Conchonaud F, Wurtz O, Boned A, Guo XJ, Rigneault H, He HT, Marguet D** (2006) Dynamic molecular confinement in the plasma membrane by microdomains and the cytoskeleton meshwork. *EMBO J* **25**: 3245-3256
- Lichtenberg D, Goni FM, Heerklott H** (2005) Detergent-resistant membranes should not be identified with membrane rafts. *Trends Biochem Sci* **30**: 430-436
- Lingwood D, Simons K** (2007) Detergent resistance as a tool in membrane research. *Nat Protoc* **2**: 2159-2165
- Lipka V, Kwon C, Panstruga R** (2007) SNARE-Ware: The Role of SNARE-Domain Proteins in Plant Biology. *Annu Rev Cell Dev Biol* **23**: 147-174
- Marguet D, Lenne PF, Rigneault H, He HT** (2006) Dynamics in the plasma membrane: how to combine fluidity and order. *EMBO J* **25**: 3446-3457
- Marmagne A, Rouet M-A, Ferro M, Rolland N, Alcon C, Joyard J, Garin J, Barbier-Brygoo H, Ephritikhine G** (2004) Identification of new intrinsic proteins in Arabidopsis plasma membrane proteome. *Mol Cell Proteomics* **3**: 675-691
- Marshansky V, Futai M** (2008) The V-type H⁺-ATPase in vesicular trafficking: targeting, regulation and function. *Curr Opin Cell Biol* **20**: 415-426
- Martin SW, Konopka JB** (2004) Lipid raft polarization contributes to hyphal growth in *Candida albicans*. *Eukaryot Cell* **3**: 675-684
- Men S, Boutte Y, Ikeda Y, Li X, Palme K, Stierhof Y-D, Hartmann M-A, Moritz T, Grebe M** (2008) Sterol-dependent endocytosis mediates post-cytokinetic acquisition of PIN2 auxin efflux carrier polarity. *Nat Cell Biol* **10**: 237-244

- Merlot S, Leonhardt N, Fenzi F, Valon C, Costa M, Piette L, Vavasseur A, Genty B, Boivin K, Muller A, Giraudat J, Leung J** (2007) Constitutive activation of a plasma membrane H⁺-ATPase prevents abscisic acid-mediated stomatal closure. *EMBO J* **26**: 3216-3226
- Miller G, Shulaev V, Mittler R** (2008) Reactive oxygen signaling and abiotic stress. *Physiol Plant* **133**: 481-489
- Meyer D** (2008) Molecular characterization of pathogen-triggered cell polarity. Dissertation **Universität zu Köln**
- Meyer D, Pajonk S, Micali C, O'Connell R, Schulze-Lefert P** (2008) Extracellular transport and integration of plant secretory proteins into pathogen-induced cell wall compartments. *Plant J*: doi: 10.1111/j.1365-1313X.2008.03743.x
- Miklis M, Consonni C, Bhat RA, Lipka V, Schulze-Lefert P, Panstruga R** (2007) Barley MLO modulates actin-dependent and actin-independent antifungal defense pathways at the cell periphery. *Plant Physiol* **144**: 1132-1143
- Mongrand S, Morel J, Laroche J, Claverol S, Carde JP, Hartmann MA, Bonneu M, Simon-Plas F, Lessire R, Bessoule JJ** (2004) Lipid rafts in higher plant cells: purification and characterization of Triton X-100-insoluble microdomains from tobacco plasma membrane. *J Biol Chem* **279**: 36277-36286
- Morel J, Claverol S, Mongrand S, Furt F, Fromentin J, Bessoule JJ, Blein JP, Simon-Plas F** (2006) Proteomics of plant detergent-resistant membranes. *Mol Cell Proteomics* **5**: 1396-1411
- Munro S** (2003) Lipid rafts: elusive or illusive? *Cell* **115**: 377-388
- Navarro L, Dunoyer P, Jay F, Arnold B, Dharmasiri N, Estelle M, Voinnet O, Jones JD** (2006) A plant miRNA contributes to antibacterial resistance by repressing auxin signaling. *Science* **312**: 436-439
- Navarro L, Zipfel C, Rowland O, Keller I, Robatzek S, Boller T, Jones JDG** (2004) The transcriptional innate immune response to flg22. Interplay and overlap with Avr gene-dependent defense responses and bacterial pathogenesis. *Plant Physiol* **135**: 1113-1128
- Nelson CJ, Hegeman AD, Harms AC, Sussman MR** (2006) A quantitative analysis of *Arabidopsis* plasma membrane using trypsin-catalyzed ¹⁸O labeling. *Mol Cell Proteomics* **5**: 1382-1395
- Ninnemann O, Jauniaux JC, Frommer WB** (1994) Identification of a high affinity NH₄⁺ transporter from plants. *EMBO J* **13**: 3464-3471
- Nishimura MT, Stein M, Hou B-H, Vogel JP, Edwards H, Somerville SC** (2003) Loss of a callose synthase results in salicylic acid-dependent disease resistance. *Science* **301**: 969-972
- Nühse TS, Bottrill AR, Jones AME, Peck SC** (2007) Quantitative phosphoproteomic analysis of plasma membrane proteins reveals regulatory mechanisms of plant innate immune responses. *Plant J* **51**: 931-940
- Obayashi T, Kinoshita K, Nakai K, Shibaoka M, Hayashi S, Saeki M, Shibata D, Saito K, Ohta H** (2007) ATTED-II: a database of co-expressed genes and *cis* elements for identifying co-regulated gene groups in *Arabidopsis*. *Nucl Acids Res* **35**: 863-869
- O'Connell RJ, Panstruga R** (2006) Tête à tête inside a plant cell: establishing compatibility between plants and biotrophic fungi and oomycetes. *New Phytol* **171**: 699-718
- Ogasawara Y, Kaya H, Hiraoka G, Yumoto F, Kimura S, Kadota Y, Hishinuma H, Senzaki E, Yamagoe S, Nagata K, Nara M, Suzuki K, Tanokura M, Kuchitsu K** (2008) Synergistic activation of the *Arabidopsis* NADPH oxidase AtrbohD by Ca²⁺ and phosphorylation. *J Biol Chem* **283**: 8885-8892

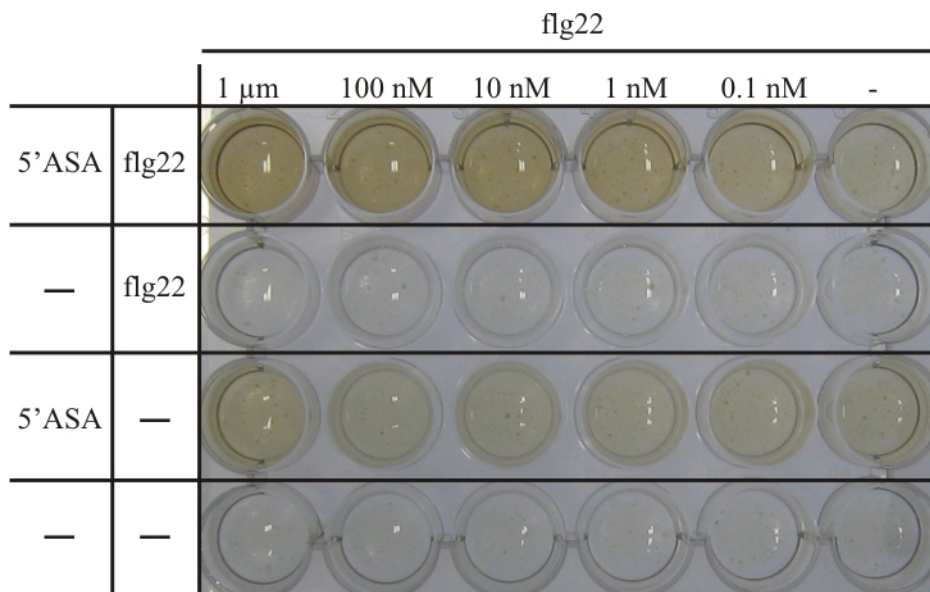
- Opalski KS, Schultheiss H, Kogel KH, Huckelhoven R** (2005) The receptor-like MLO protein and the RAC/ROP family G-protein RACB modulate actin reorganization in barley attacked by the biotrophic powdery mildew fungus *Blumeria graminis* f.sp. *hordei*. *Plant J* **41**: 291-303
- Pike LJ** (2006) Rafts defined: a report on the Keystone Symposium on Lipid Rafts and Cell Function. *J Lipid Res* **47**: 1597-1598
- Proszynski TJ, Klemm R, Bagnat M, Gaus K, Simons K** (2006) Plasma membrane polarization during mating in yeast cells. *J Cell Biol* **173**: 861-866
- Puri C, Tosoni D, Comai R, Rabellino A, Segat D, Caneva F, Luzzi P, Di Fiore PP, Tacchetti C** (2005) Relationships between EGFR signaling-competent and endocytosis-competent membrane microdomains. *Mol Biol Cell* **16**: 2704-2718
- Puri N, Roche PA** (2006) Ternary SNARE complexes are enriched in lipid rafts during mast cell exocytosis. *Traffic* **7**: 1482-1494
- Raffaele S, Mongrand S, Gamas P, Niebel A, Ott T** (2007) Genome-wide annotation of remorins, a plant-specific protein family: evolutionary and functional perspectives. *Plant Physiol* **145**: 593-600
- Rappsilber J, Ishihama Y, Mann M** (2003) Stop and go extraction tips for matrix-assisted laser desorption/ionization, nanoelectrospray, and LC/MS sample pretreatment in proteomics. *Anal Chem* **75**: 663-670
- Robatzek S, Chinchilla D, Boller T** (2006) Ligand-induced endocytosis of the pattern recognition receptor FLS2 in Arabidopsis. *Genes Dev* **20**: 537-542
- Roche Y, Gerbeau-Pissot P, Buhot B, Thomas D, Bonneau L, Gresti J, Mongrand S, Perrier-Cornet J-M, Simon-Plas F** (2008) Depletion of phytosterols from the plant plasma membrane provides evidence for disruption of lipid rafts. *FASEB J* **22**: 3980-3991
- Rosso MG, Li Y, Strizhov N, Reiss B, Dekker K, Weisshaar B** (2003) An *Arabidopsis thaliana* T-DNA mutagenized population (GABI-Kat) for flanking sequence tag-based reverse genetics. *Plant Mol Biol* **53**: 247-259
- Schaller A, Oecking C** (1999) Modulation of plasma membrane H⁺-ATPase activity differentially activates wound and pathogen defense responses in tomato plants. *Plant Cell* **11**: 263-272
- Schultheiss H, Preuss J, Pircher T, Eichmann R, Huckelhoven R** (2008) Barley RIC171 interacts with RACB in planta and supports entry of the powdery mildew fungus. *Cell Microbiol*
- Schumacher K** (2006) Endomembrane proton pumps: connecting membrane and vesicle transport. *Curr Opin Plant Biol* **9**: 595-600
- Schumacher K, Vafeados D, McCarthy M, Sze H, Wilkins T, Chory J** (1999) The *Arabidopsis det3* mutant reveals a central role for the vacuolar H⁺-ATPase in plant growth and development. *Genes Dev* **13**: 3259-3270
- Schwacke R, Schneider A, van der Graaff E, Fischer K, Catoni E, Desimone M, Frommer WB, Flugge U-I, Kunze R** (2003) ARAMEMNON, a novel database for Arabidopsis integral membrane proteins. *Plant Physiol* **131**: 16-26
- Schwessinger B, Zipfel C** (2008) News from the frontline: recent insights into PAMP-triggered immunity in plants. *Curr Opin Plant Biol* **11**: 389-395
- Seminario MC, Bunnell SC** (2008) Signal initiation in T-cell receptor microclusters. *Immunol Rev* **221**: 90-106
- Sessions A, Burke E, Presting G, Aux G, McElver J, Patton D, Dietrich B, Ho P, Bacwaden J, Ko C, Clarke JD, Cotton D, Bullis D, Snell J, Miguel T, Hutchison D, Kimmerly B, Mitzel T, Katagiri F, Glazebrook J, Law M, Goff SA** (2002) A High-Throughput Arabidopsis Reverse Genetics System. *Plant Cell* **14**: 2985-2994

- Shahollari B, Vadassery J, Varma A, Oelmüller R** (2007) A leucine-rich repeat protein is required for growth promotion and enhanced seed production mediated by the endophytic fungus *Piriformospora indica* in *Arabidopsis thaliana*. *Plant J* **50**: 1-13
- Shahollari B, Peskan-Berghöfer T, Oelmüller R** (2004) Receptor kinases with leucine-rich repeats are enriched in Triton X-100 insoluble plasma membrane microdomains from plants. *Physiol Plantarum* **122**: 397-403
- Sieber JJ, Willig KI, Kutzner C, Gerding-Reimers C, Harke B, Donnert G, Rammner B, Eggeling C, Hell SW, Grubmüller H, Lang T** (2007) Anatomy and dynamics of a supramolecular membrane protein cluster. *Science* **317**: 1072-1076
- Simons K, Toomre D** (2000) Lipid rafts and signal transduction. *Nat Rev Mol Cell Biol* **1**: 31-39
- Simons K, Ikonen E** (1997) Functional rafts in cell membranes. *Nature* **387**: 569-572
- Singer SJ, Nicolson GL** (1972) The fluid mosaic model of the structure of cell membranes. *Science* **175**: 720-731
- Sorek N, Poraty L, Sternberg H, Bar E, Lewinsohn E, Yalovsky S** (2007) Activation status-coupled transient S acylation determines membrane partitioning of a plant Rho-related GTPase. *Mol Cell Biol* **27**: 2144-2154
- Stein M, Dittgen J, Sanchez-Rodriguez C, Hou B-H, Molina A, Schulze-Lefert P, Lipka V, Somerville S** (2006) *Arabidopsis* PEN3/PDR8, an ATP Binding Cassette Transporter, contributes to nonhost resistance to inappropriate pathogens that enter by direct penetration. *Plant Cell* **18**: 731-746
- Sutter JU, Sieben C, Hartel A, Eisenach C, Thiel G, Blatt MR** (2007) Abscisic acid triggers the endocytosis of the *Arabidopsis* KAT1 K⁺ channel and its recycling to the plasma membrane. *Curr Biol* **17**: 1396-1402
- Sutter JU, Campanoni P, Tyrrell M, Blatt MR** (2006) Selective mobility and sensitivity to SNAREs is exhibited by the *Arabidopsis* KAT1 K⁺ channel at the plasma membrane. *Plant Cell* **18**: 935-954
- Thiele C, Hannah MJ, Fahrenholz F, Huttner WB** (2000) Cholesterol binds to synaptophysin and is required for biogenesis of synaptic vesicles. *Nat Cell Biol* **2**: 42-49
- Thimm O, Bläsing O, Gibon Y, Nagel A, Meyer S, Krüger P, Selbig J, Müller LA, Rhee SY, Stitt M** (2004) MAPMAN: a user-driven tool to display genomics data sets onto diagrams of metabolic pathways and other biological processes. *Plant J* **37**: 914-939
- Titapiwatanakun B, Blakeslee JJ, Bandyopadhyay A, Yang H, Mravec J, Sauer M, Cheng Y, Adamec J, Nagashima A, Geisler M, Sakai T, Friml J, Peer WA, Murphy AS** (2008) ABCB19/PGP19 stabilises PIN1 in membrane microdomains in *Arabidopsis*. *Plant J*: 10.1111/j.1365-1313X.2008.03668.x
- Torres MA, Jones JDG, Dangl JL** (2006) Reactive oxygen species signaling in response to pathogens. *Plant Physiol* **141**: 373-378
- Tsuda K, Sato M, Glazebrook J, Cohen JD, Katagiri F** (2008) Interplay between MAMP-triggered and SA-mediated defense responses. *Plant J* **53**: 763-775
- Underwood W, Somerville SC** (2008) Focal accumulation of defences at sites of fungal pathogen attack. *J Exp Bot* **59**: 3501-3508
- Valdez-Taubas J, Pelham HR** (2003) Slow diffusion of proteins in the yeast plasma membrane allows polarity to be maintained by endocytic cycling. *Curr Biol* **13**: 1636-1640
- van Damme M, Andel A, Huibers RP, Panstruga R, Weisbeek PJ, Van den Ackerveken G** (2005) Identification of *Arabidopsis* Loci Required for Susceptibility to the Downy Mildew Pathogen *Hyaloperonospora parasitica*. *Mol Plant Microbe Interact* **18**: 583-592

- van Leeuwen W, Vermeer JE, Gadella TW, Jr., Munnik T** (2007) Visualization of phosphatidylinositol 4,5-bisphosphate in the plasma membrane of suspension-cultured tobacco BY-2 cells and whole *Arabidopsis* seedlings. *Plant J* **52**: 1014-1026
- van Meer G, Voelker DR, Feigenson GW** (2008) Membrane lipids: where they are and how they behave. *Nat Rev Mol Cell Biol* **9**: 112-124
- Varet A, Hause B, Hause G, Scheel D, Lee J** (2003) The *Arabidopsis NHL3* gene encodes a plasma membrane protein and its overexpression correlates with increased resistance to *Pseudomonas syringae* pv. *tomato* DC3000. *Plant Physiol* **132**: 2023-2033
- Varet A, Parker J, Tornero P, Nass N, Nurnberger T, Dangl JL, Scheel D, Lee J** (2002) *NHL25* and *NHL3*, two *NDR1/HIN1-Like* genes in *Arabidopsis thaliana* with potential role(s) in plant defense. *Mol Plant Microbe Interact* **15**: 608-616
- Vaultier MN, Cantrel C, Vergnolle C, Justin AM, Demandre C, Benhassaine-Kesri G, Cicek D, Zachowski A, Ruelland E** (2006) Desaturase mutants reveal that membrane rigidification acts as a cold perception mechanism upstream of the diacylglycerol kinase pathway in *Arabidopsis* cells. *FEBS letters* **580**: 4218-4223
- Venable JD, Wohlschlegel J, McClatchy DB, Park SK, Yates JRrd** (2007) Relative quantification of stable isotope labeled peptides using a linear ion trap-Orbitrap hybrid mass spectrometer. *Anal Chem* **79**: 3056-3064
- Wang D, Pajerowska-Mukhtar K, Culler AH, Dong X** (2007) Salicylic acid inhibits pathogen growth in plants through repression of the auxin signaling pathway. *Curr Biol* **17**: 1784-1790
- Wessel D, Flügge UI** (1984) A method for the quantitative recovery of protein in dilute solution in the presence of detergents and lipids. *Anal Biochem* **138**: 141-143
- Willemsen V, Friml J, Grebe M, van den Toorn A, Palme K, Scheres B** (2003) Cell polarity and PIN protein positioning in *Arabidopsis* require *STEROL METHYLTRANSFERASE1* function. *Plant Cell* **15**: 612-625
- Wu R, Chen L, Yu Z, Quinn PJ** (2006) Phase diagram of stigmaterol-dipalmitoylphosphatidylcholine mixtures dispersed in excess water. *Biochim Biophys Acta* **1758**: 764-771
- Xu X, Bittman R, Dupontail G, Heissler D, Vilcheze C, London E** (2001) Effect of the structure of natural sterols and sphingolipids on the formation of ordered sphingolipid/sterol domains (rafts). Comparison of cholesterol to plant, fungal, and disease-associated sterols and comparison of sphingomyelin, cerebroside, and ceramide. *J Biol Chem* **276**: 33540-33546
- Xu X, London E** (2000) The Effect of Sterol Structure on Membrane Lipid Domains Reveals How Cholesterol Can Induce Lipid Domain Formation. *Biochemistry* **39**: 843-849
- Zipfel C** (2008) Pattern-recognition receptors in plant innate immunity. *Curr Opin Immunol* **20**: 10-16
- Zipfel C, Robatzek S, Navarro L, Oakeley EJ, Jones JD, Felix G, Boller T** (2004) Bacterial disease resistance in *Arabidopsis* through flagellin perception. *Nature* **428**: 764-767
- Zappel NF, Panstruga R** (2008) Heterogeneity and lateral compartmentalization of plant plasma membranes. *Curr Opin Plant Biol* **11**: 632-640.
- Zhang Z, Feechan A, Pedersen C, Newman M-A, Qiu J-I, Olesen KL, Thordal-Christensen H** (2007) A SNARE-protein has opposing functions in penetration resistance and defence signalling pathways. *Plant J* **49**: 302-312

- Zimmerli L, Stein M, Lipka V, Schulze-Lefert P, Somerville S (2004)** Host and non-host pathogens elicit different jasmonate/ethylene responses in *Arabidopsis*. *Plant J* **40**: 633-646

7. Supplementary Material



Supplementary Figure 1. A plate assay for the oxidative burst indicates flg22 responsiveness of Arabidopsis cultured cells.

Arabidopsis cell cultures were distributed in 1 ml aliquots into culture plates and supplied with the peroxidase substrate 5' aminosalicylic acid (5'ASA; 400 μ M) as well as different amounts of flg22 to monitor the oxidative burst. As negative controls, cells were treated with 5'ASA or flg22 only or cells were left untreated. Cell culture plates were analyzed visually 1.5 hrs after induction. The experiment was repeated once with similar results.

Supplementary Table 1. All proteins for which quantitation has been pursued. For all proteins present in both samples of a reciprocal pair quantitation was pursued. Proteins significantly enriched in DRMs after flg22 treatment are indicated in bold (p < 0.05). Functional category (FC); distance (D); maximal fold change (max fold); average fold-change (av fold); probability-value (p); number of TM domains (TM) predicted by ARAMEMNON (Schwacke et al., 2003); experimental evidence for PM association (PM, (Schwacke et al., 2003; Alexandersson et al., 2004; Marmagne et al., 2004; Nelson et al., 2006)); transcriptionally coregulated with FLS2 (Obayashi et al., 2007), number indicates rank of co-expressed gene according to ATTED; transcriptionally upregulated in response to flg22 treatment (flg22 expr, (Navarro et al., 2004; Zipfel et al., 2004)); phosphorylated after flg22 treatment (Pflg22, (Benschop et al., 2007; Nühse et al., 2007)); mutants of according genes were analyzed for flg22 responsiveness in this study (RG). enriched (enr.), dephosphorylated (de-p), phosphorylation below the significance threshold ((✓)).

| FC | AGI code and annotation | flg22 vs flg22Δ2 | | | | | | | | | | | | flg22 vs untreated | | | | flg22Δ2 vs untreated | | | | TM | PM | ATTED | flg22 expr | P flg22 |
|------------------------------------------|--------------------------------------------------------------------|------------------|--------------|--------------|--------------|--------------|--------------|--------------|--------------|--------------|--------------|--------------|--------------|--------------------|--------------|--------------|--------------|----------------------|----------|---------|-------|----|------|-------|------------|---------|
| | | 0 minutes | | | | 5 minutes | | | | 15 minutes | | | | 5 minutes | | | | 5 minutes | | | | | | | | |
| | | D | max fold | av fold | p | D | max fold | av fold | p | D | max fold | av fold | p | D | max fold | av fold | p | D | max fold | av fold | p | | | | | |
| PROTEINS RESPONDING SIGNIFICANTLY | | | | | | | | | | | | | | | | | | | | | | | | | | |
| Signalling | | | | | | | | | | | | | | | | | | | | | | | | | | |
| Receptor-like kinase | | | | | | | | | | | | | | | | | | | | | | | | | | |
| | AT5G46330 FLS2 (FLAGELLIN-SENSIT1 2) | — | — | — | — | 1,001 | 3,014 | 1,950 | 0,048 | 0,610 | 1,521 | 1,358 | 0,012 | 0,822 | 1,622 | 1,501 | 0,013 | — | — | — | — | 1 | — | 1 | ✓ | — |
| | AT3G17840 RLK902 (receptor-like kinase 902) | -0,490 | 0,949 | 0,800 | 0,131 | 1,294 | 2,096 | 1,896 | 0,000 | 1,016 | 2,018 | 1,680 | 0,014 | — | — | — | — | — | — | — | — | 1 | — | — | — | — |
| | AT3G51550 FER (FERONIA) | -0,061 | 1,026 | 0,972 | 0,939 | 1,128 | 2,320 | 1,811 | 0,000 | 0,592 | 1,416 | 1,339 | 0,201 | — | — | — | — | — | — | — | — | 1 | enr. | 158 | — | — |
| | AT3G02880 LRR transmembrane protein kinase, putative | -0,232 | 0,927 | 0,893 | 0,707 | 0,685 | 2,181 | 1,539 | 0,014 | 0,078 | 1,170 | 1,047 | 0,922 | 0,518 | 1,370 | 1,292 | 0,241 | 0,020 | 1,032 | 1,010 | 0,721 | 1 | enr. | — | ✓ | — |
| | AT5G16590 LRR transmembrane protein kinase, putative | -0,064 | 0,974 | 0,969 | 0,937 | 0,872 | 2,181 | 1,629 | 0,001 | 0,190 | 1,324 | 1,117 | 0,766 | 0,350 | 1,395 | 1,203 | 0,459 | — | — | — | — | 1 | enr. | — | — | — |
| | AT2G01820 LRR protein kinase, putative | 0,247 | 2,232 | 1,401 | 0,673 | 1,010 | 2,225 | 1,717 | 0,000 | 1,774 | 4,412 | 2,851 | 0,000 | — | — | — | — | 0,036 | 1,578 | 1,154 | 0,617 | 1 | — | — | — | — |
| | AT4G36180 LRR family protein | 0,378 | 1,369 | 1,213 | 0,494 | — | — | — | — | 1,482 | 2,769 | 2,156 | 0,000 | — | — | — | — | — | — | — | — | 1 | — | — | — | — |
| | AT1G75640 LRR family protein / protein kinase family protein | -0,989 | 0,660 | 0,617 | 0,012 | — | — | — | — | 0,621 | 1,849 | 1,421 | 0,024 | — | — | — | — | — | — | — | — | 1 | — | — | — | — |
| | AT3G23750 LRR family protein / protein kinase family protein | -0,257 | 1,025 | 0,892 | 0,673 | 0,704 | 2,320 | 1,590 | 0,030 | 0,338 | 1,722 | 1,266 | 0,563 | — | — | — | — | — | — | — | — | 1 | ✓ | — | — | — |
| | AT3G46290 protein kinase, putative | -0,157 | 0,983 | 0,928 | 0,813 | 0,791 | 2,320 | 1,628 | 0,014 | -0,021 | 1,290 | 1,025 | 0,973 | 0,548 | 1,327 | 1,308 | 0,225 | 0,443 | 1,474 | 1,260 | 0,802 | 1 | — | 224 | — | ✓ |

Supplementary Table 1 continued.

| FC | AGI code and annotation | 0 minutes | | | | flg22 vs flg22Δ2 5 minutes | | | | 15 minutes | | | | flg22 vs untreated 5 minutes | | | | flg22Δ2 vs untreated 5 minutes | | | | TM | PM | ATTED | flg22 expr | P flg22 |
|--------------------------|------------------------------------------------------------------------|-----------|----------|---------|-------|-------------------------------|--------------|--------------|--------------|--------------|--------------|--------------|--------------|---------------------------------|--------------|--------------|--------------|-----------------------------------|----------|---------|-------|-------|------|-------|------------|---------|
| | | D | max fold | av fold | p | D | max fold | av fold | P | D | max fold | av fold | p | D | max fold | av fold | p | D | max fold | av fold | p | | | | | |
| Other Transporter | | | | | | | | | | | | | | | | | | | | | | | | | | |
| ABC Transporter | | | | | | | | | | | | | | | | | | | | | | | | | | |
| | AT2G36910 PGP1 (P-Glycoprotein 1) | — | — | — | — | 0,857 | 2,657 | 1,764 | 0,041 | 0,340 | 1,781 | 1,282 | 0,599 | 0,369 | 1,487 | 1,227 | 0,443 | 0,778 | 3,623 | 2,141 | 0,710 | 10 | — | — | — | ✓ |
| | AT2G47000 PGP4 (P-Glycoprotein 4) | 0,041 | 1,091 | 1,023 | 0,957 | 1,063 | 2,371 | 1,783 | 0,001 | 0,379 | 1,213 | 1,204 | 0,493 | 0,553 | 1,321 | 1,311 | 0,225 | — | — | — | — | 12 | — | — | — | ✓ |
| | AT5G50200 WR3 (WOUND-RESPONSIVE 3); nitrate transporter | 0,127 | 1,117 | 1,066 | 0,859 | 1,248 | 2,722 | 1,985 | 0,003 | 0,512 | 1,397 | 1,290 | 0,299 | 0,589 | 1,419 | 1,337 | 0,217 | 0,018 | 1,018 | 1,009 | 0,994 | 1 | — | — | — | — |
| | AT4G13510 AMT1;1 (AMMONIUM TRANSPORT 1) | -0,240 | 0,910 | 0,889 | 0,698 | 1,073 | 2,594 | 1,849 | 0,006 | 0,700 | 1,843 | 1,460 | 0,227 | 0,542 | 1,461 | 1,313 | 0,225 | -0,176 | 0,951 | 0,918 | 0,947 | 12 | ✓ | — | ✓ | ✓ |
| | AT1G11260 STP1 (SUGAR TRANSPORTER 1) | -0,059 | 1,356 | 1,026 | 0,912 | 0,936 | 1,694 | 1,586 | 0,025 | 0,226 | 1,437 | 1,153 | 0,754 | 0,699 | 1,650 | 1,427 | 0,140 | -0,170 | 1,315 | 1,015 | 0,459 | 12 | ✓ | 32 | — | — |
| | AT3G19930 STP4 (SUGAR TRANSPORTER 4) | 0,062 | 1,641 | 1,144 | 0,919 | 0,962 | 1,722 | 1,607 | 0,020 | 0,311 | 1,504 | 1,203 | 0,585 | 0,538 | 1,478 | 1,312 | 0,225 | 0,127 | 1,602 | 1,154 | 0,738 | 12 | ✓ | — | — | — |
| | AT4G21120 AAT1 (CATIONIC AMINO ACID TRANSPORTER 1) | — | — | — | — | — | — | — | — | 0,248 | 1,243 | 1,134 | 0,686 | 0,738 | 1,449 | 1,436 | 0,013 | — | — | — | — | 14 | — | — | — | — |
| | AT5G40780 LHT1 (LYSINE HISTIDINE TRANSPORTER 1) | — | — | — | — | 1,619 | 3,372 | 2,411 | 0,004 | 0,232 | 1,324 | 1,136 | 0,707 | 0,778 | 1,782 | 1,492 | 0,013 | — | — | — | — | 11-12 | ✓ | — | ✓ | — |
| | AT3G54140 proton-dependent oligopeptide transport (POT) family protein | -0,158 | 1,093 | 0,938 | 0,813 | 0,933 | 2,861 | 1,867 | 0,048 | 0,209 | 1,591 | 1,181 | 0,632 | 0,892 | 1,594 | 1,549 | 0,049 | -0,430 | 0,833 | 0,810 | 0,817 | 11 | ✓ | — | — | — |
| Cell wall-related | | | | | | | | | | | | | | | | | | | | | | | | | | |
| | AT1G03870 FLA9 (FLA9) | 0,001 | 1,545 | 1,097 | 0,997 | 0,251 | 1,209 | 1,133 | 0,684 | 0,839 | 2,174 | 1,610 | 0,048 | — | — | — | — | — | — | — | — | 0-1 | enr. | — | — | — |
| | AT4G12420 SKU5 (skewed 5); copper ion binding | -1,124 | 1,130 | 0,712 | 0,303 | 0,882 | 1,934 | 1,580 | 0,038 | 2,241 | 8,137 | 4,621 | 0,000 | 0,121 | 2,937 | 1,660 | 0,902 | 0,070 | 1,367 | 1,075 | 0,902 | 0/GPI | enr. | — | — | — |
| | AT1G05570 CALS1/GSL6 (CALLOSE SYNTHASE 1) | — | — | — | — | — | — | — | — | 0,807 | 1,694 | 1,498 | 0,047 | — | — | — | — | — | — | — | — | 16 | — | — | — | — |

Supplementary Table 1 continued.

| FC | AGI code and annotation | 0 minutes | | | | fig22 vs fig22Δ2 5 minutes | | | | 15 minutes | | | | fig22 vs untreated 5 minutes | | | | fig22Δ2 vs untreated 5 minutes | | | | TM | PM | ATTED | fig22 expr | P fig22 |
|----------------------------------------------|----------------------------------------------------------------|---------------|--------------|--------------|--------------|-------------------------------|--------------|--------------|--------------|--------------|--------------|--------------|--------------|---------------------------------|--------------|--------------|--------------|-----------------------------------|----------|---------|-------|-------|------|-------|------------|---------|
| | | D | max fold | av fold | p | D | max fold | av fold | p | D | max fold | av fold | p | D | max fold | av fold | p | D | max fold | av fold | p | | | | | |
| Other | | | | | | | | | | | | | | | | | | | | | | | | | | |
| | AT2G45820 REM1.3 (REMORIN) | 0,366 | 1,383 | 1,209 | 0,519 | 0,985 | 2,017 | 1,660 | 0,017 | 1,047 | 2,217 | 1,738 | 0,012 | 0,953 | 1,919 | 1,623 | 0,048 | -0,107 | 1,229 | 0,981 | 0,710 | 0 | enr. | — | — | ✓ |
| | AT3G61260 REM1.2 (remorin family protein) | -0,484 | 1,104 | 0,834 | 0,325 | 1,038 | 1,944 | 1,683 | 0,012 | 0,350 | 1,276 | 1,190 | 0,541 | 0,667 | 1,766 | 1,427 | 0,162 | 0,134 | 1,289 | 1,087 | 0,817 | 0 | enr. | — | — | — |
| | AT1G11330 S-locus lectin protein kinase family protein | — | — | — | — | 1,197 | 3,276 | 2,131 | 0,030 | — | — | — | — | — | — | — | — | — | — | — | — | 1 | — | — | — | — |
| | AT1G72230 plastocyanin-like domain-containing protein | — | — | — | — | 0,505 | 1,909 | 1,384 | 0,303 | 0,441 | 1,521 | 1,267 | 0,093 | 0,173 | 1,296 | 1,105 | 0,721 | 0,110 | 1,315 | 1,128 | 0,568 | 0/GPI | — | — | — | — |
| Unknown | | | | | | | | | | | | | | | | | | | | | | | | | | |
| | AT1G32190 expressed protein | -0,207 | 0,936 | 0,904 | 0,748 | 1,152 | 2,478 | 1,863 | 0,001 | 0,845 | 1,722 | 1,526 | 0,048 | 0,685 | 1,628 | 1,415 | 0,148 | -0,125 | 1,139 | 1,001 | 0,568 | 0- | — | — | — | — |
| | AT3G44150 expressed protein | — | — | — | — | 0,892 | 2,790 | 1,825 | 0,048 | 0,426 | 1,499 | 1,256 | 0,432 | 0,713 | 1,617 | 1,430 | 0,013 | — | — | — | — | 1 | — | — | — | — |
| | AT1G17620 expressed protein | 0,094 | 1,157 | 1,053 | 0,919 | 0,803 | 2,225 | 1,606 | 0,006 | 0,398 | 1,307 | 1,219 | 0,470 | 0,562 | 1,525 | 1,331 | 0,225 | -0,075 | 1,032 | 1,016 | 0,538 | 1 | ✓ | — | — | — |
| | AT3G01290 band 7 family protein | 0,082 | 1,091 | 1,042 | 0,919 | 1,010 | 1,909 | 1,659 | 0,014 | 0,600 | 1,342 | 1,342 | 0,198 | 0,465 | 1,408 | 1,264 | 0,293 | — | — | — | — | 0- | enr. | — | ✓ | — |
| | AT1G69840 band 7 family protein | -0,056 | 1,118 | 0,982 | 0,942 | 1,286 | 2,478 | 1,950 | 0,000 | 0,628 | 1,875 | 1,431 | 0,325 | 0,736 | 1,522 | 1,437 | 0,013 | -0,263 | 0,941 | 0,927 | 0,568 | 0 | ✓ | 154 | ✓ | — |
| | AT5G62740 band 7 family protein | 0,584 | 2,225 | 1,511 | 0,455 | 1,197 | 2,861 | 1,996 | 0,009 | 0,768 | 2,096 | 1,554 | 0,364 | 0,729 | 1,684 | 1,448 | 0,013 | — | — | — | — | 0 | ✓ | — | — | — |
| PROTEINS NOT RESPONDING SIGNIFICANTLY | | | | | | | | | | | | | | | | | | | | | | | | | | |
| Signalling | | | | | | | | | | | | | | | | | | | | | | | | | | |
| Receptor-like kinase | | | | | | | | | | | | | | | | | | | | | | | | | | |
| | AT3G13380 BRL3 (BRI1-LIKE 3) | 0,831 | 12,516 | 6,348 | 0,661 | — | — | — | — | — | — | — | — | — | — | — | — | — | — | — | — | 1 | — | — | — | — |
| | AT3G51740 IMK2 (INFLORESCENCE MERISTEM RECEPTOR-LIKE KINASE 2) | -0,308 | 1,342 | 0,946 | 0,593 | 0,785 | 3,097 | 1,897 | 0,165 | 0,148 | 1,499 | 1,135 | 0,827 | — | — | — | — | — | — | — | — | 1 | — | — | — | — |
| | AT5G58150 LRR transmembrane protein kinase, putative | -0,971 | 1,058 | 0,711 | 0,019 | — | — | — | — | 0,016 | 1,694 | 1,147 | 0,974 | — | — | — | — | — | — | — | — | 1 | — | — | — | — |

Supplementary Table 1 continued.

| FC | AGI code and annotation | 0 minutes | | | | flg22 vs flg22A2 5 minutes | | | | 15 minutes | | | | flg22 vs untreated 5 minutes | | | | flg22A2 vs untreated 5 minutes | | | | TM | PM | ATTED | flg22 expr | P flg22 |
|----------------------|-----------------------------------------------------------------------------------------|-----------|----------|---------|-------|-------------------------------|----------|---------|-------|------------|----------|---------|-------|---------------------------------|----------|---------|-------|-----------------------------------|----------|---------|-------|-------|------|-------|------------|---------|
| | | D | max fold | av fold | p | D | max fold | av fold | p | D | max fold | av fold | p | D | max fold | av fold | p | D | max fold | av fold | p | | | | | |
| | AT2G01210 LRR transmembrane protein kinase, putative | — | — | — | — | 0,273 | 3194,8 | 1597,4 | 0,973 | — | — | — | — | 0,089 | 106,8 | 53,41 | 0,974 | -1,611 | 24,81 | 12,41 | 0,606 | — | — | — | — | — |
| | AT1G53730 LRR transmembrane protein kinase, putative | — | — | — | — | — | — | — | — | -0,252 | 1,039 | 0,895 | 0,813 | — | — | — | — | — | — | — | — | 1 | — | — | — | — |
| | AT3G28450 LRR transmembrane protein kinase, putative | -0,350 | 0,983 | 0,853 | 0,541 | — | — | — | — | — | — | — | — | — | — | — | — | — | — | — | — | 1 | — | — | ✓ | — |
| | AT2G26730 LRR transmembrane protein kinase, putative | -0,206 | 1,236 | 0,949 | 0,606 | — | — | — | — | — | — | — | — | — | — | — | — | — | — | — | — | 1 | ✓ | — | — | ✓ |
| | AT4G35230 protein kinase family protein | — | — | — | — | — | — | — | — | 0,117 | 1,093 | 1,059 | 0,875 | — | — | — | — | — | — | — | — | 0- | — | — | — | — |
| | AT1G70520 protein kinase family protein | 0,324 | 2,861 | 1,671 | 0,787 | — | — | — | — | — | — | — | — | — | — | — | — | — | — | — | — | 1 | — | 174 | ✓ | — |
| | AT3G17410 serine/threonine protein kinase, putative | — | — | — | — | — | — | — | — | -0,114 | 1,342 | 1,004 | 0,942 | — | — | — | — | — | — | — | — | — | — | — | — | — |
| | AT2G47060 serine/threonine protein kinase, putative | -0,044 | 1,184 | 0,996 | 0,955 | 0,320 | 1,616 | 1,231 | 0,581 | 0,378 | 1,909 | 1,334 | 0,635 | — | — | — | — | — | — | — | — | 0 | — | 164 | ✓ | — |
| | AT2G37050 kinase | 0,400 | 1,236 | 1,217 | 0,469 | 0,350 | 1,616 | 1,244 | 0,541 | 0,475 | 1,477 | 1,278 | 0,345 | 0,350 | 1,239 | 1,188 | 0,459 | — | — | — | — | 1 | enr. | — | — | — |
| Other kinases | AT5G67130 phospholipase C | 0,036 | 1,477 | 1,089 | 0,937 | — | — | — | — | 0,208 | 1,450 | 1,148 | 0,787 | — | — | — | — | — | — | — | — | 0/GPI | — | — | — | — |
| | AT1G35160 GRF4 (GENERAL REGULATORY FACTOR 4); protein phosphorylated amino acid binding | -0,539 | 1,227 | 0,854 | 0,267 | — | — | — | — | — | — | — | — | — | — | — | — | — | — | — | — | 0 | — | — | — | — |
| | AT4G23650 CDPK6 (CALCIUM-DEPENDENT PROTEIN KINASE 6) | 0,398 | 1,262 | 1,216 | 0,470 | 0,419 | 1,289 | 1,229 | 0,441 | 0,351 | 1,262 | 1,190 | 0,541 | — | — | — | — | — | — | — | — | 0- | enr. | — | — | — |
| | AT5G19450 CDPK19 (CALCIUM-DEPENDENT PROTEIN KINASE 19) | — | — | — | — | — | — | — | — | — | — | — | — | — | — | — | — | — | — | — | — | 0- | ✓ | — | — | — |

Supplementary Table 1 continued.

| FC | AGI code and annotation | flg22 vs flg22Δ2 | | | | | | | | flg22 vs untreated | | | | flg22Δ2 vs untreated | | | | TM | PM | ATTED | flg22 expr | P flg22 | | | | | |
|----|--------------------------------------------------------------------------|------------------|----------|---------|-------|-----------|----------|---------|-------|--------------------|----------|---------|-------|----------------------|----------|---------|-------|--------|-------|-------|------------|----------|------|----|---|---|---|
| | | 0 minutes | | | | 5 minutes | | | | 15 minutes | | | | 5 minutes | | | | | | | | | | | | | |
| | | D | max fold | av fold | p | D | max fold | av fold | p | D | max fold | av fold | p | D | max fold | av fold | p | | | | | | | | | | |
| | AT5G24430 calcium-dependent protein kinase, putative / CDPK, putative | — | — | — | — | — | — | — | — | 0,256 | 1,751 | 1,242 | 0,698 | — | — | — | — | — | — | — | — | — | | | | | |
| | Other signalling proteins | | | | | | | | | | | | | | | | | | | | | | | | | | |
| | AT1G66410 CAM4 (CALMODULIN 4); calcium ion binding | -0,320 | 1,614 | 1,033 | 0,711 | 0,718 | 1,521 | 1,425 | 0,110 | — | — | — | — | — | — | — | — | 0 | ✓ | — | — | — | | | | | |
| | AT4G17530 RAB1C; GTP binding | 0,141 | 1,227 | 1,082 | 0,832 | 0,318 | 1,544 | 1,214 | 0,581 | 0,312 | 1,307 | 1,173 | 0,586 | 0,469 | 1,413 | 1,267 | 0,293 | -0,237 | 0,900 | 0,890 | 0,947 | 0/gerger | ✓ | — | — | — | |
| | AT5G20010 RAN-1 (Ras-related GTP-binding nuclear protein 1); GTP binding | 0,185 | 1,183 | 1,098 | 0,766 | — | — | — | — | — | — | — | — | — | — | — | — | — | — | — | — | — | — | — | — | — | — |
| | AT5G59150 RABA2d (Rab GTPase homolog A2d) | — | — | — | — | — | — | — | — | 0,047 | 1,437 | 1,083 | 0,973 | — | — | — | — | — | — | — | — | 0/pren | — | — | — | — | — |
| | AT1G28340 LRR family protein | — | — | — | — | — | — | — | — | 0,039 | 1,078 | 1,021 | 0,944 | — | — | — | — | — | — | — | — | 1 | — | — | — | — | — |
| | Transport | | | | | | | | | | | | | | | | | | | | | | | | | | |
| | Plasma membrane ATPases | | | | | | | | | | | | | | | | | | | | | | | | | | |
| | AT5G62670 AHA11 (H ⁺)-ATPase 11) | 0,018 | 1,258 | 1,034 | 0,973 | — | — | — | — | 0,492 | 1,641 | 1,314 | 0,211 | 0,537 | 1,540 | 1,320 | 0,225 | 0,193 | 1,208 | 1,104 | 0,994 | 10 | enr. | — | — | — | — |
| | Calcium-transporting ATPases | | | | | | | | | | | | | | | | | | | | | | | | | | |
| | AT1G13210 autoinhibited Ca ²⁺ -ATPase II | 0,380 | 1,944 | 1,345 | 0,573 | — | — | — | — | 1,074 | 2,423 | 1,803 | 0,310 | — | — | — | — | — | — | — | — | 8 | — | 98 | ✓ | — | — |
| | Vacuolar H⁺-ATPases | | | | | | | | | | | | | | | | | | | | | | | | | | |
| | AT2G28520 VHA-a1 | — | — | — | — | — | — | — | — | -0,610 | 0,803 | 0,744 | 0,396 | — | — | — | — | — | — | — | — | 6 | — | — | — | — | — |
| | AT1G19910 AVA-C2 | — | — | — | — | 0,665 | 1,944 | 1,465 | 0,147 | 0,387 | 1,249 | 1,210 | 0,481 | — | — | — | — | — | — | — | — | 3 | — | — | — | — | — |
| | AT3G01390 VHA-G1 | — | — | — | — | — | — | — | — | — | — | — | — | — | — | — | — | — | — | — | — | 0 | ✓ | — | — | — | — |
| | AT1G15690 AVP1 (vacuolar-type H ⁺ -pumping pyrophosphatase 1) | -0,086 | 1,069 | 0,964 | 0,919 | 0,467 | 2,017 | 1,401 | 0,358 | — | — | — | — | 0,200 | 1,121 | 1,103 | 0,692 | — | — | — | — | 12 | ✓ | — | — | — | — |
| | ABC Transporter | | | | | | | | | | | | | | | | | | | | | | | | | | |
| | AT2G39480 PGP6 (P-Glycoprotein 6) | -0,450 | 0,877 | 0,805 | 0,387 | — | — | — | — | — | — | — | — | — | — | — | — | — | — | — | — | 11 | — | — | — | — | — |
| | AT3G62150 PGP21 (P-Glycoprotein 21) | — | — | — | — | — | — | — | — | 0,121 | 1,065 | 1,061 | 0,867 | — | — | — | — | — | — | — | — | 10-11 | — | 23 | — | — | — |

Supplementary Table 1 continued.

| FC | AGI code and annotation | 0 minutes | | | | flg22 vs flg22Δ2 | | | | 15 minutes | | | | flg22 vs untreated | | | | flg22Δ2 vs untreated | | | | TM | PM | ATTED | flg22 expr | P flg22 | |
|----|-----------------------------------------------------------------------|-----------|----------|---------|-------|------------------|----------|---------|-------|------------|----------|---------|-------|--------------------|----------|---------|-------|----------------------|----------|---------|-------|-------|------|-------|------------|---------|---|
| | | D | max fold | av fold | p | D | max fold | av fold | p | D | max fold | av fold | p | D | max fold | av fold | p | D | max fold | av fold | p | | | | | | |
| | AT1G15210 PDR7 (PLEIOTROPIC DRUG RESISTANCE 7) | 0,077 | 1,274 | 1,060 | 0,922 | — | — | — | — | — | — | — | — | — | — | — | — | — | — | — | — | 14 | — | — | — | — | ✓ |
| | Other Transporter | | | | | | | | | | | | | | | | | | | | | | | | | | |
| | AT1G61250 SC3 (SECRETORY CARRIER 3) | — | — | — | — | — | — | — | — | 0,257 | 1,694 | 1,227 | 0,652 | — | — | — | — | — | — | — | — | 4 | ✓ | — | — | — | — |
| | AT2G38290 ATAMT2 (AMMONIUM TRANSPORTER 2) | — | — | — | — | — | — | — | — | 0,326 | 1,360 | 1,186 | 0,573 | — | — | — | — | — | — | — | — | 8-9 | ✓ | 41 | ✓ | — | — |
| | AT5G43350 ATPT1 (PHOSPHATE TRANSPORTER 1) | 0,009 | 1,227 | 1,024 | 0,983 | — | — | — | — | 0,374 | 1,521 | 1,235 | 0,167 | — | — | — | — | — | — | — | — | 11-12 | ✓ | — | — | — | — |
| | AT5G64410 ATOPT4 (oligopeptide transporter 4) | 0,464 | 1,378 | 1,261 | 0,363 | — | — | — | — | 0,326 | 1,360 | 1,186 | 0,573 | — | — | — | — | — | — | — | — | 14-15 | — | 20 | — | — | — |
| | AT4G35100 PIP3 (PLASMA MEMBRANE INTRINSIC PROTEIN 3) | -0,021 | 1,396 | 1,049 | 0,966 | — | — | — | — | — | — | — | — | 0,449 | 1,301 | 1,247 | 0,300 | — | — | — | — | 6 | enr. | — | — | — | — |
| | AT4G05120 FUR1 (FUDR RESISTANT 1); nucleoside transporter | -0,045 | 1,477 | 1,063 | 0,933 | 0,582 | 2,371 | 1,559 | 0,107 | 0,287 | 1,436 | 1,179 | 0,628 | 0,335 | 1,471 | 1,207 | 0,485 | — | — | — | — | 11 | — | — | — | — | — |
| | AT2G38940 ATPT2 (PHOSPHATE TRANSPORTER 2) | -0,177 | 1,227 | 0,956 | 0,780 | 0,748 | 2,657 | 1,720 | 0,089 | 0,535 | 1,667 | 1,340 | 0,198 | 0,520 | 1,366 | 1,292 | 0,241 | — | — | — | — | 12 | ✓ | — | — | — | — |
| | AT1G65730 YSL7 (YELLOW STRIPE LIKE 7); oligopeptide transporter | — | — | — | — | — | — | — | — | 0,737 | 1,821 | 1,476 | 0,100 | — | — | — | — | — | — | — | — | 14 | — | — | — | — | — |
| | AT5G15090 voltage-dependent anion-selective channel protein, putative | 0,054 | 1,236 | 1,044 | 0,942 | 0,242 | 1,289 | 1,136 | 0,698 | 0,422 | 1,369 | 1,237 | 0,435 | 0,101 | 1,140 | 1,054 | 0,817 | — | — | — | — | 0 | ✓ | — | — | — | — |
| | AT3G54700 phosphate transporter, putative | -0,055 | 1,436 | 1,048 | 0,919 | — | — | — | — | -0,131 | 1,667 | 1,097 | 0,829 | 0,539 | 1,471 | 1,312 | 0,225 | 0,144 | 1,195 | 1,079 | 0,817 | 8 | — | — | — | — | — |
| | AT2G27810 xanthine/uracil permease family protein | 0,087 | 1,052 | 1,044 | 0,919 | 0,504 | 1,521 | 1,299 | 0,303 | -0,319 | 1,170 | 0,898 | 0,830 | — | — | — | — | — | — | — | — | 10 | — | — | — | — | — |

Supplementary Table 1 continued.

| FC | AGI code and annotation | flg22 vs flg22Δ2 | | | | | | | | | | | | flg22 vs untreated | | | | flg22Δ2 vs untreated | | | | TM | PM | ATTED | flg22 expr | P flg22 |
|----|------------------------------------------------------------------------|------------------|-------|-------|-------|-----------|-------|-------|-------|------------|-------|-------|-------|--------------------|-------|-------|-------|----------------------|-------|-------|-------|-------|------|-------|------------|---------|
| | | 0 minutes | | | | 5 minutes | | | | 15 minutes | | | | 5 minutes | | | | D | max | av | p | | | | | |
| | | D | max | av | p | D | max | av | p | D | max | av | p | D | max | av | p | D | max | av | p | | | | | |
| | AT3G47960 proton-dependent oligopeptide transport (POT) family protein | 0,028 | 1,290 | 1,043 | 0,973 | — | — | — | — | — | — | — | — | — | — | — | — | — | — | — | — | 12 | — | — | ✓ | — |
| | AT1G60030 xanthine/uracil permease family protein | — | — | — | — | — | — | — | — | 0,125 | 1,397 | 1,103 | 0,864 | — | — | — | — | — | — | — | — | 12 | — | — | — | — |
| | Cell wall-related | | | | | | | | | | | | | | | | | | | | | | | | | |
| | AT2G04780 FLA7 | -0,027 | 1,091 | 0,992 | 0,973 | -0,015 | 1,130 | 1,001 | 0,976 | 0,679 | 1,450 | 1,396 | 0,136 | 0,112 | 1,376 | 1,093 | 0,738 | — | — | — | — | 0/GPI | enr. | — | — | — |
| | AT2G45470 FLA8 | 0,344 | 1,628 | 1,244 | 0,550 | — | — | — | — | 0,624 | 1,780 | 1,408 | 0,176 | — | — | — | — | — | — | — | — | 0/GPI | enr. | — | — | — |
| | AT4G12730 FLA2 | -0,026 | 1,276 | 1,020 | 0,973 | 0,156 | 1,081 | 1,079 | 0,813 | 0,649 | 1,710 | 1,408 | 0,156 | -0,146 | 1,193 | 0,960 | 0,738 | 0,131 | 1,424 | 1,111 | 0,947 | 1 | ✓ | — | — | — |
| | AT5G55730 FLA1 | 0,078 | 1,209 | 1,051 | 0,922 | 0,232 | 1,324 | 1,136 | 0,707 | 0,574 | 1,436 | 1,329 | 0,221 | 0,023 | 1,358 | 1,055 | 0,947 | 0,052 | 1,367 | 1,068 | 0,994 | 0/GPI | — | — | — | — |
| | AT5G44130 FLA13 | 0,157 | 2,146 | 1,345 | 0,827 | -0,248 | 0,955 | 0,888 | 0,686 | 0,483 | 2,203 | 1,466 | 0,632 | 0,017 | 1,226 | 1,028 | 0,947 | 0,204 | 1,883 | 1,266 | 0,994 | 0/GPI | enr. | — | — | — |
| | AT5G48450 SKS3 (SKU5 Similar 3); copper ion binding | -0,045 | 1,262 | 1,010 | 0,955 | 0,618 | 1,567 | 1,368 | 0,179 | 0,423 | 1,477 | 1,251 | 0,435 | 0,077 | 1,187 | 1,048 | 0,862 | 0,087 | 1,289 | 1,067 | 0,994 | 0 | — | — | — | — |
| | AT5G49720 KOR1 (KORRIGAN); hydrolyzing O-glycosyl compounds | 0,065 | 1,360 | 1,072 | 0,937 | 0,850 | 2,936 | 1,860 | 0,095 | 0,227 | 1,544 | 1,176 | 0,541 | 0,485 | 1,326 | 1,269 | 0,281 | — | — | — | — | 1 | ✓ | — | — | — |
| | AT1G75680 glycosyl hydrolase family 9 protein | -0,335 | 0,877 | 0,849 | 0,565 | 0,289 | 1,641 | 1,225 | 0,626 | -0,433 | 1,039 | 0,834 | 0,758 | — | — | — | — | — | — | — | — | 0-1 | enr. | — | — | — |
| | AT2G17120 peptidoglycan-binding LysM domain-containing protein | -0,134 | 1,156 | 0,957 | 0,846 | 0,351 | 1,342 | 1,197 | 0,541 | — | — | — | — | 0,089 | 1,449 | 1,101 | 0,817 | 0,087 | 1,631 | 1,186 | 0,622 | 0/GPI | — | — | ✓ | — |
| | AT1G65610 endo-1,4-beta-glucanase, putative / cellulase, putative | — | — | — | — | — | — | — | — | 0,378 | 1,591 | 1,251 | 0,299 | — | — | — | — | — | — | — | — | 1 | — | — | — | — |
| | Intracellular trafficking | | | | | | | | | | | | | | | | | | | | | | | | | |
| | AT5G09810 ACT7 (ACTIN 7) | 0,196 | 1,369 | 1,127 | 0,758 | — | — | — | — | 0,716 | 1,464 | 1,421 | 0,110 | — | — | — | — | — | — | — | — | 0 | — | — | — | — |
| | AT3G12110 ACT11 (ACTIN 11) | — | — | — | — | — | — | — | — | — | — | — | — | -0,394 | 0,869 | 0,825 | 0,247 | — | — | — | — | — | — | — | — | — |
| | AT1G04820 TUA4 (tubulin alpha-4 chain) | 0,142 | 1,156 | 1,075 | 0,832 | 0,263 | 1,342 | 1,153 | 0,661 | 0,446 | 1,324 | 1,247 | 0,393 | 0,099 | 1,245 | 1,065 | 0,817 | -0,019 | 1,125 | 1,047 | 0,456 | 0 | ✓ | — | — | — |

Supplementary Table 1 continued.

| FC | AGI code and annotation | flg22 vs flg22A2 | | | | | | | | | | | | flg22 vs untreated | | | | flg22A2 vs untreated | | | | TM | PM | ATTED | flg22 expr | P flg22 |
|-------------------|--------------------------------------------------------------------------------------------------------|------------------|----------|---------|-------|-----------|----------|---------|-------|------------|----------|---------|-------|--------------------|----------|---------|-------|----------------------|----------|---------|-------|-------|------|-------|------------|---------|
| | | 0 minutes | | | | 5 minutes | | | | 15 minutes | | | | 5 minutes | | | | 5 minutes | | | | | | | | |
| | | D | max fold | av fold | p | D | max fold | av fold | p | D | max fold | av fold | p | D | max fold | av fold | p | D | max fold | av fold | p | | | | | |
| | AT5G11150 VAMP713 (vesicle-associated membrane protein 713) | — | — | — | — | — | — | — | — | 0,483 | 1,356 | 1,270 | 0,331 | 0,258 | 1,200 | 1,137 | 0,594 | — | — | — | — | 1 | — | — | — | — |
| | AT5G08080 SYP132 (syntaxin 132); t-SNARE | — | — | — | — | — | — | — | — | 0,514 | 1,316 | 1,287 | 0,299 | — | — | — | — | — | — | — | — | 1 | enr. | — | — | — |
| | AT5G46860 VAM3 (syntaxin 22); t-SNARE | — | — | — | — | — | — | — | — | — | — | — | — | — | — | — | — | — | — | — | — | 1 | — | — | — | — |
| | AT3G08530 clathrin heavy chain, putative | — | — | — | — | — | — | — | — | 0,697 | 2,272 | 1,572 | 0,532 | — | — | — | — | — | — | — | — | 0 | ✓ | — | — | — |
| Metabolism | | | | | | | | | | | | | | | | | | | | | | | | | | |
| | AT3G07160 ATGSL10 (GLUCAN SYNTHASE-LIKE 10) | 0,560 | 1,342 | 1,316 | 0,237 | — | — | — | — | — | — | — | — | — | — | — | — | — | — | — | — | 14 | ✓ | — | — | — |
| | AT5G13000 ATGSL12 (GLUCAN SYNTHASE-LIKE 12) | — | — | — | — | — | — | — | — | 0,177 | 1,118 | 1,091 | 0,780 | — | — | — | — | — | — | — | — | 11 | — | — | — | — |
| | AT4G26690 MRH5/SHV3 (morphogenesis of root hair 5); glycerophosphodiester phosphodiesterase/ kinase | 0,281 | 1,710 | 1,240 | 0,633 | 0,121 | 1,065 | 1,061 | 0,867 | 0,326 | 1,614 | 1,234 | 0,636 | — | — | — | — | — | — | — | — | 1 | — | — | ✓ | — |
| | AT5G54500 FQR1 (FLAVODOXIN-LIKE QUINONE REDUCTASE 1) | 0,297 | 1,198 | 1,158 | 0,608 | — | — | — | — | 0,325 | 1,324 | 1,181 | 0,573 | — | — | — | — | — | — | — | — | 0-1 | enr. | — | — | — |
| | AT1G66480 PMI2 (plastid movement impaired 2) | — | — | — | — | 0,392 | 1,227 | 1,212 | 0,477 | 0,652 | 1,600 | 1,392 | 0,156 | — | — | — | — | — | — | — | — | 0 | — | — | — | ✓ |
| | AT4G20830 FAD-binding domain-containing protein | -0,052 | 1,143 | 0,987 | 0,944 | 0,623 | 1,751 | 1,401 | 0,176 | 0,704 | 1,545 | 1,418 | 0,120 | 0,249 | 1,358 | 1,149 | 0,606 | 0,136 | 1,411 | 1,110 | 0,994 | 0 | — | — | ✓ | — |
| | AT3G07390 AIR12 (Auxin-Induced in Root cultures 12); extracellular matrix structural constituent | 0,075 | 1,183 | 1,046 | 0,924 | 0,326 | 1,360 | 1,186 | 0,573 | 0,525 | 1,396 | 1,297 | 0,286 | 0,122 | 1,226 | 1,072 | 0,802 | 0,165 | 1,242 | 1,094 | 0,738 | 0/GPI | — | — | — | — |

Supplementary Table 1 continued.

| FC | AGI code and annotation | flg22 vs flg22Δ2 | | | | | | | | | | | | flg22 vs untreated | | | | flg22Δ2 vs untreated | | | | TM | PM | ATTED | flg22 expr | P flg22 |
|---------------------|---------------------------------------------------------------------------|------------------|----------|---------|-------|-----------|----------|---------|-------|------------|----------|---------|-------|--------------------|----------|---------|-------|----------------------|----------|---------|-------|-------|------|-------|------------|---------|
| | | 0 minutes | | | | 5 minutes | | | | 15 minutes | | | | 5 minutes | | | | 5 minutes | | | | | | | | |
| | | D | max fold | av fold | p | D | max fold | av fold | p | D | max fold | av fold | p | D | max fold | av fold | p | D | max fold | av fold | p | | | | | |
| | ATCG00680 encodes for CP47, subunit of the photosystem II reaction center | — | — | — | — | — | — | — | — | — | — | — | — | — | — | — | — | 0,201 | 6,532 | 3,359 | 0,994 | — | — | — | — | — |
| | AT1G64760 glycosyl hydrolase family 17 protein | -0,408 | 1,316 | 0,913 | 0,550 | 0,187 | 1,209 | 1,101 | 0,766 | 0,340 | 1,491 | 1,214 | 0,470 | — | — | — | — | — | — | — | — | 0/GPI | — | — | — | — |
| | AT3G13560 glycosyl hydrolase family 17 protein | -0,048 | 1,586 | 1,094 | 0,942 | 0,237 | 1,948 | 1,298 | 0,718 | 0,417 | 2,018 | 1,382 | 0,673 | — | — | — | — | — | — | — | — | 0/GPI | — | — | — | — |
| | AT5G42100 glycosyl hydrolase family 17 protein | -0,020 | 1,093 | 0,995 | 0,973 | 0,273 | 1,290 | 1,152 | 0,646 | -0,157 | 1,130 | 0,945 | 0,813 | — | — | — | — | — | — | — | — | 0/GPI | — | — | — | — |
| | AT3G58100 glycosyl hydrolase family 17 protein | 0,080 | 1,905 | 1,236 | 0,919 | 0,529 | 1,360 | 1,298 | 0,280 | 0,697 | 1,891 | 1,469 | 0,124 | — | — | — | — | — | — | — | — | 0/GPI | — | — | — | — |
| | AT5G56590 glycosyl hydrolase family 17 protein | -0,199 | 1,697 | 1,091 | 0,813 | — | — | — | — | 0,699 | 1,697 | 1,433 | 0,123 | — | — | — | — | — | — | — | — | 0/GPI | — | — | — | — |
| | AT4G31140 glycosyl hydrolase family 17 protein | -0,055 | 1,052 | 0,977 | 0,942 | 0,191 | 1,307 | 1,115 | 0,766 | 0,666 | 1,450 | 1,387 | 0,147 | — | — | — | — | — | — | — | — | 0/GPI | — | — | — | — |
| | AT5G58090 glycosyl hydrolase family 17 protein | -1,879 | 0,611 | 0,435 | 0,088 | 0,018 | 1,342 | 1,050 | 0,973 | 0,252 | 1,276 | 1,140 | 0,466 | 0,183 | 1,302 | 1,111 | 0,710 | — | — | — | — | 0/GPI | enr. | — | — | — |
| | AT5G55480 glycerophosphoryl diester phosphodiesterase family protein | -0,104 | 1,143 | 0,966 | 0,905 | 0,235 | 1,243 | 1,128 | 0,707 | 0,340 | 1,249 | 1,183 | 0,559 | 0,167 | 1,628 | 1,176 | 0,710 | — | — | — | — | 0/GPI | — | — | — | — |
| | AT4G36750 quinone reductase family protein | 0,213 | 1,586 | 1,182 | 0,741 | 0,208 | 1,243 | 1,115 | 0,748 | 0,386 | 1,262 | 1,209 | 0,481 | 0,391 | 1,443 | 1,230 | 0,404 | 0,044 | 1,229 | 1,039 | 0,994 | 0-1 | enr. | — | — | — |
| | AT4G27270 quinone reductase family protein | — | — | — | — | — | — | — | — | — | — | — | — | 0,453 | 1,296 | 1,249 | 0,300 | — | — | — | — | 0-1 | yes | — | — | — |
| | AT2G04350 long-chain-fatty-acid--CoA ligase family protein | -0,185 | 1,081 | 0,926 | 0,766 | — | — | — | — | 0,886 | 1,909 | 1,579 | 0,155 | — | — | — | — | — | — | — | — | 1 | — | — | — | — |
| | AT1G13440 GAPC-2; glyceraldehyde-3-phosphate dehydrogenase | 0,293 | 1,437 | 1,182 | 0,619 | — | — | — | — | 0,582 | 1,477 | 1,338 | 0,211 | 0,231 | 1,296 | 1,132 | 0,622 | 0,124 | 1,492 | 1,167 | 0,485 | 0 | ✓ | — | — | — |
| Stress/Redox | AT3G09440 heat shock cognate 70 kDa protein 3 (HSC70-3) | -0,436 | 1,078 | 0,841 | 0,300 | — | — | — | — | 0,596 | 1,697 | 1,377 | 0,198 | — | — | — | — | — | — | — | — | 0 | — | — | — | — |

Supplementary Table 1 continued.

| FC | AGI code and annotation | 0 minutes | | | | flg22 vs flg22A2 5 minutes | | | | 15 minutes | | | | flg22 vs untreated 5 minutes | | | | flg22A2 vs untreated 5 minutes | | | | TM | PM | ATTED | flg22 expr | P flg22 |
|----|------------------------------------------------------------------|-----------|----------|---------|-------|-------------------------------|----------|---------|-------|------------|----------|---------|-------|---------------------------------|----------|---------|-------|-----------------------------------|----------|---------|-------|-------|------|-------|------------|---------|
| | | D | max fold | av fold | p | D | max fold | av fold | p | D | max fold | av fold | p | D | max fold | av fold | p | D | max fold | av fold | p | | | | | |
| | AT4G38670 pathogenesis-related thaumatin family protein | — | — | — | — | — | — | — | — | 0,115 | 1,213 | 1,068 | 0,877 | — | — | — | — | — | — | — | — | 0 | — | — | — | — |
| | AT3G52470 harpin-induced family protein / HIN1 family protein | -0,188 | 1,356 | 0,984 | 0,713 | 0,610 | 1,518 | 1,358 | 0,188 | 0,028 | 1,356 | 1,057 | 0,973 | 0,593 | 1,700 | 1,376 | 0,217 | 0,058 | 1,468 | 1,094 | 0,817 | 1 | — | — | — | — |
| | AT5G42980 TRX3 (thioredoxin H-type 3) | — | — | — | — | — | — | — | — | — | — | — | — | -0,619 | 1,537 | 0,946 | 0,568 | — | — | — | — | — | — | — | — | — |
| | AT4G20260 DREPP plasma membrane polypeptide family protein | 0,144 | 1,532 | 1,142 | 0,830 | 0,086 | 1,117 | 1,045 | 0,919 | 0,596 | 1,641 | 1,367 | 0,198 | 0,153 | 1,193 | 1,083 | 0,741 | 0,033 | 1,392 | 1,067 | 0,974 | 0 | enr. | — | — | — |
| | AT3G44110 J3 (DnaJ homologue 3) | 0,284 | 1,236 | 1,152 | 0,632 | — | — | — | — | — | — | — | — | 0,296 | 1,389 | 1,175 | 0,540 | 0,191 | 1,160 | 1,100 | 0,798 | 0 | — | — | — | — |
| | Protein modification | | | | | | | | | | | | | | | | | | | | | | | | | |
| | AT1G53100 acetylglucosaminyltransferase | — | — | — | — | — | — | — | — | 0,456 | 1,948 | 1,375 | 0,571 | — | — | — | — | — | — | — | — | 1-2 | — | — | — | — |
| | AT2G05920 subtilase family protein | — | — | — | — | 0,020 | 1,249 | 1,033 | 0,973 | — | — | — | — | — | — | — | — | -0,142 | 0,994 | 0,983 | 0,622 | 0 | — | — | — | — |
| | AT3G02740 aspartyl protease family protein | -0,036 | 1,213 | 1,005 | 0,967 | — | — | — | — | — | — | — | — | — | — | — | — | — | — | — | — | 0/GPI | — | — | — | — |
| | AT3G49870 ARLA1C (ADP-ribosylation factor-like A1C); GTP binding | — | — | — | — | — | — | — | — | — | — | — | — | — | — | — | — | — | — | — | — | 0 | ✓ | — | — | — |
| | AT1G10630 ADP-ribosylation factor, putative | — | — | — | — | 0,640 | 1,499 | 1,374 | 0,165 | — | — | — | — | — | — | — | — | — | — | — | — | 0- | ✓ | — | — | — |
| | AT1G33120 60S ribosomal protein L9 (RPL90B) | 0,198 | 1,184 | 1,105 | 0,758 | — | — | — | — | — | — | — | — | — | — | — | — | — | — | — | — | 0 | — | — | — | — |
| | AT2G16360 40S ribosomal protein S25 (RPS25A) | 0,198 | 1,456 | 1,145 | 0,580 | — | — | — | — | — | — | — | — | — | — | — | — | — | — | — | — | 0 | — | — | — | — |
| | AT3G04840 40S ribosomal protein S3A (RPS3aA) | — | — | — | — | — | — | — | — | — | — | — | — | — | — | — | — | — | — | — | — | 0 | — | — | — | — |

Supplementary Table 1 continued.

| FC | AGI code and annotation | 0 minutes | | | | flg22 vs flg22Δ2 5 minutes | | | | 15 minutes | | | | flg22 vs untreated 5 minutes | | | | flg22Δ2 vs untreated 5 minutes | | | | TM | PM | ATTED | flg22 expr | P flg22 | |
|----------------|--------------------------------------------------------------------------------------------|-----------|----------|---------|-------|-------------------------------|----------|---------|-------|------------|----------|---------|-------|---------------------------------|----------|---------|-------|-----------------------------------|----------|---------|-------|-----|------|-------|------------|---------|---|
| | | D | max fold | av fold | p | D | max fold | av fold | p | D | max fold | av fold | p | D | max fold | av fold | p | D | max fold | av fold | p | | | | | | |
| | AT1G23410 40S ribosomal protein S27A (RPS27aA) | -0,069 | 1,342 | 1,019 | 0,933 | — | — | — | — | 0,220 | 1,781 | 1,239 | 0,758 | — | — | — | — | — | — | — | — | 0 | — | — | — | — | |
| | AT1G27400 60S ribosomal protein L17 (RPL17A) | — | — | — | — | — | — | — | — | 0,542 | 1,980 | 1,420 | 0,517 | — | — | — | — | — | — | — | — | 0 | — | — | — | — | |
| | AT1G22780 PFL (POINTED FIRST LEAVES); structural constituent of ribosome | — | — | — | — | — | — | — | — | 0,299 | 1,324 | 1,169 | 0,606 | — | — | — | — | — | — | — | — | 0 | — | — | — | — | |
| | AT3G53020 STV1 (SHORT VALVE1); structural constituent of ribosome | 0,336 | 1,290 | 1,184 | 0,563 | — | — | — | — | — | — | — | — | — | — | — | — | — | — | — | — | 0 | — | — | — | — | |
| | AT1G02780 EMB2386 (EMBRYO DEFECTIVE 2386); structural constituent of ribosome | 0,092 | 1,170 | 1,053 | 0,919 | 0,517 | 1,436 | 1,296 | 0,296 | -0,025 | 1,058 | 0,990 | 0,973 | — | — | — | — | 0,030 | 1,195 | 1,076 | 0,443 | 0 | — | — | — | — | — |
| | AT4G20360 RABE1b/Rab8D (Rab GTPase homolog E1b); translation elongation factor | — | — | — | — | — | — | — | — | — | — | — | — | — | — | — | — | — | — | — | — | 0 | — | — | — | — | |
| | AT5G02500 HSC70-1 (heat shock cognate 70 kDa protein 1); ATP binding | -0,023 | 1,065 | 0,992 | 0,973 | 0,748 | 1,477 | 1,443 | 0,093 | 0,067 | 1,130 | 1,038 | 0,919 | 0,241 | 1,340 | 1,143 | 0,617 | — | — | — | — | 0 | — | — | — | — | — |
| | AT1G71220 UDP-glucose:glycoprotein glucosyltransferase | -0,508 | 1,616 | 0,996 | 0,176 | 1,151 | 5,373 | 2,974 | 0,254 | 0,516 | 2,423 | 1,554 | 0,698 | 0,643 | 1,618 | 1,389 | 0,175 | — | — | — | — | 0-1 | — | — | — | — | — |
| | AT1G07920 elongation factor 1-alpha / EF-1-alpha | 0,660 | 1,863 | 1,444 | 0,152 | — | — | — | — | 0,578 | 2,232 | 1,511 | 0,466 | 0,300 | 1,277 | 1,164 | 0,539 | -0,197 | 1,255 | 0,993 | 0,459 | 0 | — | — | — | — | — |
| RNA/DNA | | | | | | | | | | | | | | | | | | | | | | | | | | | |
| | AT1G22530 SEC14 cytosolic factor family protein / phosphoglyceride transfer family protein | 0,064 | 1,586 | 1,129 | 0,918 | — | — | — | — | — | — | — | — | — | — | — | — | — | — | — | — | 0 | enr. | — | — | — | — |
| | AT1G58220 myb family transcription factor | — | — | — | — | — | — | — | — | — | — | — | — | -1,485 | 22,84 | 11,42 | 0,568 | — | — | — | — | 0 | — | — | — | — | — |

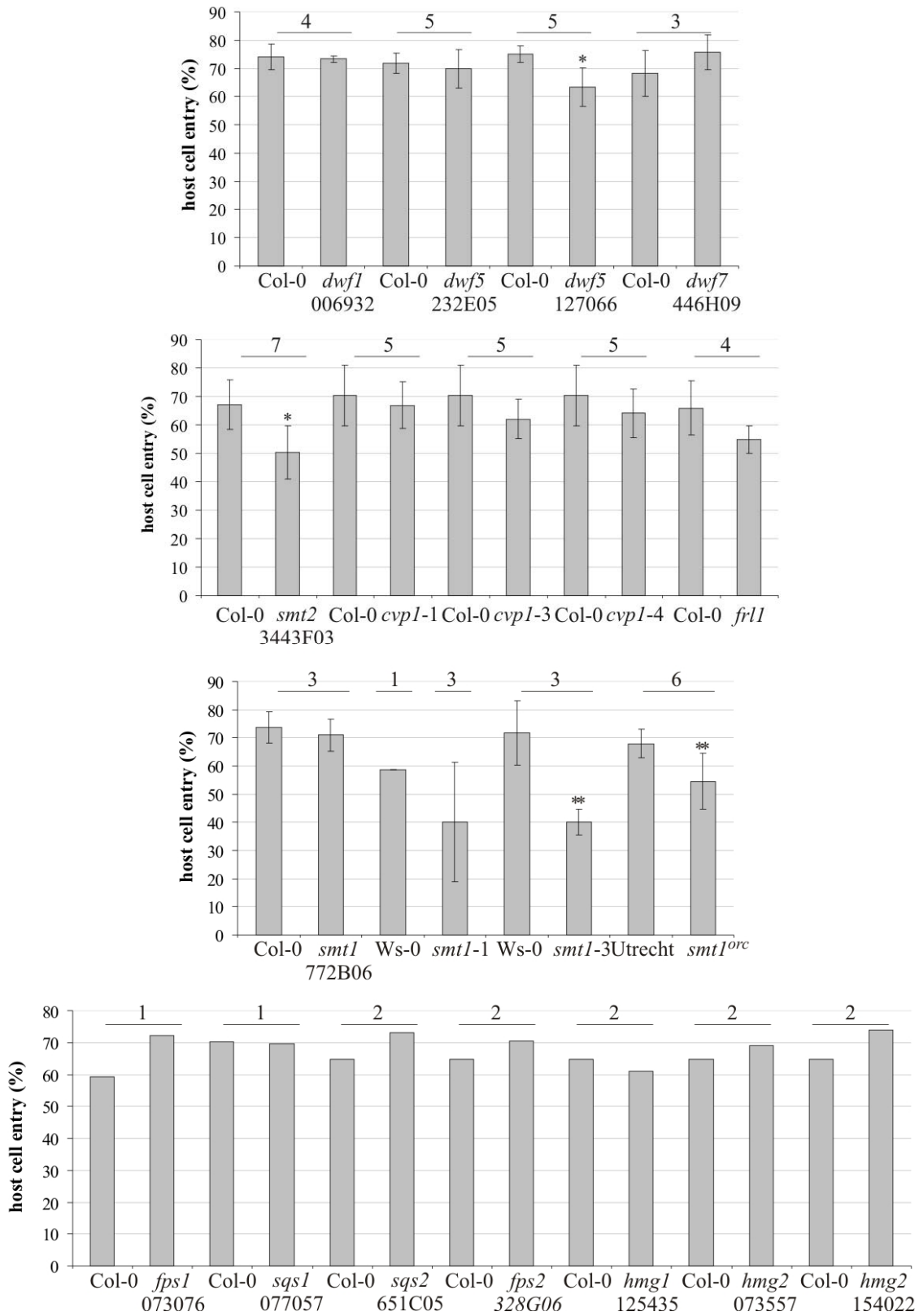
Supplementary Table 1 continued.

| FC | AGI code and annotation | 0 minutes | | | | flg22 vs flg22Δ2 5 minutes | | | | 15 minutes | | | | flg22 vs untreated 5 minutes | | | | flg22Δ2 vs untreated 5 minutes | | | | TM | PM | ATTED | flg22 expr | P flg22 |
|----------------|---------------------------------------------------------------|--------------|--------------|--------------|--------------|-------------------------------|----------|---------|-------|------------|----------|---------|-------|---------------------------------|----------|---------|-------|-----------------------------------|----------|---------|-------|-------|------|-------|------------|---------|
| | | D | max fold | av fold | p | D | max fold | av fold | p | D | max fold | av fold | p | D | max fold | av fold | p | D | max fold | av fold | p | | | | | |
| | AT1G72320 APUM23 (ARABIDOPSIS PUMILIO 23); RNA binding | — | — | — | — | — | — | — | — | — | — | — | — | — | — | — | — | — | — | — | — | 0 | ✓ | — | — | — |
| | AT5G48800 phototropic-responsive NPH3 family protein | -0,090 | 0,987 | 0,957 | 0,919 | — | — | — | — | — | — | — | — | — | — | — | — | — | — | — | — | 0-1 | — | — | — | ✓ |
| Other | AT2G44790 UCC2 (UCLACYANIN 2); copper ion binding | — | — | — | — | — | — | — | — | — | — | — | — | 0,127 | 1,106 | 1,065 | 0,798 | — | — | — | — | 0/GPI | — | — | ✓ | — |
| | AT5G51480 SKS2 (SKU5 SIMILAR 2); copper ion binding | -0,157 | 1,104 | 0,940 | 0,813 | 0,439 | 1,499 | 1,262 | 0,404 | 0,623 | 1,464 | 1,361 | 0,176 | 0,235 | 1,340 | 1,140 | 0,622 | 0,258 | 1,584 | 1,198 | 0,994 | 0/GPI | — | — | — | — |
| | AT4G25240 SKS1 (SKU5 SIMILAR 1); copper ion binding | -0,131 | 0,949 | 0,938 | 0,851 | 0,351 | 1,641 | 1,250 | 0,541 | 0,496 | 1,360 | 1,278 | 0,313 | 0,300 | 1,395 | 1,178 | 0,539 | -0,054 | 1,160 | 0,989 | 0,994 | 0/GPI | — | — | — | — |
| | AT4G16120 ATSEB1 | — | — | — | — | 0,411 | 2,225 | 1,449 | 0,211 | 0,624 | 1,360 | 1,358 | 0,176 | — | — | — | — | — | — | — | — | 0 | — | — | — | — |
| | AT5G15350 plastocyanin-like domain-containing protein | -0,230 | 0,910 | 0,893 | 0,708 | 0,513 | 1,843 | 1,370 | 0,299 | 0,411 | 1,324 | 1,227 | 0,455 | — | — | — | — | -0,100 | 1,360 | 1,014 | 0,994 | 0 | enr. | — | — | — |
| | AT4G31840 plastocyanin-like domain-containing protein | 0,154 | 1,559 | 1,153 | 0,815 | 0,005 | 1,156 | 1,013 | 0,983 | 0,405 | 1,437 | 1,236 | 0,465 | 0,184 | 1,096 | 1,095 | 0,710 | -0,016 | 1,392 | 1,050 | 0,994 | 0/GPI | — | — | — | — |
| Unknown | AT2G41800 expressed protein | 0,692 | 3,170 | 1,896 | 0,044 | 0,608 | 1,808 | 1,406 | 0,190 | 0,664 | 2,347 | 1,582 | 0,303 | 0,269 | 1,862 | 1,280 | 0,568 | -0,329 | 1,295 | 0,927 | 0,710 | 0 | — | — | — | — |
| | AT1G54920 expressed protein | — | — | — | — | — | — | — | — | — | — | — | — | — | — | — | — | — | — | — | — | 0 | — | — | — | — |
| | AT2G01080 harpin-induced family protein / HIN1 family protein | — | — | — | — | — | — | — | — | — | — | — | — | — | — | — | — | — | — | — | — | 1 | — | — | ✓ | — |
| | AT4G24290 similar to NSL1 (NECROTIC SPOTTED LESIONS 1) | — | — | — | — | — | — | — | — | 0,396 | 1,047 | 0,847 | 0,470 | — | — | — | — | — | — | — | — | 1-2 | — | — | — | — |
| | AT4G15630 integral membrane family protein | — | — | — | — | — | — | — | — | 0,314 | 1,766 | 1,268 | 0,748 | — | — | — | — | — | — | — | — | — | — | — | — | — |

Supplementary Table 1 continued.

| FC | AGI code and annotation | fig22 vs fig22Δ2 | | | | | | | | | | | | TM | PM | ATTED | fig22 expr | P fig22 | | | | | |
|----|-----------------------------|------------------|----------|---------|-------|-----------|----------|---------|-------|------------|----------|---------|-------|----|----------|---------|------------|---------|---|---|---|---|---|
| | | 0 minutes | | | | 5 minutes | | | | 15 minutes | | | | | | | | | | | | | |
| | | D | max fold | av fold | p | D | max fold | av fold | p | D | max fold | av fold | p | D | max fold | av fold | p | | | | | | |
| | AT5G40640 expressed protein | — | — | — | — | 0,748 | 1,909 | 1,450 | 0,093 | — | — | — | — | — | — | — | — | — | 5 | — | — | — | ✓ |
| | AT1G18180 expressed protein | -0,083 | 1,397 | 1,028 | 0,919 | 0,499 | 2,722 | 1,660 | 0,325 | — | — | — | — | — | — | — | — | — | 6 | ✓ | — | — | — |
| | AT1G29980 expressed protein | -0,075 | 1,081 | 0,970 | 0,924 | 0,514 | 2,181 | 1,470 | 0,088 | — | — | — | — | — | — | — | — | — | 1 | — | — | — | — |
| | AT1G45688 expressed protein | — | — | — | — | 0,937 | 3,097 | 1,953 | 0,088 | -0,025 | 1,170 | 1,002 | 0,973 | — | — | — | — | — | 1 | — | — | — | — |

Supplementary Table 2. On CD only.



Supplementary Figure 2. *Golovinomyces orontii* infection phenotypes of Arabidopsis wild type and all sterol biosynthesis mutant lines used in this study.

Quantitative analysis of host cell entry was performed at 48 hpi. Results represent mean \pm s.d. The number of biological replicates is indicated above the bars. Asterisks indicate a significant difference from wild-type accessions (** = $p < 0.01$; * = $p < 0.05$, Student's t-test).

8. Author's contributions

Chapter 1 is an introduction to the topic of microdomains and membrane rafts in plant membranes, the main focus of my PhD thesis. This introduction has been published as a review in *Current Opinion in Plant Biology* (Zappel and Panstruga, 2008). The manuscript was written by Ralph Panstruga and Nana F. Zappel to different parts and edited together:

| Chapter | Author |
|---------|--------------------------------|
| 1.1 | Nana F. Zappel |
| 1.2 | Nana F. Zappel |
| 1.3 | Nana F. Zappel |
| 1.4 | Nana F. Zappel |
| 1.5 | Nana F. Zappel |
| 1.6 | Nana F. Zappel/Ralph Panstruga |
| 1.7 | Nana F. Zappel |
| 1.8 | Nana F. Zappel |
| 1.11 | Nana F. Zappel |

The results presented in chapter 3.1 are the result of collaboration with Sylwia Kierszniowska and Waltraud Schulze (MPI for Molecular Plant Physiology in Golm).

| Author | Contribution |
|----------------------|--------------------------------------------------------------------------------------------------------------------------------------------------------------------------------|
| Nana F. Zappel | experiment design manuscript writing PM and DRM isolation sample preparation for MS analysis ratiometric quantification callose assay oxidative burst assays |
| Sylwia Kierszniowska | metabolic labeling PM and DRM isolation sample preparation for MS analysis MS analysis ratiometric quantification |
| Sharon A. Kessler | generation of transgenic lines SAK116-6 and SAK97-18 |
| Hiroko Asano | isolation of <i>fer</i> mutant |

| | |
|-------------------|-------------------------------------------------------------------|
| Ueli Grossniklaus | experiment design on work with <i>fer</i> , SAK116-6 and SAK97-18 |
| Silke Robatzek | experiment design manuscript editing |
| Waltraud Schulze | experiment design |
| Ralph Panstruga | experiment design manuscript editing |

| Figure/Table | Author |
|------------------------|-------------------------------------|
| Figure 2 | Nana F. Zappel/Ralph Panstruga |
| Figure 3 | Nana F. Zappel |
| Figure 4 | Nana F. Zappel |
| Figure 5 | Nana F. Zappel |
| Figure 6 | Nana F. Zappel |
| Figure 7 | Nana F. Zappel |
| Table 3 | Nana F. Zappel/Sylwia Kierszniowska |
| Supplementary Figure 1 | Nana F. Zappel |
| Supplementary Table 1 | Nana F. Zappel/Sylwia Kierszniowska |

Work presented in chapter 3.2 was carried out the MPI for Plant Breeding Research (Cologne).

| Author | Contribution |
|----------------|--------------------------------------------------------------------------------------------------------------------------------------------------------------------------------------------------------------------------------------------------------------------------------------------------------------------------------------------------------|
| Nana F. Zappel | experiment design manuscript writing western blot on DRMs M β CD treatment assay SNARE complex detection in DRMs isolation of T-DNA insertion lines pathogen assays generation of mutant lines expressing GFP-AtPEN1 quantitative analysis of GFP-AtPEN1 focal accumulation using OPERA microscope and Acapella software |
| Dorit Meyer | establishment of OPERA analysis |
| Kurt Stüber | writing of the Acapella script for quantitative focal accumulation analysis |
| Anzu Minami | generation of lipocalin antiserum |
| Yoko Tominaga | generation of lipocalin antiserum |
| Matsuo Uemura | experiment design concerning the lipocalin antiserum |

AUTHORS'S CONTRIBUTIONS

| | |
|---------------------|---------------------------------------------|
| Paul Schulze-Lefert | experiment design concerning OPERA analysis |
| Ralph Panstruga | experiment design manuscript editing |

| Figure/Table | Author |
|------------------------|----------------|
| Figure 8 | Nana F. Zappel |
| Figure 9 | Nana F. Zappel |
| Figure 10 | Nana F. Zappel |
| Figure 11 | Nana F. Zappel |
| Figure 12 | Nana F. Zappel |
| Supplementary Figure 2 | Nana F. Zappel |
| Figure 13 | Nana F. Zappel |
| Figure 14 | Nana F. Zappel |
| Table 4 | Nana F. Zappel |
| Table 2 | Nana F. Zappel |

Acknowledgements

Ich möchte mich herzlich bei allen bedanken, die mich während der Anfertigung meiner Doktorarbeit unterstützt haben; ganz besonders bei:

Ralph Panstruga für die Möglichkeit meine Arbeit in seiner Gruppe durchzuführen. Vielen Dank für Deine intensive und hilfreiche Betreuung und Förderung.

Prof. Paul Schulze-Lefert für die stetige Unterstützung, vielen Anregungen und Vorschläge.

Silke Robatzek nicht nur für Ihre exzellente Betreuung als „second supervisor“, sondern auch als Mentorin.

Prof. U.-I. Flüge für die Übernahme des Korreferats.

Prof. T. Bisseling für die Übernahme des externen Koreferats.

Prof. M. Hülskamp für die Übernahme des Prüfungsvorsitzes.

Waltraud Schulze und Sylwia Kierszniowsks für die enge Zusammenarbeit in dem Proteomiks-Projekt.

Prof. G. Van den Ackerveken, Prof. I. Adamska, Prof. M. Uemura, Prof. U. Grossniklaus, Matthew Humphry and Armin Töller for kindly sharing antibodies and seed material.

I thank Rockefeller University Press for the permissions to reproduce a previously published figure.

Everybody from the Panstruga/PSL team for their daily support in the lab and their kind help when once again they had to fill in for me or carry something heavy - especially Anja Reinstädler, Chiara Consonni, Sarah Schmidt, Justine Lorek, Mark Kwaaitaal, Sandra Noir und Simone Pajonk.

Sophia Mersmann, Susanne Salomon und dem restlichen Robatzek Team dafür, dass sie ihre Expertise mit mir geteilt haben.

Vera Göhre, meiner Tischnachbarin, für Ihr offenes Ohr und Ihre wertvollen Ratschläge - einem stets klaren Kopf, wenn meiner mal wieder nicht wollte.

Aurélie Huser for thoughtful discussions and spending time apart from work.

Jessika Adrian meiner „süßen Freundin aus dem Coupland Department“ und Nachbarin für die gemeinsamen Jahre.

Steffen Keinath für seine Aufmerksamkeit, Unterstützung und nicht zuletzt Geduld jeden einzelnen Tag!

Meinen Eltern und meiner Familie für ihre grenzenlose Hilfe, Unterstützung und Förderung ohne die ich nicht hier wäre.

Ich widme diese Doktorarbeit meiner Mutter.

Erklärung

Ich versichere, dass ich die von mir vorgelegte Dissertation selbständig angefertigt, die benutzten Quellen und Hilfsmittel vollständig angegeben und die Stellen der Arbeit - einschließlich Tabellen, Karten und Abbildungen -, die anderen Werken im Wortlaut oder dem Sinn nach entnommen sind, in jedem Einzelfall als Entlehnung kenntlich gemacht habe; dass diese Dissertation noch keiner anderen Fakultät oder Universität zur Prüfung vorgelegen hat; dass sie - abgesehen von den auf Seite III angegebenen Teilpublikationen - noch nicht veröffentlicht worden ist sowie, dass ich eine solche Veröffentlichung vor Abschluss des Promotionsverfahrens nicht vornehmen werde. Die Bestimmungen dieser Promotionsordnung sind mir bekannt. Die von mir vorgelegte Dissertation ist von Prof. Dr. Paul Schulze-Lefert betreut worden.

Köln, 6. Dezember 2008

Nana Zappel

Lebenslauf

Angaben zur Person

Name: Nana Friderike Zappel
Geburtsdatum/-ort: 23. November 1979 in Göttingen
Nationalität: deutsch
Familienstand: ledig

Ausbildung

seit 08/2005 **Promotions-Studium** an der Universität zu Köln, Köln, Deutschland
Max-Planck-Institut für Züchtungsforschung, unter der Leitung von Prof.
Dr. P. Schulze-Lefert
Stipendium der *International Max-Planck-Research School*

09/2003 – 06/2005 **Master-Studium** an der Universität Wageningen, Wageningen,
Niederlande
Fachbereich Pflanzenbiotechnologie, Hauptfach: Pflanzenpathologie
Abschluss: Master of Plant Biotechnology *cum laude*

09/1999 – 02/2003 **Bachelor-Studium** Agrarwissenschaften an der
Universität Hohenheim, Stuttgart, Deutschland
Abschluss: Bachelor of Science

09/2001 – 10/2002 **Universidad Politécnica de Valencia**, Valencia, Spanien

09/1998 – 07/1999 **Leibniz Kolleg**, Tübingen, Deutschland

06/1998 **Abitur**, Theodor-Heuss-Gymnasium, Göttingen, Deutschland

Köln, 6. Dezember 2008

Nana Zappel

